Modeling a NOx Storage and Reduction Catalyst

by

Jasdeep Singh Mandur

A thesis

presented to the University of Waterloo

in fulfillment of the

thesis requirement for the degree of

Master of Applied Science

in

Chemical Engineering

Waterloo, Ontario, Canada, 2009

AUTHOR'S DECLARATION

I hereby declare that I am the sole author of this thesis. This is a true copy of the thesis, including any required final revisions, as accepted by my examiners.

I understand that my thesis may be made electronically available to the public.

Jasdeep S. Mandur

Abstract

Lean burn engines are more fuel efficient than standard stoichiometric-burn engines but at the same time, the conventional three-way catalyst is not effective in reducing the NOx in oxygen-rich exhaust. One of the recent advancements in exhaust after treatment technologies for lean burn engines is the NOx storage and reduction (NSR) methodology. In this mechanism, NOx is stored on the storage component of a NSR catalyst during normal engine operation. However, before the catalyst reaches its saturation capacity, an excess of fuel is injected to the engine for a very short period resulting in reductant rich exhaust and during this period, NOx is released and subsequently reduced to N_2, therefore, restoring the storage capacity of the catalyst. The operation is cyclic in nature, with the engine operating between an oxygen rich feed for long periods and a fuel rich feed for relatively shorter periods. To implement this technology in the most efficient way, a detailed understanding of the NSR chemistry under different operating conditions is required.

For the past few years, several authors have studied the NSR systems using both experimental and modeling techniques. However, most of the models proposed in the literature were calibrated against the steady cyclic operation where the NOx profiles are similar for each cycle. In real life situations, the engine operation changes with different driving conditions, occurring due to sudden acceleration, roads in hilly areas, non-uniform braking, etc., which results in operation with a number of different transient cycle-to-cycle regimes depending upon the frequency with which the engine operation is altered. Due to such varying conditions, it is very important to investigate the significance of transients observed between the two different steady cycle-to-cycle operations for the optimization and control purposes.

Also, the models in the literature are specific to the catalyst used in the study and therefore, their adaptation to other NSR catalysts is not straightforward. Therefore, one of the main motivations behind this research work is to develop a general approach to explain the storage dynamics. Moreover, the existing models have not studied the regeneration mechanisms, which is very important to explain the cyclic data in complete operation including both transients and steady state cycles.

In this study, a pseudo one-dimensional model of a commercial NOx storage/release (NSR) catalyst is presented. The NOx storage is considered to be mass transfer limited, where as the storage proceeds, the barium carbonate particle is converted into the nitrate and for further storage, the NOx has to diffuse through this growing nitrate layer and a after certain depth, this penetration becomes nearly impossible.

To explain the transient nature of the cyclic NOx profile, it is hypothesized that when incomplete regeneration occurs, only part of the nitrate is converted back to carbonate. Therefore, the nitrate layer increases in thickness with each cycle, thus making further storage increasingly more difficult. The shrinking core concept with incomplete storage in the lean phase followed by incomplete regeneration of the nitrate layer during the regeneration phase accounts for a net drop in storage capacity of the catalyst in each cycle, which continues decreasing until the amount of sites regenerated equal the amount used in NOx storage.

The number of unknown parameters used for fitting were reduced by parameter sensitivity analysis and then fitted against a NOx profile at the reactor exit.

The overall amount of NOx that can be stored in the lean phase of the cycle depends on the extent of regeneration that can be achieved during the previous rich phase, which in turn depends directly on the concentration of reductants in the feed. Therefore, there is a trade-off between the amount of fuel used and the NOx emissions. The proposed model can be potentially used to improve this trade-off by using model-based optimization techniques.

Acknowledgements

First of all, I would like to thank Prof. Hector Budman for providing me with an opportunity to work on this challenging project. I also thank him for his consistent support and the guidance he provided throughout this project.

Also, I would like to thank Prof. William Epling for offering his extensive knowledge in the field of NOx reduction in NSR systems. The brainstorming sessions, that I had with him and Prof. Hector, helped me a lot in understanding the insights of NSR catalyst and therefore, achieving my goal to such an extent.

The support of my family will remain unforgettable throughout my life. The encouragement from my parents to try new things and their willingness to answer my questions always motivated me and acted as one of the pillars of my success. I am really blessed to have them as a part of my life.

These two years that I spent in UW would have not been so enjoyable without the help of my friends and I would like to thanks all of them, especially Mukesh, Mayur Mundhwa, Ketan Prajapati, Varun Malhotra, Prashant, Rosendo, Walid-Al-Gerwi and Mohammad Shams for being there with me.

In the end, I would like to thank Natural Sciences and Engineering Research Council, Canada for the financial support for this project.

Table of Contents

List of Figures

List of Tables

Chapter 1
Introduction

1.1 Overview

It has been predicted that, over the next few decades, the present oil supply will not be sufficient to meet the ever-growing demand. In response to this prediction, industrial countries at the forefront of technology have already started investing in novel methodologies to utilize fossil fuels efficiently and to harness renewable energy resources. Vehicles are one of the major consumers of oil reserves. Hence, automotive manufacturers face a major challenge of utilizing available oil resources efficiently without affecting the growing economy. Climate change, observed over the past few years, has brought the public to a common understanding that the strong and effective measures to control global warming and strict environment regulations on harmful emissions are needed. In this scenario, automotive companies have two major tasks, first to increase fuel economy and second to reduce emissions to the minimum set by Environmental Protection Agency (EPA) regulations.

Diesel engines are known to be more fuel efficient than gasoline engines but at the same time, they suffer certain disadvantages such as heavier in size, lower RPM range etc., which limit their use in regular vehicles. Although the gasoline engines have been the preferable choice for regular vehicles for a long period, the recent focus on achieving higher fuel economy resulted in their modified operation, where the engines will have to be operated under lean burn conditions. In lean burn engines, fuel is burnt in the presence of excess air which is different from the conventional operation where fuel and oxygen are fed in a stoichiometric ratio. Although fuel economy increases in lean burn engines, the conventional after-treatment systems based on traditional three-way catalyst are no longer effective in reducing NOx emissions in the exhaust of these engines. The reason is that in the presence of excess oxygen, CO and H_2 are reduced immediately into CO_2 and H_2O respectively and the final exhaust contains unacceptable amounts of NOx which remain un-reacted. The higher amount of NOx in the exhaust is also a major problem in lean burn diesel engines. The recent advancements in the after treatment systems for lean burn diesel/gasoline engines led to the development of two different approaches: (●) Selective Catalytic Reduction (SCR) methodology and (●) NOx Storage and Reduction (NSR) methodology

1.1.1 Selective Catalytic Reduction

In the SCR methodology, the catalyst reacts selectively with the reductants and NOx. There are two sub-categories of SCR: ammonia/urea-based and hydrocarbon-based. The ammonia/urea based SCR

technology is well proven and has been widely implemented for stationary applications such as emissions from the industrial boilers. However, its implementation in vehicular after-treatment systems requires well designed on-board anhydrous ammonia or aqueous urea injection systems and highly sensitive equipment to monitor any ammonia slip which may occur. The hydrocarbon based SCR systems have shown relatively lower NOx reduction efficiencies and also the development of these systems has not progressed as far as ammonia/urea based SCR systems.

1.1.2 NOx Storage and Reduction

In the NOx storage and release (NSR) methodology, the after treatment system is equipped with a specially designed NSR catalyst. During normal lean burn operation, NOx in the exhaust gets stored on the storage particles present in NSR catalyst. When the catalyst gets saturated, fuel rich feed is fed to the engine for a very short period which results in reductant rich exhaust. In this reducing environment, stored NOx is released and subsequently reduced by the reductants, thus restoring the original storing capacity of the catalyst. This operation is cyclic in nature with a lean phase corresponding to the normal engine operation and a rich phase corresponding to fuel-rich injections.

In this thesis, the reactions and associated mechanisms involved in the NOx storage and release technology will be studied.

1.2 NOx storage and release catalyst

The NSR catalyst has a monolith-type structure where each of the channel walls is coated with an alumina layer acting as a washcoat. Typically, the washcoat is doped with an alkali or alkaline earth metal used to trap the NOx as nitrates and precious metal components responsible for performing a series of red-ox reactions. The standard formulation used in literature is $Pt/Ba/Al_2O_3$. In this study, an industrial catalyst is being considered which is more complex as compared to the standard catalyst. However, for confidentiality reasons the exact formulation of the catalyst is not given. In addition to basic constituents, it contains ceria compounds that act as a washcoat stabilizer and additional precious metals other than Platinum (Pt), such as rhodium (Rh) etc. The typical model catalyst is schematically represented in Figure 1-1

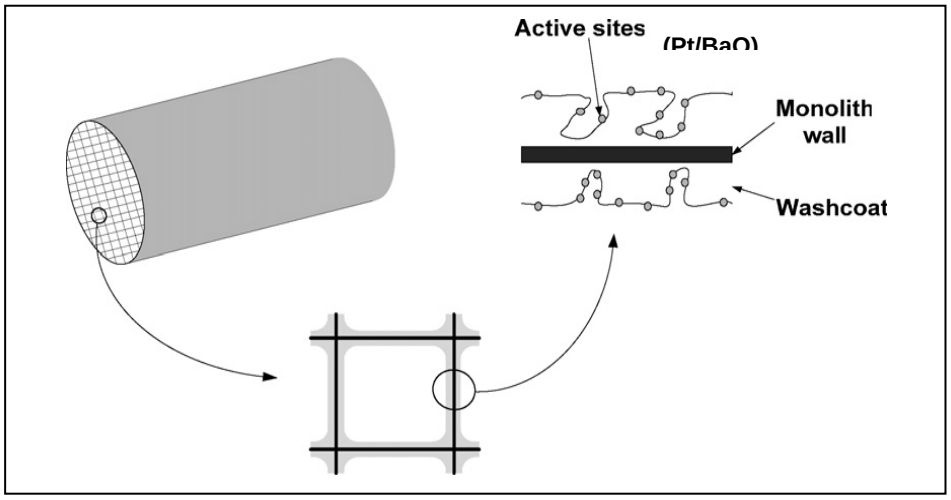

Figure 1-1: Representation of Typical NSR catalyst (Tomasic 2007)

1.3 NOx storage and release mechanism

The NSR mechanism is cyclic in nature with the engine alternating between lean burn and fuel rich conditions. The overall cycle can be divided into four basic reaction steps (Epling et al., 2004):

(i) NO oxidation to NO_2

(ii) NO and NO_2 storage on barium particles in the form of nitrates and nitrites

(iii) Regeneration of barium particles by reductants releasing NO

(iv) Reduction of NO into N_2 by reductants

1.3.1 Lean Phase

During nominal engine operation, lean burn conditions generate oxygen rich exhaust which is the feed for the NSR catalyst. In the terminology used in NSR systems, this period is referred to as the lean phase. Due to the oxidizing environment, NOx cannot be reduced and therefore is trapped within the catalyst in the form of barium nitrate (or nitrite). Since, it has been experimentally observed that NO_2 is more readily stored on barium particles as compared to NO (Forzatti et al., 2006; Jozsa et al., 2004), NO oxidation over a Pt site is a crucial step in the storage process. During the initial couple of seconds, the amount of NOx observed at the catalyst exit is nearly zero, and after a certain delay, the NO concentration starts increasing non-uniformly, resulting in a typical S-Shaped NOx profile as shown in Figure 1-2a. This increase in the NOx concentration is attributed to the fact that the storage

capacity of the catalyst continues to decrease as more and more barium nitrate is formed. The duration of the lean phase is based on the storage capacity of the catalyst and targeted percentage reduction in the NOx emissions.

1.3.2 Rich Phase

When a significant amount of NOx starts appearing at the catalyst exit or alternatively, when the amount of NOx stored starts to decrease below its target value, the storage capacity of the catalyst has to be restored to its original level to remain below a target NOx emissions value. At that moment, corresponding to time 400 seconds in Figure 1-2b, the engine operation is switched to the fuel rich conditions to produce reductant rich exhaust. When this exhaust is fed to the catalyst, reductants react with barium nitrate in the reducing environment, restoring the barium to its original form. This period is referred to as the rich phase in the terminology of NSR systems and is relatively shorter in duration than the lean phase. The duration of the rich phase has to be selected very carefully because the fuel-rich engine operation results in extra consumption of fuel and this consumption should be kept to a minimum to make the operation economically viable. Thus, the amount of reductants should be just sufficient to restore the storage capacity but without affecting significantly the fuel consumption.

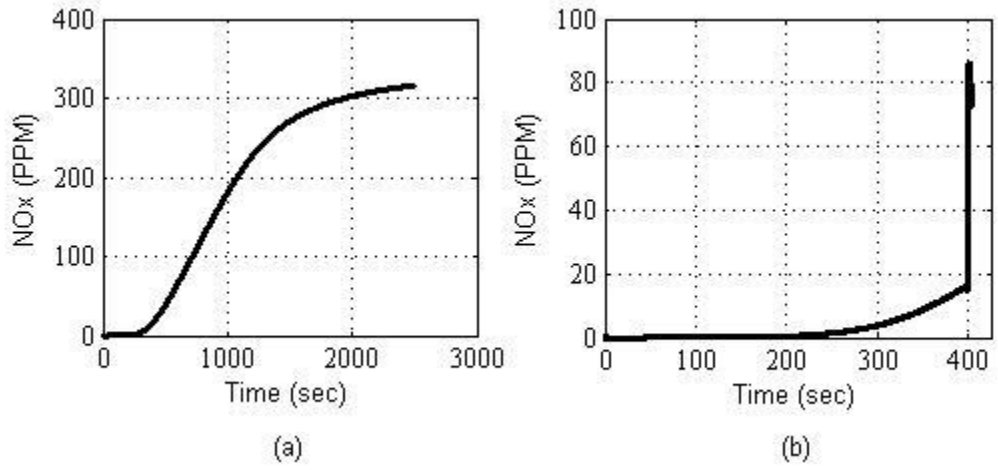

Figure 1-2: Simulated results of a typical NSR cycle in a current work. (a) Lean Phase (b) Rich Phase

Regeneration of storage sites result in the release of stored NOx mostly in the form of NO and the released NO is subsequently reduced to N_2 by reductants. The competitive nature of these two reactions, i.e. NO release and NO reduction, results in a characteristic "spike" or "puff" observed for NO concentration profiles during the rich phase, as shown in Figure 1-2b.

1.3.3 Cyclic Operation of NSR

When the engine is operated via alternating between the lean burn and fuel rich conditions repeatedly, cyclic operation results. In the experiments performed on this catalyst (Al-Harbi Thesis, 2008), it has been observed that with fresh catalyst, i.e. completely regenerated catalyst before the cyclic operation started, cyclic operation can be subdivided into two regimes: a transient cycle-to-cycle regime which is then followed by steady cycle-to-cycle regime as shown in Figure 1-3. For simplicity, although both regimes are cyclic in nature, the first regime will be referred to as "transient operation" whereas the second regime will be referred to as "steady-periodic operation".

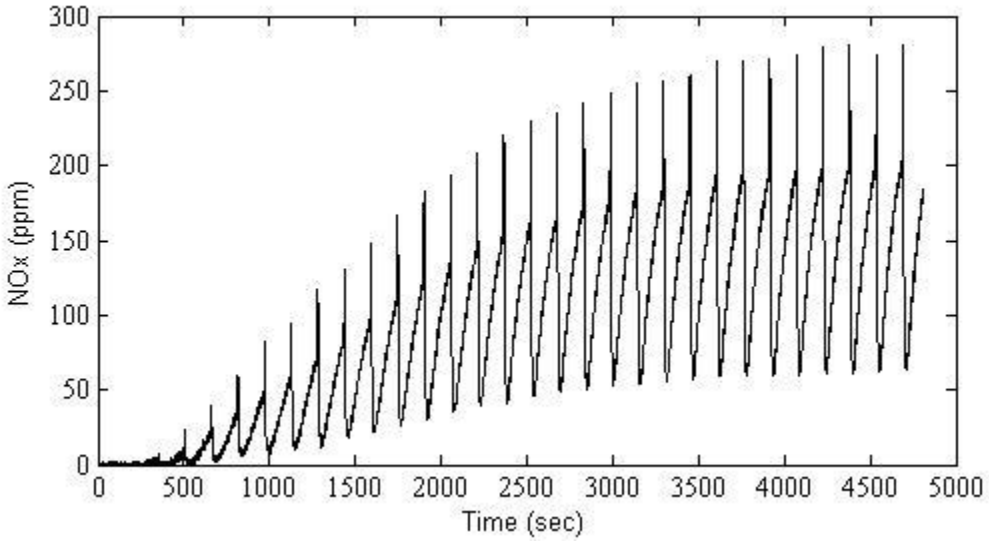

Figure 1-3: NOx concentration at the catalyst exit for cyclic operation with lean time of 150 sec and rich time of 5 sec. Experimental details include: Lean phase composition of 300 ppm NO, 10% O_2, 5% CO_2, 5% H_2O and rest N_2; Rich phase composition of 1.5% CO, 5% CO_2, 5% H_2O and rest N_2; Temperature = 300 ^oC (Al-Harbi & Epling, 2009)

Referring to Figure 1-3, the transient regime corresponds to the period where the NOx concentration amplitudes and baseline of the NOx profile change over time (until approximately 4000 seconds in Figure 1-3) whereas in the steady-periodic regime both the amplitude of oscillations and the baseline of the NOx profile remain constant (after 4000 seconds in Figure 1-3). The durations of both the lean and rich phases have individual effects on the period for which operation will remain in the transient regime. As discussed earlier, during the rich phase the partially reduced storage capacity of the catalyst is regenerated by the reductants. If the duration of the rich phase or correspondingly, the net amount of reductants entering the catalyst is sufficient enough to provide complete regeneration along the entire length of catalyst, then there will be no transient regime in the cycle-to-cycle operation. The reason is that if the regeneration achieved during the rich phase is complete the lean phase will start at each cycle from the same storage capacity. In this case the duration of the lean phase will only affect the shape of NOx profile during lean and the same NOx exit profile will be observed in every cycle afterwards. In the case of incomplete regeneration, the number of cycles in the transient cycle-to-cycle regime depends on the duration of the lean phase. If the lean phase is sufficiently long to achieve saturation of storage capacity along the entire length of reactor already during just the first cycle, then only the first cycle will be different in terms of cycle-to-cycle NOx profile, and from the second cycle and on, steady periodic operation will occur. Following this reasoning as the duration of the lean phase decreases, the number of cycles in the transient cycle-to-cycle regime is expected to increase.

Since the amount of reductants used in the rich phase has to be kept to a minimum for economic considerations, the experiments reviewed and used in the current work were conducted with rich feed concentrations of 1.5% CO and a rich phase period of 5 seconds. The results for 1.5% CO are shown in Figure 1-3 and it can be seen clearly that cyclic operation is in transient cycle-to-cycle regime for a very long duration, nearly 4000 seconds as mentioned above.

1.3.4 Objective of the Research

The NSR operation is fairly complex since it involves a number of variables affecting its overall response. The different durations of the lean and rich phases and the different reductant compositions used during operation have a great affect on NOx emissions and associated fuel consumption. To implement NSR technology in the most efficient way, a detailed understanding of the effect of the transport and reaction mechanisms under different operating conditions is required. Mathematical modeling can be a very useful tool in understanding this complex system and to suggest optimal operating conditions for achieving a better trade-off between NOx emissions and fuel consumption

from model-based optimization. The model could also be used to make predictions within a predictive closed loop control strategy for the process.

Several different models have been proposed to describe the NOx storage and subsequent release/reduction processes (Olsson et al., 2005; Tuttlies et al., 2004; Schmieber et al., 2007; Guthenke et al., 2007). However, most of these models were focused on describing the different possible mechanisms in the storage process and were calibrated against data obtained in steady periodic operation. Very few attempts were made to explain the transient operation. From a practical point of view the transient regime is of great importance because due to frequent engine startup and during city driving, the exhaust system is expected to operate most of the time in a transient regime rather than a steady periodic one. Moreover, in reality, engine operation changes with different driving conditions occurring due to sudden acceleration, roads in hilly areas, non-uniform braking, etc., which results in operation with a number of different transient cycle-to-cycle regimes depending upon the frequency with which the engine operation is altered. Due to such varying conditions, it is very important to investigate the significance of transients observed between the two different steady cycle-to-cycle operations. Thus, an optimization that will be relevant for the actual operation of this system should be based on a model that correctly describes the transient operation of the catalyst. As stated above the available literature is lacking in the mathematical description of the transient regime. Moreover, in the literature, different possible mechanisms were used to explain the storage dynamics and were specific to the catalysts used in the study. Therefore, their adaptation to other NSR catalyst formulations is not straightforward.

Following the above, the overall objectives of the research can be summarized as follows:

i. To propose a general approach to model the storage dynamics of an industrial NSR catalyst, that can be easily adapted to any other catalyst formulation.

ii. To calibrate this model with experimental data and to predict both steady periodic as well as transient operation of the system.

iii. To identify the important process parameters to be optimized to achieve a better trade-off between NOx emissions and fuel consumption.

Chapter 2
Literature Review

The overall cyclic nature of a NSR catalyst can be described in five basic sequential steps (Epling et al., 2004). However, a detailed study has shown the presence of multiple reaction pathways and different mechanisms, thus adding difficulty to the understanding and modeling of the operation. In this chapter, the various efforts made in the past by different research groups to understand the complexity of NSR chemistry will be discussed.

The exhaust of a lean burn engine contains NOx, mostly in the form of NO. When the oxygen rich exhaust is fed to the NSR catalyst during the lean phase, NOx can undergo following three reactions:

- NO oxidation to NO_2
- NO storage on storage particles.
- NO_2 storage on storage particles.

However, it has been experimentally shown that the NO_2 storage occurs more readily, or at faster rates, as compared to NO storage (Forzatti et al., 2006; Jozsa et al., 2004). Forzatti et al. studied the NOx storage over $Pt/Ba/Al_2O_3$ catalyst with three types of feed compositions; $NO + O_2$, $NO_2 + O_2$ and NO only. It was observed that using $NO + O_2$ instead of $NO_2 + O_2$ resulted in little difference in the amount of NOx stored, with a decrease of only 3%, whereas using only NO had a significant effect, with 45% less stored over a fixed 5 min lean period. It was concluded that the NO_2 is an important intermediate during the storage process and, therefore, in order to maximize the NOx trap efficiency, the NO oxidation step becomes very important.

2.1 NO Oxidation

NO oxidation is a reversible reaction, which is kinetically limited at lower temperature and thermodynamically limited at higher temperatures.

2.1.1 NO oxidation over noble metals

Detailed studies of the overall reaction rate have been conducted for different precious metals over different support materials. Studies have shown that the extent of NO oxidation is higher over Pt based catalysts as compared to Palladium (Pd) or Rhodium (Rh) based catalysts (Ohtsuka, 2001; Ohtsuka and Tabata, 2001). Xue et al. studied the effect of loading and dispersion of Pt on NO oxidation for three different types of supports; SiO_2, Al_2O_3 and ZrO_2. The activities of all three types

of catalysts were observed to increase as the Pt loading increased and as the amount of Pt exposed on the surface increases. On the other hand, the larger Pt particles were found to result in higher catalytic activity in the case of Pt/SiO_2 catalysts and this size-dependence was relatively weaker for Pt/Al_2O_3 catalysts, becoming almost negligible for Pt/ZrO_3 catalysts. Moreover, it was also shown that SiO_2 has very little influence on the Pt/SiO_2 catalysts performance whereas Al_2O_3 and ZrO_2 support materials influence the behavior of corresponding Pt-containing catalysts to a relatively greater extent.

In a recent study, Mulla et al. have reported strong inhibition of the NO oxidation reaction by NO_2 and this has been attributed to the fact that NO_2 adsorbs preferentially on the surface, keeping it oxidized and thus preventing the adsorption of other species. Thus, most of the surface oxygen comes from the dissociation of NO_2 rather than from the dissociation of O_2. This is also confirmed in the studied by Segner et al. (1992) and Parker and Koel (1990), where it is reported that the high sticking coefficient of NOx makes it a very effective source of surface oxygen.

2.1.2 NO Oxidation over NSR catalyst

Since NO oxidation is a key step in the NOx storage process, Olsson et al (2005) conducted a comparative study of NO oxidation to assess the effect of storage particles on oxidation kinetics. Olsson et al. studied NO oxidation on both $Pt/BaO/Al_2O_3$ and Pt/Al_2O_3 catalysts and found that in the presence of BaO particles, the maximum attainable NO conversion was significantly decreased. One of the explanations presented for this notable change was a decrease in Pt dispersion, either due to the coverage of some Pt sites by $Ba(NO_3)_2$ particles, which are nearly 3 times larger in volume than BaO, or due to the formation of inactive Pt oxides by slow oxidation of some Pt particles. It was also found that in the case of NO oxidation over the $Pt/BaO/Al_2O_3$ catalyst, there is no thermodynamic limitation until about 400^oC whereas over the Pt/Al_2O_3 catalyst, NO oxidation becomes thermodynamically limited around 300^oC.

2.2 NOx Storage

NO oxidation is followed by the storage of NOx on alkali/alkaline earth metal compounds. Based on experimental studies it has been observed that the storage capacity has a strong dependency on different catalyst formulations and operating conditions. Due to this, multiple reactions pathways and mechanisms have been proposed. The corresponding findings of these studies are summarized in the following sub-sections.

2.2.1 The Factors affecting the storage capacity of an NSR catalyst

2.2.1.1 Effect of alkali/alkaline earth metals

In the common formulation of an NSR catalyst, Ba is a common choice for serving as storage medium. However, the effect of using other alkali/alkaline earth metals on the NOx storage performance has been also investigated. For example Kobayashi et al. (1997) and Takahashi et al. (1996) reported that the basicity of a storage particle is directly related to the percentage of NOx stored and the earth metals in order of their decreasing basicity are reported as K > Ba > Sr $\geq$ Na > Ca > Li $\geq$ Mg. The study by Gill et al. indicated that potassium results in higher performance over 350^{o}C but below this temperature barium shows better results. Also, the barium nitrates formed during the storage process are more stable than other nitrates, therefore suggesting the barium as a preferred choice for trapping medium.

2.2.1.2 Effect of feed compositions

The feed conditions are also found to have significant effect on the storage capacity of the catalyst, especially the CO_2 and H_2O levels. Detailed studies by Nova et al. (2002) and Lietti et al. (2001) have shown that, in the presence of CO_2 and H_2O, the barium can exist in the form of oxide, carbonate and hydroxide. They also found that a thermodynamic equilibrium exists between these three states where this equilibrium depends on both feed composition and temperature. It was also reported that the NOx is first stored on BaO, then on $Ba(OH)_2$ and finally on $BaCO_3$. The stability of different states of barium was observed to be directly related to their acidic character as per the following hierarchical sequence: $BaO < Ba(OH)_2 < BaCO_3 < Ba(NO_2)_2 < Ba(NO_3)_2 < BaSO_4$. Since the $Ba(OH)_2$ and $BaCO_3$ are more stable than BaO, their presence on the surface is expected to hinder the overall storage capacity. Toops et al. studied the individual and the combined effects of CO_2 and H_2O on the storage capacity for a $Pt/K/Al_2O_3$ catalyst. The presence of 5% CO_2 decreased the storage capacity by 45% at 250^{o}C whereas 5% H_2O resulted in a decrease of 16% at 300^{o}C. However, a decrease of only 11% in the overall storage capacity was observed with the combined presence of H_2O and CO_2, each at a 5% concentration level. This is attributed to the fact that the presence of H_2O will shift the equilibrium between $BaCO_3$ and $Ba(OH)_2$ in the $BaCO_3 + H_2O \leftrightarrow Ba(OH)_2 + CO_2$ reaction, towards the right of this reaction, thus increasing the amount of hydroxide on the surface. Since the hydroxide is less stable than the carbonate, the ability to store NOx increases as compared to the cases where the two gases are individually fed into the system.

2.2.1.3 Effect of gas temperature

In studies investigating the temperature dependency of the storage capacity, it has been observed that NOx storage increases with temperature, reaching a maximum at around 350^{o}C and decreases thereafter (Epling et al., 2003; Mahzoul et al., 1999; Fridell et al., 1999). At lower temperatures, NO oxidation is kinetically limited and therefore it becomes the rate limiting step in the storage process. For temperatures above 400^{o}C, Fridell et al. observed a decrease in the thermal stability of nitrates/nitrites with respect to temperature thus explaining the reduced capability of storage particles to store NOx as observed at higher temperatures. In cyclic operation, the barium sites in the form of oxides, carbonates or hydroxides that are converted into nitrates/nitrites during the lean phase are regenerated back during the rich phase by reductants. At low temperatures, the extent of regeneration of storage sites is kinetically limited and therefore, the surface was observed to retain nitrate/nitrite species resulting in a decrease of the storage capacity for the next lean phase (Epling et al., 2004). To address this limitation, either higher temperatures or higher reductant compositions can be used to achieve nearly 100% regeneration, thus providing approximately the same storage capacity during each subsequent NSR cycle.

2.2.2 Reaction pathways and mechanisms

Based on the above discussion, the different inlet gas compositions and the presence of different types of storage particles lead to the occurrence of multiple reaction pathways and associated mechanisms. In the presence of active oxygen species, barium sites are observed to store NO_2 and NO, mainly in the form of nitrates (Mahzoul et al., 1999; Prinetto et al., 2001; Fridell et al., 1999). Mahzoul et al. (1999) suggested that the barium particles close to the Pt sites are more active in the storage process. This has been corroborated by several studies where NO oxidation over a Pt site has been suggested as a key step due to the relative preference for NO_2 storage. The proposed reactions to describe the storage process are as follows:

$$O_2 \leftrightarrow 2O^* \quad \text{... (2.1)}$$

$$BaO + 2NO_2 + O^* \leftrightarrow Ba(NO_3)_2 \quad \text{... (2.2)}$$

$$BaO + 2NO + 3O^* \leftrightarrow Ba(NO_3)_2 \quad \text{... (2.3)}$$

The presence of nitrites under certain conditions, such as low temperature, suggested the possibility of NO oxidation reaction to proceed according in two steps; NO is initially stored as nitrite

and subsequently the nitrite is oxidized into a nitrate (Mahzoul et al., 1999; Lietti et al., 2001). These two reactions are as follows:

$$BaO + 2NO + O^* \rightarrow Ba(NO_2)_2 \quad \text{... (2.4)}$$

$$Ba(NO_2)_2 + 2O^* \rightarrow Ba(NO_3)_2 \quad \text{... (2.5)}$$

Lietti et al. (2001) have also suggested another reaction path to explain the presence of both nitrite and nitrate sites, where the dimerization of NO_2 to N_2O_4 is followed by a disproportionation reaction as follows:

$$2NO_2 \rightarrow N_2O_4 \quad \text{... (2.6)}$$

$$2BaO + 2N_2O_4 \rightarrow Ba(NO_2)_2 + Ba(NO_3)_2 \quad \text{... (2.7)}$$

Although due to their thermal instability at higher temperatures nitrite sites have not been directly observed in experiments, they may exist as intermediates.

For the barium sites close to Pt, the feed O_2 can be justified as a source of active oxygen atom via O_2 dissociation reaction: $O_2 \leftrightarrow 2O^*$, but as those sites get saturated, the role of this reaction diminishes. Epling et al. (2004) illustrated the role of NO_2 as a possible oxidant for the storage sites away from Pt via the disproportionation reaction: $BaO + 3NO_2 \rightarrow Ba(NO_3)_2 + NO$

Several studies have demonstrated the existence of multiple storage sites and the significant effect of Pt/Ba proximity on the overall NOx storage (Epling et al., 2004; Mahzoul et al., 1999; Lietti et al., 2001). Based on the different topology of active sites of Pt and storage components, three distinct pathways for NOx storage have been suggested (Epling et al., 2004). A schematic overview of these pathways is shown in Figure 2-1. The first type of surface, represented by Figure 2-1 (A) contains two types of storage sites; one in a close proximity to Pt (Type I) and another site away from the Pt sites (Type II). The Type I storage particles account for a rapid NOx storage using both O_2 and NO_2 as the oxygen source, whereas Type II still contribute to the storage but at very slow rate and trapping is exclusively done via disproportionation mechanism with no O_2 participation. The second type of surface, represented by Figure 2-1 (B) contains two types of Pt sites. The Pt sites in a close proximity to Ba (Type I) are responsible for the trapping mechanism, whereas the Pt sites away from Ba (Type II) account for oxidation activities. However, this model does not account for slower trapping of NOx observed after the "NOx slip" begins (Epling et al., 2004). This suggests that extra Ba sites are needed, that are located away from the Pt sites.

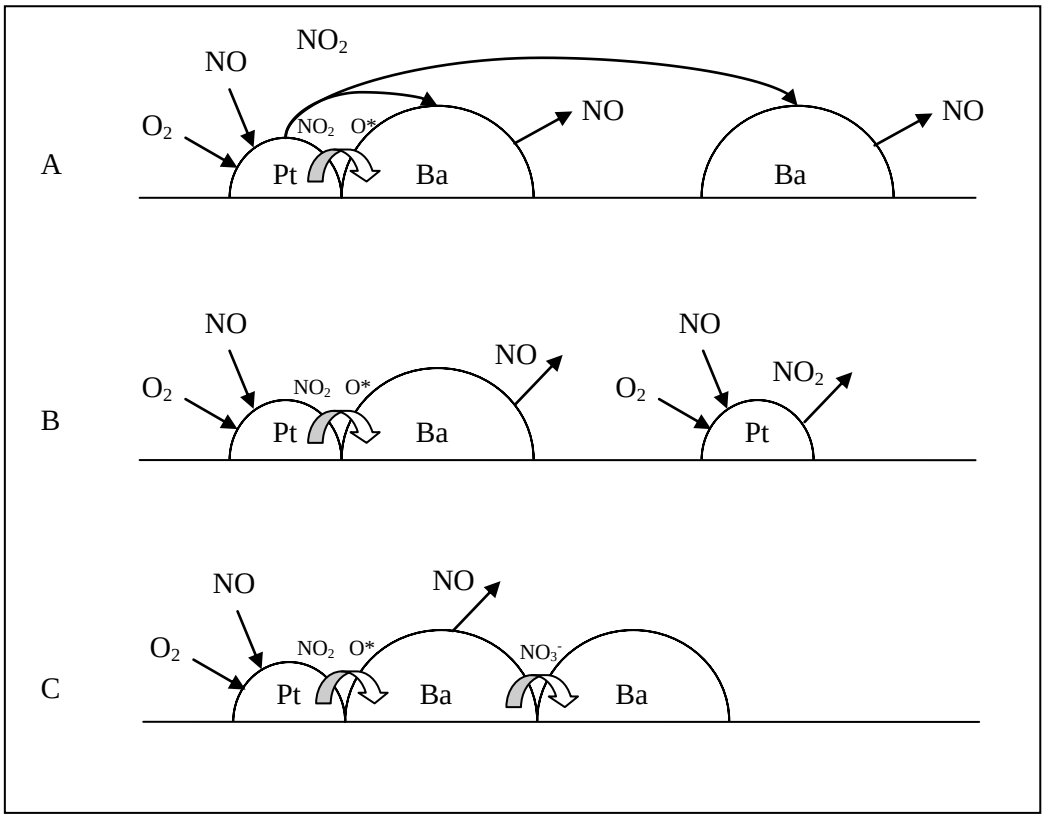

Figure 2-1: Reaction schematics of three proposed pathways for NOx sorption on Pt/Ba-based NSR catalyst.

The third type of surface, represented by Figure 2-1 (C), accounts for a nitrate spill - over type mechanism. The Ba sites close to Pt get saturated immediately and then the storage rate decreases due to the resistance offered by a growing nitrate layer. This type of surface topology has been used by Olsson et al. (2005) as the basis of a two dimensional shrinking core model. A shrinking core model accounting for the different types of barium particles has been used in this research and is described in detail in later chapter of this thesis.

2.3 Reductant Evolution

The storage capacity of the catalyst continues to decrease with time due to the formation of nitrates/nitrites and after a certain delay, the NOx level in the exit stream starts to increase. Around the point where the exit NOx amount is just about to cross the maximum limit, set by EPA regulations, the storage capacity must be regenerated so that the NOx can be stored again. To regenerate the depleted storage capacity, the catalyst surface must be exposed to a reducing environment which is generally obtained by switching the engine operation to fuel rich conditions.

However, it has been studied that the reductants may undergo substantial changes before actually involved in the regeneration of nitrates/nitrites (Epling et al., 2004). The water gas shift (WGS) reaction is well-known on precious metals and since the NSR catalyst contains Pt/Rh/Pd as their main constituents, the possibility of WGS reaction over NSR catalyst was studied by several authors. Li et al., observed that with a feed composition of 10% H_2O, 10% CO_2 and 1.2% CO over an industrial NSR catalyst, nearly 1.1% H_2 was produced. In another study by Theis et al. with $Pt/Ba/Al_2O_3$ and $Pt/K/Al_2O_3$ catalysts, the reverse WGS reaction was monitored by adding 10% H_2O to the H_2 feed during sulfation events. The study showed that without H_2O, significant amounts of CO were produced whereas with H_2O, 64% less CO was observed. Since the rich feed generally contains CO_2 and H_2O, reductants can undergo a substantial change and give different results from the one without considering WGS reaction.

The industrial NSR catalyst likely contains ceria due to its wide functionality such as stabilizing the washcoat, improving thermal resistance and increasing the catalytic activity of precious metals. Ceria has a tendency to store oxygen during lean phase, which is represented by oxygen storage capacity (OSC). If OSC is present, during the rich phase, a certain amount of reductant can be consumed in regenerating the oxygen storage capacity (Mahzoul et al., 2001) and the greater the OSC, more is reductant required.

2.4 NOx release and reduction

During the regeneration of storage sites, the stored NOx is first released and then subsequently reduced to N_2. The unconverted NOx, observed as a “puff/peaks” in the exit NOx profile clearly indicates the occurrence of these two reactions in a sequence but with relatively different rates. The overall efficiency of the operation to regenerate the maximum amount of storage sites, while keeping the amount of unconverted NOx to the minimum, is a function of several variables, such as type of reductant, feed composition, catalyst formulation and operating conditions.

The different reductants, such as CO, H_2 and hydrocarbons, have different regeneration and reduction abilities, which are dependent on operating conditions. In studies by Mahzoul et al. and Abdulhamid et al., it was observed that at low temperatures, H_2 is an effective reductant for both NOx reduction and regeneration of storage sites whereas CO remains inactive and with increases in the temperature, the efficiency of CO increases and becomes nearly the same as H_2 at relatively higher temperature. Mahzoul et al. also studied the combined effect of CO and H_2 and observed that adding CO reduced the effects of H_2 at low temperatures, whereas both reductants were equally effective and

showed an additive effect at high temperatures. To explain the reduced activity of CO at low temperature, it was proposed that some of the Pt sites could have been poisoned by CO.

The effect of temperature on the NOx release and reduction mechanism is highly complicated. One set of data (Fridell et al., 1999) reported an increase in the NOx peak with temperature while in other study (Nova et al., 2002), release was reported to decrease. At low temperatures, both NOx release and reduction are totally dependent on the ability of catalyst to activate the reductants. Although the reductant activity is not a limitation at higher temperatures, nitrates/nitrites are relatively less stable (Kabin et al., 2004). Therefore, the rate of nitrate/nitrite self decomposition and resulting NOx release accelerates faster than the rate of NOx reduced. Since propylene was used as a reductant, the theory of reductant activation was ruled out in explaining the results by Fridell et al. and Nova et al. However, the amount of NOx trapped in the lean phase was different in each study and, therefore, can contribute to the self decomposition of nitrates/nitrites in a different way.

The release of NOx was observed even in the absence of reductants (Balcon et al., 1999; Liu and Anderson). One possibility explaining the release was the reduction in the partial pressures of NOx and O_2, which changes the existing equilibrium away from otherwise stable nitrates/nitrites, resulting in their self decomposition. The role of other gases present in the exhaust was also studied by several authors. Amberntsson et al. demonstrated that the presence of CO_2 enhanced NOx release, which became more significant with increasing CO_2 concentrations. Thermodynamic calculations in their study clearly described a correlation between CO_2 amounts and nitrate stabilities. It was also showed that the presence O_2 has a suppressive effect on NOx release. Nearly 75% of the trapped NOx were released with a 5% CO_2/Ar mixture and this amount reduced to nearly 47% when mixture of 10% O_2/ 5% CO_2/ Ar was used. Both NO_2 and NO were observed in the release but NO_2 amounts remained unaffected whereas amounts of NO reduced remarkably in the presence of O_2. It was suggested that the decrease in NO release was due to the formation of Pt-O, which reduces the Pt sites available for the NO oxidation.

2.4.1 Reaction pathways and mechanisms

The release of NOx can be explained by two paths:

- Self decomposition of nitrates/nitrites in the absence of O_2 or increase in the temperature
- Reactions of nitrates/nitrites with reductants

Studies by Lietti et al., Mahzoul et al. and Liu and Anderson have reported that in the absence of O_2 or NOx in the feed or increase in the temperature, equilibrium between storage sites and nitrate/nitrite species shifts toward right and therefore NOx is released. The proposed reactions were:

$$Ba(NO_3)_2 \leftrightarrow BaO + 2NO_2 + O^* \quad \text{... (2.8)}$$

$$Ba(NO_3)_2 \leftrightarrow BaO + 2NO + 3O^* \quad \text{... (2.9)}$$

In the reductant involved mechanism by Liu and Anderson, the reductant molecule (or its activated form spilled over from Pt) interacts directly with the nitrates to form nitrites which then releases NO and O_2 as follows:

$$(NO_3^-)_2 \rightarrow (NO_2^-)_2 \rightarrow {O_2}^- + 1/2O_2 + 2NO \quad \text{... (2.10)}$$

Similar mechanism by Nova et al. was based on the activation of reductants over Pt, followed by their spill-over on the Al_2O_3 support towards the nitrates that will decompose into NOx. The NOx will be then reduced either on Pt sites or directly by spilled over reductant.

The mechanism for the reduction of NO by precious-metal sites, as proposed by James et al., postulates that the reductant reduces the precious-metal site, which then participates in NO decomposition. In another mechanism by Olsson et al., the reductant is activated on precious-metal sites and then reacts directly with NOx.

The straight stoichiometric path for the regeneration of storage sites and reduction of stored NOx to N_2 was also proposed. (Lietti et al., 1999)

$$Ba(NO_2)_2 + 3H_2 \leftrightarrow BaO + N_2 + 3H_2O \quad \text{... (2.11)}$$

$$Ba(NO_2)_2 + 3H_2 \leftrightarrow BaO + N_2 + 3H_2O \quad \text{... (2.12)}$$

$$Ba(NO_3)_2 + 5H_2 \leftrightarrow BaO + N_2 + 5H_2O \quad \text{... (2.13)}$$

2.5 Modeling Studies

Based on experimental studies conducted over a wide range of operating conditions, different mathematical models have been proposed to describe the reaction paths and associated mechanisms present in the NSR process (Olsson et al. 2001, 2002, 2005, 2006; Koci et al., 2004, 2007; Guthenke et al., 2007; Schmeißer et al., 2007; Tuttlies et al., 2004; Kromer et al., 2007; Jirat et al., 1999).

Olsson et al. (2001, 2002) proposed a detailed model in an attempt to describe all possible surface adsorption and desorption reactions occurring on Pt and BaO catalytic sites. Accordingly, they included a large number of reactions that were either producing or consuming different intermediate surface species. In their second study, Olsson et al., (2005, 2006) formulated a global kinetic model of lesser complexity, as compared to their previous study, by neglecting the reactions involving faster formation and consumption of surface intermediates.

The rapid NOx storage occurring during the initial period of lean phase, followed by the slow escape of NOx out of the reactor has been attributed to the mass transport limitation either in the wash-coat or within the barium particles (Kojima et al., 2001; Hepburn et al., 1996, 1998). The proposed global kinetic model of Olsson et al. (2005, 2006) included the mass transfer limitations in the barium particles by modifying the kinetic rate equations for both NO and NO_2 storage reactions. These modifications were done based on three main assumptions:

- The barium particles are spherical in shape
- The barium nitrate layer formed over the carbonate-nitrate interface is of a uniform thickness
- The rate of diffusion throughout the nitrate layer is constant with respect to radial position and is equal to the rate of reaction at the carbonate-nitrate interface.

From the experimental study, Olsson et al. (2005) also observed that only a fraction of the barium particles are used in NOx storage reactions. Therefore, they modified their shrinking core model to include an inactive core in the center of barium particles which is not accessible to the gas. Tuttlies et al. (2004) proposed a 2-D model that accounts for the effect of mass transfer limitation by considering the barium particles to be porous in structure. In this model, the diffusion limitation by both barium carbonate and barium nitrate was considered unlike the model by Olsson et al. (2005), where the diffusion through only barium nitrate was considered. Since the barium nitrate has nearly twice the molar volume of barium carbonate, the diffusion coefficient within the solid phase of the barium particles was considered to decrease with the formation of a relatively dense nitrate layer. This fact was used to explain the unavailability of storage sites beyond a certain coverage limit. The model of Tuttlies et al (2004) was further simplified into a one dimensional model by Schmeißer et al. (2007). In a recent study by Kromer et al. (2008), two different one-dimensional NOx storage models were proposed to account for the mass transfer limitation in the storage process. In one model, two layers of particles were considered and it was proposed that once the NOx is stored on the particles in first layer, they diffuse to the second layer to react again and the overall storage step is controlled by the mass transfer coefficient between these two layers. In the other model of Kromer et al., two parallel

pathways with relatively different rates were suggested to account for the effect of neighboring Pt and BaO particles on NOx storage. The concept of two different wash-coat layers with different catalytic activity was also used by Koci et al. (2004) to explain the different storage capacities at low and high temperatures. However, in this study, it was proposed that the type and loading of precious metals and storage components on one wash-coat layer is different from that of the second wash-coat layer. Accordingly, the activity of both layers is described by two different reaction rates' dependencies with respect to temperature.

Although the proposed models in the literature have explained the various possible NOx storage mechanisms, few studies have focused on the regeneration steps, i.e. the rich phase. During this phase, apart from regeneration of nitrates/nitrites and NOx reduction, reductants are also involved in reactions such as oxidation of reductants, water gas shift reaction and reactions with ceria. The proposed models by Koci et al. (2004, 2007), Guthenke et al. (2007), Tuttlies et al. (2004) and Schmeißer et al. (2007) contains all the possible reactions, where the kinetics of the oxidation reactions were taken from Voltz et al. (1973).

Few attempts have been made to fit the models to the data obtained from cyclic operation. Olsson et al. (2005) modified the reaction kinetics for regeneration/release and reduction reactions to fit the net NOx coming out of the catalyst. However, they tested only one cycle where complete regeneration during the rich phase was obtained. Güthenke et al. (2007) have recently tested their model during steady cyclic operation using the exit NOx concentration data. However, the coverage profiles were not reported in that study and therefore it is unclear what the extent of regeneration in that work was. The proposed models by Koci et al. (2004, 2007) have shown some fitting to exit NOx data during steady cyclic operation but no predictions for the coverage profiles were made.

However, the simulation results in the both Güthenke et al and Koci et al studies predicted the behavior of NOx profile in transient cyclic operation based on an incomplete regeneration of nitrates/nitrites. Tuttlies et al. (2004) predicted the NOx profile in transient cyclic operation and they also reported simulated results for coverage profiles in the barium particles along the catalyst length. However, they did not show any fitting with experimental data. The recent study by Schmeißer et al. 2007 showed the fitting of their model to the transient operation but the study was limited to only the first two cycles. These results show that incomplete regeneration may have occurred during the transient but there is no experimental data for verification. It should be noted that only the studies by Tuttlies et al. and Schmeißer et al. consider the transient operation whereas all the other modeling work reported in this section considered steady periodic operation. Moreover, the barium carbonate/nitrate coverage profiles were also not reported in most of these studies and therefore, there

is no significant information one can extract to adapt these models to explain the transient cyclic data. The amount of reductant used in these studies was between 2-3%, which may be sufficient to regenerate nearly 100% of the barium carbonate in the rich phase of first cycle, therefore resulting in only the steady state operation for which these models have reported the fitting.

Chapter 3
Model Formulation

The industrial catalyst modeled in this work was provided by Cummins. Although the exact formulation of this catalyst cannot be presented for confidentiality reasons, some of its main characteristics will be discussed in this chapter to justify the proposed mathematical model. For example, unlike the catalyst with a standard formulation of $Pt/BaO/Al_2O_3$, this catalyst includes different types of precious metals (Pt/Rd/Pd etc.) with different loadings, different types of storage sites and also contains ceria particles (Al-Harbi & Epling, 2009). This formulation results in an increased operating temperature range and in larger amounts of NOx that can be reduced as compared to a catalyst with the standard formulation. The chemistry of a standard NSR catalyst has been studied extensively by different authors but few studies have focused on the industrial NSR catalyst (Tuttlies et al., 2004; Schmieber et al. 2007; Koci et al., 2007). Moreover, the proposed models in the literature are specific to the catalyst used in each particular study and cannot be adapted for different formulations easily as said in earlier chapters. In the present study, an approach to model an industrial catalyst has been presented that permits to deal with general types of catalysts' formulations by using a variable diffusion function within a shrinking core model. A mathematical model that combines a pseudo-homogeneous 1D model of the mass transfer equations with the aforementioned shrinking core model is presented in the following sections.

3.1 Mechanistic Details of the Catalyst

The catalyst, modeled in the study, has a monolith structure with a circular cross section. It is partitioned into number of square channels, where the channel walls are coated with an alumina based washcoat. The washcoat has an irregular surface area, thus presenting a non-uniform cross section for the gas to flow. The channel can be divided into two sections: a bulk phase where the gas flows along the channel length and a washcoat phase where the gas diffuses and then reacts.

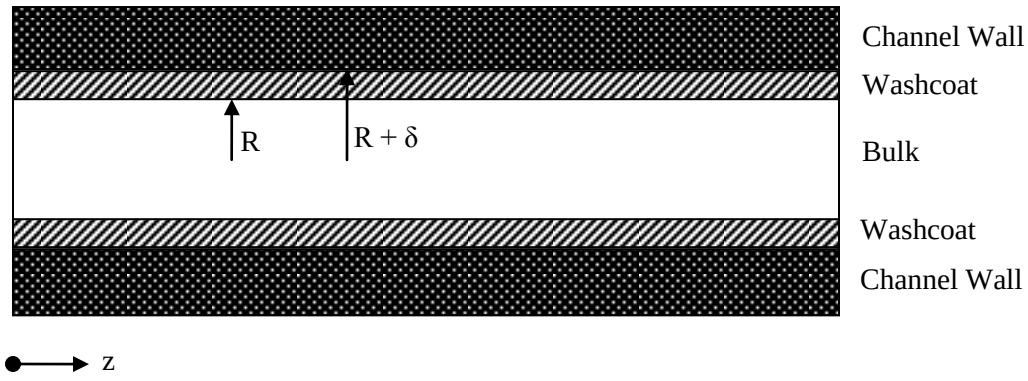

Figure 3-1: A schematic representation of a monolith channel

The reaction products then diffuse back into the bulk phase and flow out along with rest of the gas stream. A schematic representation of the channel is shown in Figure 3-1. For simplicity, the thickness of the washcoat layer was assumed to be uniform with a circular cross-section and is represented by δ. The reactor data to be used were obtained with a catalyst sample that was taken from a larger monolith block with a cell density of 300 cells per square inch (cpsi). The sample had a diameter of 0.912 inch and a total length of about 3 inches (data provided by Meshari and Epling). Based on the sample diameter and cell density, the number of channels was calculated to be 169. The previous models in literature have considered the washcoat thickness to be 20-60 microns. Since there is no uniform boundary between the washcoat and the bulk phase and the catalyst structure is not accurately known, the washcoat thickness was assumed to be 40 microns.

3.2 Assumptions

- Since the gas velocity in the bulk phase and the length-to-diameter ratio of the channel are very high, the radial dependency of the bulk gas concentrations and temperature were assumed to be negligible. On the other hand, the effects of thermal and concentration boundary layers were accounted for in the model using mass and heat transfer coefficients.
- The change in gas temperature during the lean phase was observed to be negligible and therefore, isothermal conditions were assumed in the model. An instantaneous temperature rise was observed during the rich phase but since the rich phase (5 sec) is much shorter than the lean phase (150 sec), the high gas temperature value was assumed constant throughout the rich phase, still maintaining the isothermal assumption.

- The gas velocity was also assumed to be constant throughout the channel because the change in the overall gas volume due to reactions was observed to be very low (1-2%). The effect of temperature rise on the gas velocity was also neglected due to the isothermal assumption listed above.
- Based on the gas velocity, the flow conditions were found to be laminar. Correspondingly, the estimated pressure drop across the channel length was found to be as low as 10^{-4} atm and hence it was neglected.
- Due to the high gas velocity used in the study (~ 2 m/s), the rate of axial convection was assumed to be very high as compared to the rate of axial dispersion and therefore, the latter was neglected.
- The wash-coat thickness used in the model is of the order of microns and therefore it is very low as compared to the volume of the monolith channel. Thus, due to the high aspect ratio (L/D), radial variations in the gas concentrations in the wash-coat were also neglected.
- Since all the reactions are catalytic and the catalyst particles are supported on the washcoat layer, all the reactions were assumed to occur only in the washcoat.

3.3 Mass Balance

Based on the assumptions listed above, a spatial pseudo homogeneous 1-D model was formulated. Since the gas is flowing through all the channels at a uniform rate, only one channel was modeled. The cross sectional area of the channel was considered to be circular as mentioned above. For simplicity, the mixture of $BaCO_3$, $Ba(OH)_2$ and BaO is referred to as $BaCO_3$ and that of $Ba(NO_3)_3$ and $Ba(NO_3)_2$ as $Ba(NO_3)_3$. However, the effect of different forms of barium compounds was lumped into the rate constants. The justification for this assumption will be discussed in a later section. The following subsection summarizes the mass balance equations that model the change in concentrations of gas species and catalytic surfaces in each phase.

3.3.1 Bulk Phase

The gas entering the monolith channel travels along the channel length due to convection and simultaneously diffuses into the washcoat. Since the residence time of the gas in the bulk phase is about 1-2 seconds, the gas was also considered to be accumulating at different axial points along the channel length. Therefore, the change in gas compositions in the bulk phase for i^{th} component, C_{gi} can be modeled by following equation:

$$\frac{\partial C_{gi}}{\partial t} = -v\frac{\partial C_{gi}}{\partial z} + \frac{k_c a}{\varepsilon^g}\left(C_{si} - C_{gi}\right) \quad \text{... (3.1)}$$

where:

v is gas velocity, m/s

k_c is the boundary layer mass transfer coefficient, m/s

ε^g is fraction of bulk phase volume in total volume (bulk + washcoat)

C_{gi} is gas phase concentration of i^{th} species, mol/m^3/sec

C_{si} is washcoat phase concentration of i^{th} species, mol/m^3/sec

3.3.2 Washcoat phase

After diffusing into the washcoat, the gas species react on the surface of the catalytic sites. Although most of the reactions take place on the surface of the catalyst particles, the NOx storage reactions are considered to be occurring at the interface of barium nitrate and barium carbonate within the barium particle. This mechanism is modeled by a shrinking core model that is presented in a later section. The gas species involved in the storage reactions have to diffuse through the barium nitrate layer before reacting at the interface. Accordingly, the change in gas compositions in the washcoat phase, C_{si} can be modeled by an accumulation rate, a rate of mass transferred from the bulk into the washcoat, a rate of diffusion into the barium particles and a consumption or production rate due to the catalytic reactions at the surface as follows:

$$\frac{\partial C_{si}}{\partial t} = \frac{k_c a}{\varepsilon^s * (1-\varepsilon^g)}\left(C_{gi} - C_{si}\right) + D_i\frac{\partial C_{si}}{\partial r} + \frac{1}{\varepsilon^s}\left(\sum_{j=1}^{J} \nu_{i,j}\, {R_j}^s\right) \quad \text{... (3.2)}$$

where,

ε^s is the fraction of washcoat volume in total volume (bulk + washcoat)

D_i is the diffusion of i^{th} species within the nitrate layer, m/sec

r is the radial coordinate within the spherical barium particle, m

R_j^s is the rate of j^{th} reaction at the catalyst surface expressed in terms of active washcoat volume, mol/m^3/sec

Since the storage reactions are assumed to be occurring at the interface, the mass balance through the nitrate layer can be modeled by an accumulation rate and a rate of diffusion through the nitrate layer. The volume of gas trapped within the catalyst particles present in the washcoat is assumed to be very small as compared to the accumulation terms related to the volume of gas in the washcoat and the bulk. Based on this assumption, the accumulation term within the barium particles is considered as negligible and therefore, the mass balance within the particle is given by a mass balance equation and a corresponding boundary condition as follows:

$$0 = D_i \frac{\partial^2 C_{si}}{\partial r^2} \quad \text{... (3.3)}$$

$$with, \qquad \left(D_i \frac{\partial C_{si}}{\partial r}\right)_{r=r_i} = \sum_{j=1}^{J} \nu_{i,j} \, {R_j}^f \quad \text{... (3.4)}$$

where:

R_j^f is the rate of j^{th} reaction at the interface within the barium particles expressed in terms of active washcoat volume, mol/m^3/sec

r_i is the position of the barium nitrate-barium carbonate interface within the spherical barium particle, m

Since the rate of diffusion was constant throughout the nitrate layer and is equal to rate of reaction at the interface, the concentration of gas species at the interface can be related to its washcoat concentration using equation 3.3 and equation 3.4. Therefore, equation 3.2 can be expressed in terms of washcoat concentration as follows:

$$\frac{\partial C_{si}}{\partial t} = \frac{k_c a}{\varepsilon^s * (1 - \varepsilon^g)} \left(C_{gi} - C_{si}\right) + \left(\sum_{j=1}^{J} \nu_{i,j} \, {R_j}^f\right) + \frac{1}{\varepsilon^s}\left(\sum_{j=1}^{J} \nu_{i,j} \, {R_j}^s\right) \quad \text{... (3.5)}$$

In this way, the concentrations in the washcoat and the bulk can be obtained from the solution of algebraic equations 3.3 and 3.4 coupled with the differential equation 3.5.

The reaction rates considered in this study also depend on the fraction of the catalyst utilized in each reaction. The mass balance to calculate the catalyst fraction utilized in a particular reaction, also referred to as the catalyst coverage, is given as follows:

$$\frac{\partial \theta_m}{\partial t} = \frac{1}{{\psi_m}^{cap}} \left(\sum_{j=1}^{J} \nu_{m,j} \, {R_j}^f \right) \quad \text{... (3.6)}$$

where,

θ_m is the catalyst coverage (fraction)

ψ_m^{cap} is the storage capacity of catalyst, mol/m^3

R_j is the rate of jth reaction expressed in the terms of washcoat volume, mol/m^3/sec

3.4 Initial and Boundary conditions

3.4.1 Initial Conditions

At the beginning of cycle, the catalyst was assumed to be fully regenerated, meaning that the ceria as well as the barium particles were present in their original un-reacted form. It was also considered that the catalyst was not exposed to the feed before. Accordingly, the initial conditions for all the species can be written as follows:

$$C_{gi}(z)_{t=0} = 0 \quad \text{... (3.7)}$$

$$C_{si}(z)_{t=0} = 0 \quad \text{... (3.8)}$$

$$\theta_{BaCO_3}(z)_{t=0} = 1 \quad \text{... (3.9)}$$

$$\theta_{Ba(NO_3)_2}(z)_{t=0} = 0 \quad \text{... (3.10)}$$

$$\theta_{Ce_2O_3}(z)_{t=0} = 1 \quad \text{... (3.11)}$$

$$\theta_{CeO_2}(z)_{t=0} = 0 \quad \text{... (3.12)}$$

3.4.2 Boundary Conditions

In principle, since the model is 1-D, boundary conditions at the inlet of channel and the exit of channel are needed. However, since the gas phase concentrations are only dependent on the first order derivative of the concentration with respect to axial position, only the boundary conditions of gas phase concentrations at the inlet are needed. These conditions are specified as follows:

$$C_{gi}(t)_{z=0} = C_{inlet} \quad \text{... (3.13)}$$

3.5 Reaction Kinetics

In the current modeling work, all the reactions that have been reported earlier in the literature in connection with the NSR process were considered. Although few of the reaction kinetics were used in their original reported form, most of them were modified to account for the particular NSR chemistry on the non-standard catalyst modeled in this study.

3.5.1 NO oxidation Reaction

The NO oxidation is considered as a critical step in NOx storage operation. In principle the kinetics of this reaction are complex since it involves different intermediates appearing at the Pt surface. To simplify this reaction, a lumped kinetic model for NO oxidation was proposed by Olsson et al. (2005) that does not include the intermediates' kinetics. In some other studies by Mulla et al. (2007), Guthenke et al. (2007), Schmieber et al. (2007) and Koci et al. (2004, 2007), the NO oxidation kinetics were observed to be strongly inhibited by NO_2. The inhibition effect of reductants was also considered in some models (Koci et al., 2007; Guthenke et al., 2007) but most of the studies on NSR catalyst have neglected the reductants' inhibition effect. In the present model, the experiments were conducted with NO present only in the lean phase during which no reductant was injected. Therefore, only NO_2 inhibition was considered in the model. Accordingly, the reaction and the corresponding rate expression as adapted from Guthenke et al. (2007) after eliminating the CO and C_3H_6 inhibition terms is given as follows:

$$NO + \frac{1}{2}O_2 \overset{r_1}{\leftrightarrow} NO_2 \quad \text{... (3.14)}$$

$$r_1 = k_1 * \left(c_{NO} * c_{O_2}^{0.5} - \frac{c_{NO_2}}{K_1^{eq}}\right) \Big/ \left(1 + K_1 * c_{NO_2}^{0.7}\right) \quad \text{... (3.15)}$$

3.5.2 NOx storage reaction

The NOx storage reactions have been extensively studied in the literature. The negligible amount of NOx at the exit of the catalyst observed during the initial couple of seconds and followed by a slower

increase in NOx is attributed to the decrease in storage capacity of the catalyst. To model the time histories of the NOx exit concentrations, several mechanisms have been proposed:

i. Using diffusion in the barium particles through a growing nitrate layer (Olsson et al., 2005, Tuttlies et al., 2007, Schmieber et al., 2007)

ii. Using reaction rate expressions that depend on a high power of the coverage (Guthenke et al., 2007)

iii. Using a two layers approximation, mentioned in the literature review, with mass transfer limitations between them (Kromer et al., 2008) and

iv. Using two types of barium particles, one close to Pt sites and another away from them, that have different storage capacities (Kromer et al., 2008)

Most of the studies considered the barium particles either in a 100% oxide or a 100% carbonate form at the start of operation and did not account for the substantial changes in barium distribution between the oxide, carbonate and hydroxide forms due to the presence of CO_2 and H_2O. Moreover, only two different storage capacities based on either two different wash coats or two different barium particles were reported. Since the catalyst can have more than two types of storage mechanisms, the adaptation of these models to other catalyst formulations is not straightforward. Therefore, in the present model, a general approach is presented which can be adapted for any kind of catalyst based on calibration to experimental data.

The barium in the catalyst bed may be originally present solely as an oxide. However, when the catalyst is exposed to the lean phase gas compositions, due to the thermodynamic stability of $BaCO_3$ and $Ba(OH)_2$ over BaO, there is a possibility that the barium is converted immediately into $BaCO_3$ and $Ba(OH)_2$ depending on the concentrations of CO_2 and H_2O in the feed. Therefore, in the proposed model, the barium is considered to be present in any of the three forms; carbonate, hydroxide or oxide. Considering that the barium particle is porous in structure, the gas species have to diffuse into the barium particles and therefore due to resistance, the inner core of the barium particle may remain as oxide during the operation whereas the shell around this core can be either in carbonate, hydroxide or a combination of both forms. This will result in a varying storage capacity within the barium particle.

In the experimental studies reported in literature, it has also been observed that the proximity of Pt to Ba particles affects the overall storage capacity because the barium particles close to Pt can store NOx very easily as compared to the particles away from Pt (Kromer et al., 2008). Moreover, it has been also observed that the presence of multiple types of washcoat layers can affect the activity of

barium particles (Koci et al., 2004; Kromer et al., 2008). Since the catalyst under study, have different types of storage sites, this fact will contribute to a complex kinetic behavior. Therefore, to capture this complexity while maintaining the ease of application of the model to any catalytic system, a shrinking core approach model is used as described in the following subsection.

3.5.2.1 Shrinking core model

To account for the multiple types of barium particles with different levels of proximity to the Pt particles, an "artificial" barium particle is assumed, which is spherical in shape. The outer layer of this particle up to a certain depth will represent the type of barium particle that can store the NOx immediately. The next inner layer up to certain thickness will represent some other type of barium particle which will have relatively lower activity than the particles in the upper layer but higher activity than the particles in subsequent inner layers. To describe this multilayered arrangement an equivalent diffusion coefficient is used such as the diffusion values decrease with respect to depth. This equivalent diffusion coefficient is formulated as a nonlinear function of particle depth and this function will depend on the catalyst being used. To simplify the model and reduce the number of unknown parameters, the reaction of only $BaCO_3$ was considered but in reality it represents the mixture of BaO, $BaCO_3$ and $Ba(OH)_2$. The NO and NO_2 storage reactions reported in the literature were adapted as below:

$$2NO_2 + \frac{1}{2}O_2 + BaCO_3 \xrightarrow{r_2} Ba(NO_3)_2 + CO_2 \quad \text{... (3.16)}$$

$$2NO + \frac{3}{2}O_2 + BaCO_3 \xrightarrow{r_3} Ba(NO_3)_2 + CO_2 \quad \text{... (3.17)}$$

The rate expressions for these reactions were modified to account for the shrinking core model and the derivation is given in the following subsection.

3.5.2.2 Derivation of the Shrinking core model

For simplicity, the barium particle is considered to be spherical in shape with the total radius, given by r_{tot}. For the fresh catalyst, the NOx species will react on the surface of this particle. As the reaction proceeds, the barium carbonate is consumed and therefore the radius of the carbonate core decreases. The pictorial representation of the barium particle at any time t is shown in Figure 3.2.

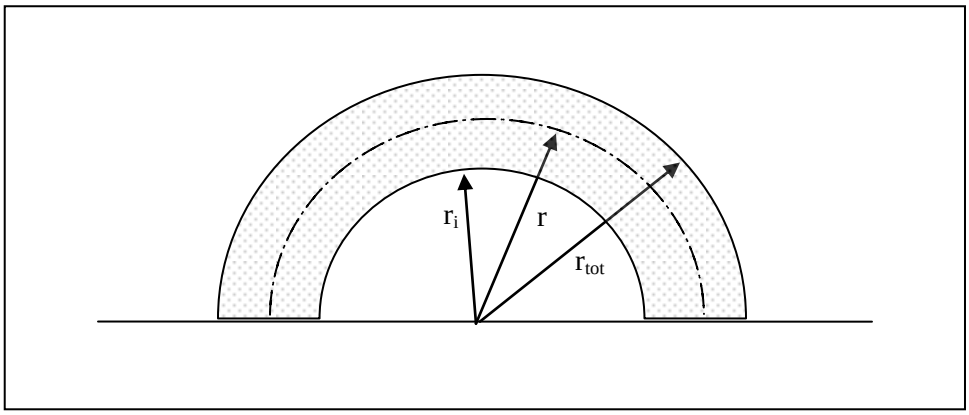

Figure 3-2: Representation of the barium particle in shrinking core model

The radius of the inner carbonate core is given by r_i and r represents the radial position within the barium particle. During the storage process, the NOx has to diffuse through the nitrate layer, being continuously formed around the carbonate core. There is no reaction within the nitrate layer and therefore the mass balance across this nitrate layer rate is given by:

$$D_{NO_x} * \frac{d^2 c_{NO_x}}{dr^2} = 0 \quad \text{... (3.18)}$$

After integration above equation reduces to,

$$D_{NO_x} * \frac{dc}{dr} = R_{diff} \quad \text{... (3.19)}$$

where, R_{diff} is the rate of diffusion in the nitrate per unit surface area.

This rate is assumed to be constant by Olsson et al. (2005) but in this study, it is considered to be decreasing with the consumption of carbonate. The reason behind varying diffusivity has been explained in the previous subsection. However, its justification will be given in the next chapter on results and discussion.

Integrating equation 3.21, assuming the rate of diffusion to be constant, will give the algebraic expression relating the NOx concentration at the carbonate-nitrate interface to the NOx concentration at the particle surface.

$$R_{diff'} = \frac{4 * \pi * D_{NO_x}}{r_{tot} - r_i} * \left(c_{NOx}^{r=r_{tot}} - c_{NOx}^{r=r_i}\right) * r_i * r_{tot} \quad \text{... (3.20)}$$

where, $R_{diff'} = R_{diff} * 4 * \pi * r_i^2$

Since oxygen is present in the excess as compared to NOx, the rate of reaction per barium particle at the interface is given by:

$$r = k * \theta_{BaCO_3} * c_{NOx}^{r=r_i} \quad \text{... (3.21)}$$

At the interface, the rate of diffusion is equal to the rate of reaction and therefore, is given by:

$$k * \theta_{BaCO_3} * c_{NOx}^{r=r_i} = \frac{4 * \pi * D_{NO_x}}{r_{tot} - r_i} * \left(c_{NOx}^{r=r_{tot}} - c_{NOx}^{r=r_i}\right) * r_i * r_{tot} \quad \text{... (3.22)}$$

After rearranging the above equation, the NOx concentration at the interface can be written as:

$$c_{NOx}^{r=r_i} = \frac{c_{NOx}^{r=r_{tot}}}{1 + \frac{k * \theta_{BaCO_3} * (r_{tot} - r_i)}{4 * \pi * D_{NO_x} * r_i * r_{tot}}} \quad \text{... (3.23)}$$

Putting this expression into equation 3.23, the rate expression can be expressed in term of NOx concentration at the particle surface. The revised rate expression is given as:

$$r = k * \theta_{BaCO_3} * \frac{c_{NOx}^{r=r_{tot}}}{1 + \frac{k * \theta_{BaCO_3} * (r_{tot} - r_i)}{4 * \pi * D_{NO_x} * r_i * r_{tot}}} \quad \text{... (3.24)}$$

Although the rate expression was assumed to be independent of oxygen concentration, it was decided to include the oxygen dependency in the final rate expression.

Since the exact structure of the catalyst in unknown, the varying rate of diffusion cannot be expressed explicitly. Therefore, the above derivation was adapted from Olsson et al. (2005), where the constant rate of diffusion was assumed to derive the rate expression, and the varying diffusion function is then incorporated in the model by a nonlinear expression for the diffusion as follows:

$$D_{eff} = A * \frac{exp\left(-B * \left(1 - \frac{r_1}{r_{tot}} - C\right)\right)}{1 + exp\left(-B * \left(1 - \frac{r_1}{r_{tot}} - C\right)\right)} \quad \text{... (3.25)}$$

where A, B and C are the parameters to be estimated from the experimental data.

The final rate expression for NO and NO_2 storage reactions will be given by:

$$r_2 = \psi_{NOx} * \frac{k_2}{1 + k_2 \frac{r_{tot} - r_i}{D_{eff_{NO_2}}} \frac{r_i}{r_{tot}} \theta_{BaCO_3}} * c_{NO_2} * \theta_{BaCO_3} * c_{O_2}^{0.25} \quad \text{... (3.26)}$$

$$r_3 = \psi_{NOx} * \frac{k_3}{1 + k_3 \frac{r_{tot} - r_i}{D_{eff_{NO}}} \frac{r_i}{r_{tot}} \theta_{BaCO_3}} * c_{NO} * \theta_{BaCO_3} * c_{O_2}^{0.75} \quad \text{... (3.27)}$$

In some studies, these reactions have been reported as reversible reactions. However, in the current work, the reversibility is accounted for by using the self decomposition of barium nitrates as discussed in detail in a later subsection.

3.5.3 Ceria Reactions

The catalyst modeled in the current study also contains the ceria. The amount of ceria present on the catalyst determines its capacity to trap oxygen and this capacity is generally referred to as the oxygen storage capacity (OSC). Moreover, the ceria has an important role during the rich phase because it has been experimentally observed that the amount of ceria particles that are regenerated is nearly the same as the amount of regenerated barium particles. Therefore, the reaction of ceria with reductants can significantly affect the extent of regeneration of NOx storage sites. The ceria reactions have been studied extensively for the 3-way catalytic converters. Assuming that there are no physical interactions of ceria particles with barium particles, the same reactions used for 3-way catalytic converters can be used for the NSR system. These reactions and their rate expressions are as follows:

$$Ce_2O_3 + \frac{1}{2}O_2 \xrightarrow{r_4} 2CeO_2 \quad \text{... (3.28)}$$

$$CO + 2CeO_2 \xrightarrow{r_5} CO_2 + Ce_2O_3 \quad \text{... (3.29)}$$

$$H_2 + 2CeO_2 \xrightarrow{r_6} H_2O + Ce_2O_3 \quad \text{... (3.30)}$$

$$r_4 = k_4\, \psi_{O_2} C_{O_2} \left(1 - \theta_{CeO_2}\right) \quad \text{... (3.31)}$$

$$r_5 = k_5\, \psi_{O_2} C_{CO}\, \theta_{CeO_2} \quad \text{... (3.32)}$$

$$r_6 = k_6\, \psi_{O_2} C_{H_2}\, \theta_{CeO_2} \quad \text{... (3.33)}$$

3.5.4 Oxidation Reactions of Reductants

When the reactor feed is switched from the lean to rich phase, instead of the expected sudden change in the gas concentrations, it was observed that there is a period during which the concentration of reductants is increasing whereas the oxygen concentration is decreasing. This behaviour is believed to be associated to the time constant of the valve effecting the switching operation. Moreover, it is also expected that it will take some time for the oxygen present in a reactor from the last lean phase to deplete and its rate of decrease may depend upon the rate of gas convection. Therefore, although the gas compositions used in experiments contain no oxygen during rich phase, certain amount of oxygen will be present for some period of time and consequently the oxidation reactions of reductants will have to be considered.

The only reductant used in the feed during the rich phase was CO but since in the presence of CO_2 and H_2O the CO can undergo a water gas shift reaction and produce H_2, the following oxidation reactions were included in the study:

$$CO + \frac{1}{2} O_2 \xrightarrow{r_7} CO_2 \quad \text{... (3.34)}$$

$$H_2 + \frac{1}{2} O_2 \xrightarrow{r_8} H_2O \quad \text{... (3.35)}$$

The rate expressions given by Voltz et al. (1973) for these reactions have been adapted for NSR systems by several authors (Koci et al., 2004, 2007; Jirat et al., 1999; Guthenke et al., 2007). Since propylene was not used in the experiments for this study, the inhibition term corresponding to the propylene effect was removed and consequently the reduced rate expressions used in the model are given as follows:

$$r_7 = k_7 \frac{C_{CO} C_{O_2}}{(1 + K_7 C_{CO})^2 (1 + K_1 C_{NO}^{0.7})} \quad \text{... (3.36)}$$

$$r_8 = k_8 \frac{C_{H_2} C_{O_2}}{(1 + K_8 C_{CO})^2 (1 + K_1 C_{NO}^{0.7})} \quad \text{... (3.37)}$$

3.5.5 Water Gas Shift (WGS) Reaction

It has been observed that the type and amount of reductants have a significant effect on the NOx release/reduction reactions, thereby affecting the overall NSR efficiency. Since the reductants can undergo substantial changes via WGS reaction before being actually involved in the release/reduction reactions (Li et al., 2001; Theis et al., 2001), a model that ignores WGS reaction may not be able to explain the rich phase dynamics.

Since the rich feed in this study also contains CO_2 and H_2O in addition to CO, the water gas shift reaction was considered in the model to account for H_2 production. The rate expression based on stoichiometry was used to describe this reaction as follows

$$H_2O + CO \overset{r_9}{\leftrightarrow} H_2 + CO_2 \quad \text{... (3.38)}$$

$$r_9 = k_9 \left(C_{CO} C_{H_2O} - \frac{C_{CO_2} C_{H_2}}{K_9^{eq}} \right) \quad \text{... (3.39)}$$

3.5.6 NOx Release/Reduction Reactions

The following two additional mechanisms were considered in the model to explain the NOx release:

- Self decomposition of nitrates/nitrites
- Regeneration of nitrates/nitrites by reductants.

It has been experimentally observed that when the oxygen and NOx concentrations were dropped to zero during the rich phase, the barium nitrates/nitrites formed during the lean phase decomposed into the carbonate, oxide or hydroxide forms of barium resulting in the release of NOx. Therefore, NO and NO_2 storage reactions were reported as reversible reactions in the literature and whenever the equilibrium shifts towards NOx and O_2, these reactions will contribute to the release of NO and NO_2 respectively.

It is not exactly known whether nitrates decompose into carbonates, oxides or hydroxides because there is a strong equilibrium between these three forms of barium due to the presence of CO_2 and H_2O

in sufficiently higher amounts, as discussed earlier. Even if barium decomposes into the oxide form first, due to the thermodynamic equilibrium between these three forms of barium, oxide will convert immediately into the carbonate and the hydroxide considering that both reactions are fast enough.

The previous studies have also considered the reactions involving only carbonates. However, if it is assumed that the barium nitrate is decomposing only into the carbonate form and if the following equilibrium reaction is used during the rich phase:

$$2NO + \frac{3}{3}O_2 + BaCO_3 \leftrightarrow Ba(NO_3)_2 + CO_2 \quad \text{... (3.40)}$$

Based on the thermodynamics calculation for above equilibrium reaction and forward rate constant obtained from the fitting of the experimental data, the amounts of NOx being released are too high as compared to the experimental observations. Additional details are provided in the next chapter. Therefore, it was concluded that the barium nitrate can decompose into both carbonate and hydroxide form and since the catalyst composition is unknown, the ratio of carbonates and hydroxides cannot be explicitly calculated. This also supports the conclusion derived in an earlier subsection on NOx storage reactions that barium always is present as BaO, $BaCO_3$ and $Ba(OH)_2$ in different proportions. However, to simplify the model, $BaCO_3$ was again used to represent the mixture of BaO, $BaCO_3$ and $Ba(OH)_2$ in the rich phase as done for the storage reactions. The proposed reactions used in the model are as follows:

$$Ba(NO_3)_2 + CO_2 \xrightarrow{r_{10}} 2NO + \frac{3}{2}O_2 + BaCO_3 \quad \text{... (3.41)}$$

$$Ba(NO_3)_2 + CO_2 \xrightarrow{r_{11}} 2\,NO_2 + \frac{1}{2}O_2 + BaCO_3 \quad \text{... (3.42)}$$

From experiments at 300^{o}C with no reductants in the rich phase, it was observed that the amounts of NOx being released are not same during the rich phase of every cycle. Several reasons can explain this behaviour such as the occurrence of self decomposition reactions mentioned above. However, when these reactions were included in the model, it was observed that the rate expressions based on simple reaction stoichiometry were not able to explain the amounts of NOx being observed. Instead, the rate of decomposition was found to be increasing in an exponential way as the amount of nitrate increases, and therefore a sigmoid was used to represent the observed nonlinear behaviour because of its flexibility in calibrating the model. Thus, the modified rate expressions used in the model are as follows:

$$r_{10} = k_{10} * \psi_{NOx} * \frac{1}{\left(1 + \exp\left(-X_1 * \left(\theta_{Ba(NO_3)_2} - Y_1\right)\right)\right)} \quad \text{... (3.43)}$$

$$r_{11} = k_{11} * \psi_{NOx} * \frac{1}{\left(1 + \exp\left(-X_2 * \left(\theta_{Ba(NO_3)_2} - Y_2\right)\right)\right)} \quad \text{... (3.44)}$$

The second reaction mechanism contributing to the release of NOx is the reaction of nitrates/nitrites with reductants. Since the CO can form H_2 via the WGS reaction, the reactions of barium nitrate with both CO and H_2 were considered. A similar approach, as explained in above sections, was used to represent the mixture of carbonate, oxide and hydroxide forms of barium. The reactions and the corresponding rate expressions used in the study are given as follows:

$$3CO + Ba(NO_3)_2 \xrightarrow{r_{12}} BaCO_3 + 2NO + 2CO_2 \quad \text{... (3.45)}$$

$$3H_2 + Ba(NO_3)_2 \xrightarrow{r_{13}} BaCO_3 + 2NO + 2H_2O \quad \text{... (3.46)}$$

$$r_{12} = k_{12} * \psi_{NOx} * C_{CO} * \theta_{Ba(NO_3)_2} \quad \text{... (3.47)}$$

$$r_{13} = k_{13} * \psi_{NOx} * C_{H_2} * \theta_{Ba(NO_3)_2} \quad \text{... (3.48)}$$

The NO reduction reactions and the corresponding rate expressions based on the reactant stoichiometry were used in the study and are as follows:

$$CO + NO \xrightarrow{r_{14}} CO_2 + \frac{1}{2}N_2 \quad \text{... (3.49)}$$

$$H_2 + NO \xrightarrow{r_{15}} H_2O + \frac{1}{2}N_2 \quad \text{... (3.50)}$$

$$r_{14} = k_{14} * C_{CO} * C_{NO} \quad \text{... (3.51)}$$

$$r_{15} = k_{15} * C_{H_2} * C_{NO} \quad \text{... (3.52)}$$

All the reactions along with their rate expressions have been listed in the Appendix A.

3.6 Feed Composition

The experimental results used in this modeling work for the calibration of the mathematical model were conducted by Al-Harbi and Epling (Al-Harbi Thesis, 2008; Al-Harbi and Epling, 2009). The

feed compositions used in their experimental study were based on either the typical values used in previous experimental studies or the exhaust data reported in real-time engine operation. The gas flow-rate was maintained at 14.32 L/min for all the experiments and the feed compositions' values are summarized in Table 3-1.

3.7 Solution Method

The COMSOL Multiphysics and MATLAB software were used for the model development in this work. A finite element methodology within the COMSOL package was used to solve the system of partial and ordinary differential equations of the proposed model. The general form of PDE available in COMSOL was used as per the following equation:

$$e_a \frac{\partial^2 u}{\partial t^2} + d_a \frac{\partial u}{\partial t} + \nabla . \Gamma = F \quad \text{... (3.53)}$$

With the general form of boundary conditions, represented either as:

Neumann boundary condition: $-n.\Gamma = G$ or

Dirichlet boundary condition: $-n.\Gamma = G + (\partial R/\partial u)^T \mu \; ; R = 0$

These standard equations were then customized to formulate the bulk and wash-coat mass balances as summarized in Table 3-2.

Gas Species	Lean Phase Compositions	Rich Phase Compositions
NO	330 ppm	0 ppm
O_2	10%	0%
CO_2	5%	5%
H_2O	5%	5%
CO	0%	1.5% or 3%
N_2	80%	89.5% or 87%

Table 3-1: Feed compositions during lean and rich phase

Parameters of general PDE	Bulk Phase	Washcoat Phase	
	Gas Species	Gas Species	Surface Species
u	C_{gi}	C_{si}	θ_m
e_a	0	0	0
d_a	1	1	1
Γ	0	0	0
F	$-v\frac{\partial C_{gi}}{\partial z}+\frac{k_c a}{\varepsilon^g}(C_{si}-C_{gi})$	$\frac{k_c a}{\varepsilon^s * (1-\varepsilon^g)}(C_{gi}-C_{si})+\left(\sum_{j=1}^{J}\nu_{i,j}\ {R_j}^f\right)+\frac{1}{\varepsilon^s}\left(\sum_{j=1}^{J}\nu_{i,j}\ {R_j}^s\right)$	$\frac{1}{{\psi_m}^{cap}}\left(\sum_{j=1}^{J}\nu_{m,j}\ R_j\right)$
$G_{z=0}$	0	0	0
$G_{z=L}$	0	0	0
$R_{z=0}$	$C_{gi}(t)_{z=0}=C_{inlet}$	0	0
$R_{z=L}$	0	0	0

Table 3-2: Representation of Mass Balance equations along with boundary conditions in general PDE form

Chapter 4
Results and Discussion

The proposed model for the NSR cyclic operation consists of a total of 15 reactions as summarized in Appendix A. Since in the experimental study by Meshari, the gas composition of the feed contains no reductants during the lean phase, all the reductant based reactions have no role during the lean phase. Therefore, the kinetics of storage reactions can be estimated independently by solving the model only for the lean phase. Following these arguments, this chapter summarizing the model results and discussion is divided into two sections: a first section where the kinetics of NOx storage reactions will be estimated based on the model with no reductant based reactions and a second section where the kinetics of the reductant based reactions will be estimated to fit the NOx profiles at the catalyst exit obtained during the cyclic operation.

4.1 Lean Phase Kinetics

The preliminary independent study for predicting the system dynamics during the lean phase includes the following reactions:

$$NO + \frac{1}{2}O_2 \overset{r_1}{\leftrightarrow} NO_2 \quad \text{... (4.1)}$$

$$2NO_2 + \frac{1}{2}O_2 + BaCO_3 \overset{r_2}{\leftrightarrow} Ba(NO_3)_2 + CO_2 \quad \text{... (4.2)}$$

$$2NO + \frac{3}{2}O_2 + BaCO_3 \overset{r_3}{\leftrightarrow} Ba(NO_3)_2 + CO_2 \quad \text{... (4.3)}$$

$$Ce_2O_3 + \frac{1}{2}O_2 \overset{r_4}{\rightarrow} 2CeO_2 \quad \text{... (4.4)}$$

The ceria reaction given by equation 1.4 has been extensively studied for the 3-way catalytic convertors and since, has been used in the NSR modeling studies without any modifications, the kinetics reported in the literature were used in the current model as an initial estimate. Although, the NO and NO_2 storage reactions have been considered in the literature as reversible reactions, it was observed in the current study that the kinetics of the forward and backward reactions do not reconcile with the expected thermodynamic equilibrium between the barium carbonate and the barium nitrate. Additional explanations regarding this thermodynamic equilibrium are presented later in this chapter. To study the reversibility of the storage reactions in detail, experimental data was used where the

catalyst was exposed for a certain fixed duration (150 seconds) to feed gas with a composition typically used during the lean-phase and then, for a very short period of time (5 seconds), the percentage of NO and O_2 in the feed was dropped to zero so that the extent of reactions given by equations 1.2 and 1.3 in the backward direction can be estimated. This operation was repeated until the saturation limit of the catalyst for storing NOx was reached. The data for NOx profile at the catalyst exit, measured during these experiments, is shown in Figure 4-1.

4.1.1 NO oxidation

As discussed in an earlier chapters the kinetics of NO oxidation reaction is considered as a key step in the storage process. Therefore, before estimating the kinetics of NOx storage reactions, the kinetics of NO oxidation reaction has to be estimated first.

In the case of multiple reactions equilibria, the steady state concentrations of the components participating in these reactions will be governed by an overall equilibrium constant. Instead, for preliminary estimation, it was proposed that after the catalyst reaches its saturation limit to store NOx, the concentrations of NO and NO_2 in the exit stream will be governed by only the equilibrium related to the NO oxidation reaction. Accordingly, the kinetic parameters of NO oxidation, as given by reaction 1.1, were obtained based on the percentage conversion of NO which was calculated from the steady state concentrations of NO and NO_2 in the experimental data shown in Figure 4-1.

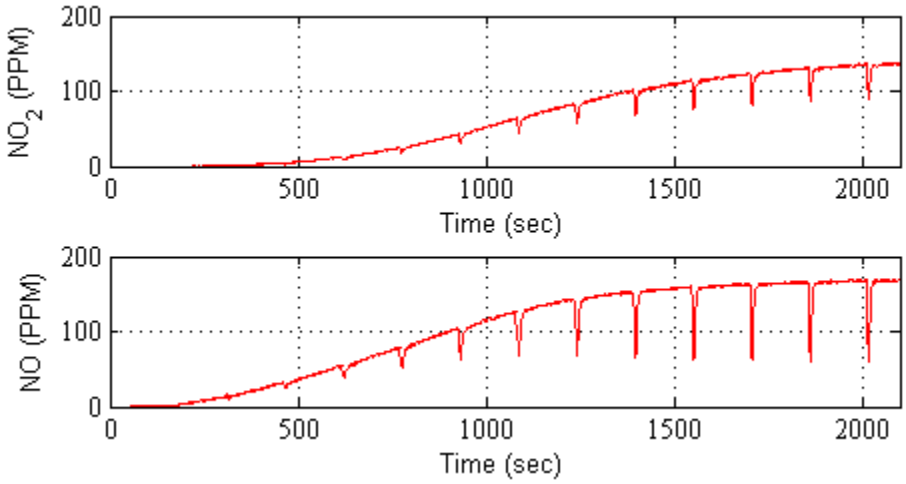

Figure 4-1: The NOx profile at the catalyst exit during a start-up cyclic experiment

After assuming the values of pre-exponential factor and activation energy reported by Olsson et al. (2005) as an initial guess, the pre-exponential factor was further tuned to match the percentage conversion predicted by the model with that observed from the experiment. Estimation of the rate constant is dependent on the mass transfer coefficient between the bulk and washcoat concentrations and therefore will have to be modified accordingly if the value of mass transfer coefficient has to be changed.

4.1.2 NO_2 and NO storage kinetics

The storage model proposed by Olsson et al. (2005) was used for obtaining initial estimates of the kinetic parameters involved in the NOx storage reactions. As seen in Figure 4-1, the NO and NO_2 are being completely stored for a certain initial time period, nearly 200 seconds for NO and 400 seconds for NO_2 . Based on this experimental observation it was concluded that a minimum value of the mass transfer coefficient is required to fit the simulated and experimental NOx profiles during the time period where full storage occurred. In general there are expected to be many different combinations of mass transfer coefficient values and kinetic reaction parameters that could result in acceptable agreement between the experiments and the simulations. In this particular study, two different mass transfer values were considered. For each one of these mass transfer coefficient values, the NO oxidation kinetics were estimated as per the procedure outline in the previous section and then, starting with the initial values given by Olsson et al. (2005), the rate constants for both NO and NO_2 storage reactions were gradually increased for each simulation run until a good fitting between the simulated and experimental NOx profiles for the initial 400 seconds Figure 4-1 was observed. The assumed model parameters for the last three simulation runs are listed in the Table 4-1. The simulation results with a mass transfer coefficient of 0.015 m/s and 0.05 m/s are shown in Figure 4-2 and Figure 4-3 respectively. It can be seen from the figures that with the mass transfer coefficient of 0.015 m/s, the rate constants used in Simulation Run 2 give better convergence than those used in Simulation Run 1 and afterwards there is no further improvement in the convergence. However, with the mass transfer coefficient of 0.15 m/s, even the rate constants used in Simulation Run 1 result in good agreement between experiments and simulations.

Number of Runs	Rate constants for NOx storage reactions	
	NO storage	NO_2 storage
Run 1	$1 * 10^2 * \exp(-\frac{20000}{8.314 * 573})$	$20 * 10^7 * \exp(-\frac{80000}{8.314 * 573})$
Run 2	$5 * 10^2 * \exp(-\frac{20000}{8.314 * 573})$	$20 * 10^7 * \exp(-\frac{80000}{8.314 * 573})$
Run 3	$10 * 10^2 * \exp(-\frac{20000}{8.314 * 573})$	$20 * 10^7 * \exp(-\frac{80000}{8.314 * 573})$

Table 4-1: The rate constants for the NO and NO_2 storage reactions used for studying the effect of mass transfer coefficient

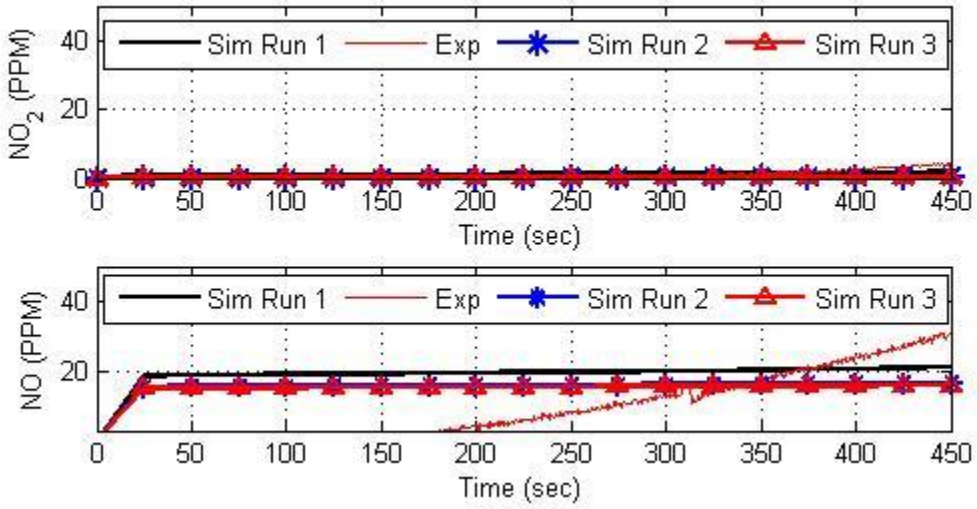

Figure 4-2: The comparison of simulated and experimental NOx profiles with the mass transfer coefficient of 0.015 m/s

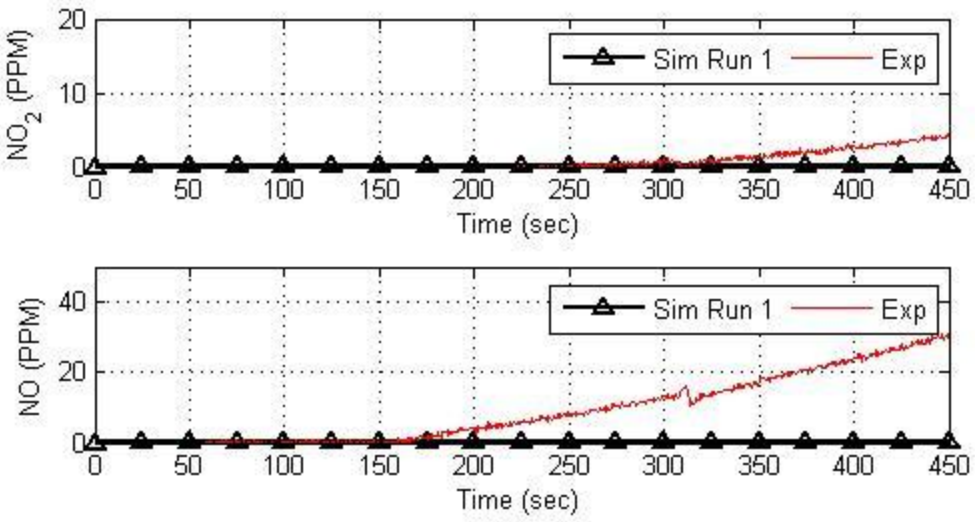

Figure 4-3: The comparison of simulated and experimental NOx profiles with the mass transfer coefficient of 0.05 m/s

Therefore, it was concluded that the mass transfer coefficient had to be higher than 0.015 m/s for the catalyst under study but the exact value was yet to be determined with additional experimental data. For the next few simulations, the mass transfer value of 0.05 m/s was used as an initial estimate.

After estimating a lower bound for the mass transfer coefficient necessary to reconcile the first part of the data in Figure 4-1, the model was simulated in a cyclic manner according to the experimental scenario in Figure 4-1. The rate constants used in these cyclic operation simulations are listed in Table 4-2. As a first attempt, the NOx storage reactions were considered to be reversible where the forward rate constants were used as listed in Table 4-2 and the backward rate constants were obtained from thermodynamic equilibrium calculations as reported by Olsson et al. (2005). Somewhat acceptable fitting was observed during the lean phase but the model predicted very high NO_2 concentration values during the rich phase, as shown in Figure 4-4. In a second set of simulations, for which the NOx storage reactions were considered to be irreversible, the simulated concentrations were observed to be very low as compared to the experimental data as shown in Figure 4-5.

Reactions	Rate Constants
NO oxidation	$2.42 * 10^6 * \exp(-\frac{40000}{8.314 * 573})$
NO storage	$1 * 10^2 * \exp(-\frac{20000}{8.314 * 573})$
NO_2 storage	$20 * 10^7 * \exp(-\frac{80000}{8.314 * 573})$

Table 4-2: The initial values for rate constants used in the model to fit cyclic experimental data with no reductants.

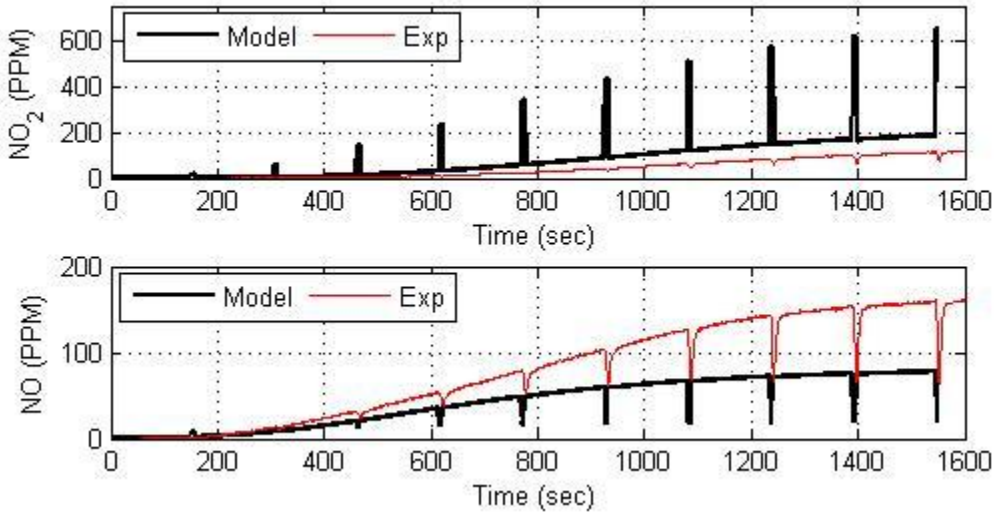

Figure 4-4: The simulated and experimental NOx profiles with the reversible NOx storage reactions as proposed by Olsson et al. (2005).

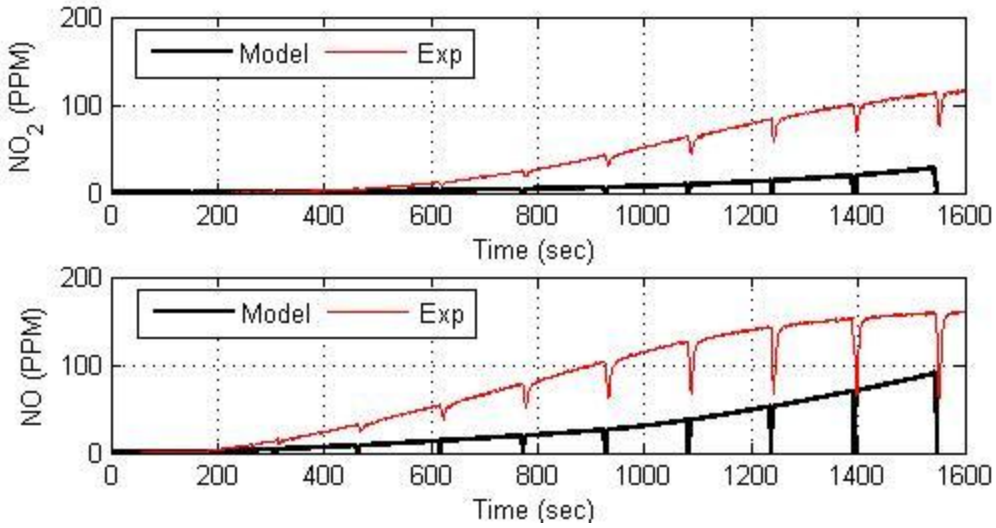

Figure 4-5: The simulated and experimental NOx profiles with the irreversible NOx storage reactions.

From these two comparative studies, it was concluded that although the NOx storage reactions are expected to be reversible, the equilibrium constant, as reported by Olsson et al. 2005, is not correct for the catalyst under study. Also, since the study by Olsson et al. (2005) considered the thermodynamic equilibrium between barium carbonate and barium nitrate, the above simulation results indicate that the barium is not present only in these two forms. Due to the presence of CO_2 and H_2O in the feed, there is a strong possibility that the barium can be converted into both carbonate and hydroxide forms during the initial few seconds of the lean phase as discussed in earlier chapters. The co-existence of barium carbonate and barium hydroxide can result in a modified equilibrium between storage sites and barium nitrates, and this could explain that the equilibrium constant can be lower than the one reported by Olsson et al. (2005).

To account for the presence of both barium carbonate and barium hydroxide within the catalyst while maintaining a small number of equations for describing the storage process, the mixture of $BaCO_3$ and $Ba(OH)_2$ was lumped together into one $BaCO_3$ concentration term. Therefore, the reactions given by equations 4.2 and 4.3 are now assumed to represent the balances for the combined concentrations of $BaCO_3$ and $Ba(OH)_2$. Owing to this lumping of the concentration of two species into one single term and the uncertainty associated with the different forms in which barium particles can be present, the forward and the backward reactions were written separately and their corresponding kinetics were estimated by fitting the simulated NOx profiles with the experimental

data given by Figure 4-1. The resulted reactions separated into their forward and backward directions are listed below:

$$2NO_2 + \frac{1}{2}O_2 + BaCO_3 \xrightarrow{r_{2f}} Ba(NO_3)_2 + CO_2 \quad \text{... (4.5)}$$

$$Ba(NO_3)_2 + CO_2 \xrightarrow{r_{2b}} 2NO_2 + \frac{1}{2}O_2 + BaCO_3 \quad \text{... (4.6)}$$

$$2NO + \frac{3}{2}O_2 + BaCO_3 \xrightarrow{r_{3f}} Ba(NO_3)_2 + CO_2 \quad \text{... (4.7)}$$

$$Ba(NO_3)_2 + CO_2 \xrightarrow{r_{3b}} 2NO + \frac{3}{2}O_2 + BaCO_3 \quad \text{... (4.8)}$$

Additional modifications made in the model to match the experimental data are as follows:

1. Since it was concluded from the results shown in Figure 4-4 and Figure 4-5 that the equilibrium constant for the reversible NOx storage reactions has to be less than the value reported by Olsson et al. (2005), another option to match the experimental data and the simulations could be that the backward reactions would proceed with lower reaction rates. However, it was found that even assuming lower rates for the backward reactions were not sufficient for matching the simulated and experimental NOx profiles in the lean phase. Therefore, it was proposed that there needs to be another resistance to the storage process which is progressively increasing as the storage process proceeds. Olsson et al. (2005) had previously proposed the possibility of diffusion limitation within the barium particle. The simulated results in the Figure 4-4 and Figure 4-5 included the proposed diffusion limitation but the assumption of such limitation was also found insufficient to account for the aforementioned increasing resistance to storage Therefore, it was hypothesized that this increasing resistance may be attributed to either Ba/Pt proximity effect or the presence of different storage sites. As discussed in the previous chapters, both of these mechanisms can explain the differences in storage reaction rates for different barium particles which are necessary for matching the model to the experimental results. To account for these mechanisms an imaginary spherical barium particle was, therefore, proposed where the outer layer represents the particles that can store the NOx rapidly whereas in subsequent deeper layers the difficulty to store NOx is progressively increasing. The detailed description of such particles has been provided in the last chapter. It should be noted that the particle used in this description does not represent an actual physical description of a barium particle within the

problem but it is rather used as a mathematical abstraction to describe the mechanism of resistance to storage due to the proximity of a barium site to a Pt site. The use of this imaginary particle led to the formulation of a shrinking core similar to the one proposed by Olsson et al. (2005) but with the difference that the spherical core used in the current study represents the multiple types of barium particles and the varying diffusion coefficient is used to represent the progressively decreasing reactions rates as the barium particles in the outer layer gets consumed and deeper layers have to be used. In order to provide for flexibility to shape any kind of diffusion barrier, a sigmoid was used to express the diffusion coefficient as a function of the radius representing the barium carbonate-nitrate interface at any given moment. Accordingly, the diffusion coefficient expression used in the model is as follows:

$$D_{eff} = A * \frac{exp\left(-B * \left(1 - \frac{r_1}{r_{tot}} - C\right)\right)}{1 + exp\left(-B * \left(1 - \frac{r_1}{r_{tot}} - C\right)\right)} \quad \text{... (4.9)}$$

where, A, B and C are the parameters describing the nonlinear sigmoid function

2. To estimate the kinetics for the backward reactions given by equations 4.6 and 4.8, the rate expression based on the reactant stoichiometry was used as an initial estimate. However, from Figure 4-1, it can be seen that the amount of NO_2 and NO during the rich phase is continuously increasing in a nonlinear manner. Since the CO_2 is present in excess as compared to other reactants, the rate expression was considered to be a function of only barium nitrate fraction and consequently, the nonlinearity in the rate expressions was represented by a sigmoid with respect to barium-nitrate coverage. The proposed rate expressions are listed in the last chapter as equations 3.35 and 3.36.

Based on these two modifications to the model, the rate constants for the forward and the backward reactions (given by the equations 4.5, 4.6, 4.7 and 4.8) and parameters describing the proposed diffusion expression (given by the equation 4.9) were estimated by extensive trial and error. A very close fit was obtained between the simulated and the experimental NOx profiles at the reactor exit and the results are shown in Figure 4-6. The estimated rate expressions and the diffusion function are listed in Table 4-3 and the Table 4-4 respectively.

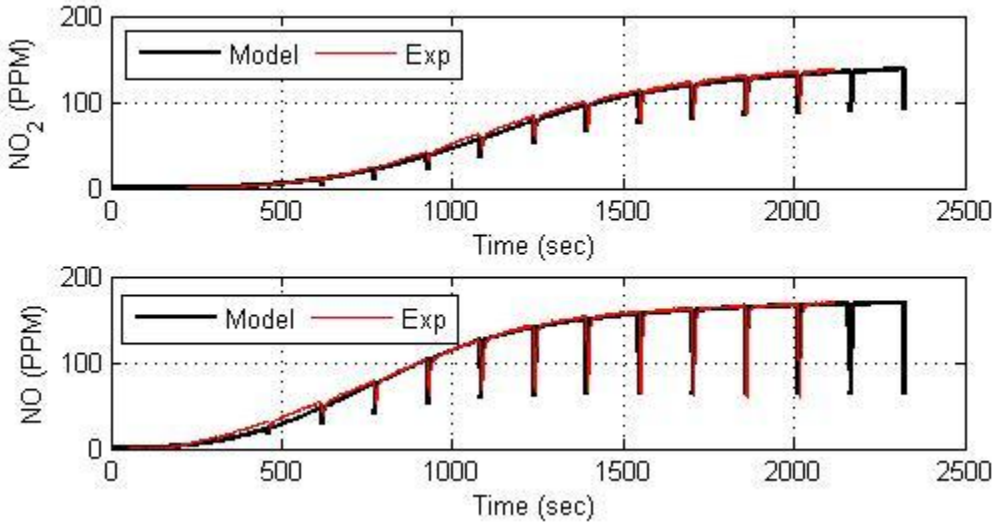

Figure 4-6: The simulated and experimental NOx profiles with the proposed modifications in the model structure with mass transfer coefficient of 0.05 m/s.

Reactions	Rate Expressions
Forward NO_2 storage, r_{2f}	$\frac{1.5}{\left(1+1.5*\frac{l}{D_{NO_2}}*\frac{r_1}{r_{tot}}*\theta_{BaCO_3}\right)}$
Forward NO storage, r_{3f}	$\frac{152.7789}{\left(1+152.7789*\frac{l}{D_{NO}}*\frac{r_1}{r_{tot}}*\theta_{BaCO_3}\right)}$
Backward NO_2 storage, r_{2b}	$\frac{1.175*2*10^{-4}}{1+\exp\left(-20*\left(\theta_{Ba(NO_3)_2}-0.525\right)\right)}$
Backward NO storage, r_{3b}	$\frac{1.5*0.375*10^{-4}}{1+\exp\left(-20*\left(\theta_{Ba(NO_3)_2}-0.35\right)\right)}$

Table 4-3: The estimated values for the rate constants used in the modified model to fit cyclic experimental data with no reductants.

Species	Diffusion Expression
D_{NO_2}	$11*10^{-9}*\frac{exp\left(-8*\left(1-\frac{r_1}{r_{tot}}-0.15\right)\right)}{1+exp\left(-8*\left(1-\frac{r_1}{r_{tot}}-0.15\right)\right)}$
D_{NO}	$1.75*10^{-9}*\frac{\exp\left(-4*\left(1-\frac{r_1}{r_{tot}}-0.01\right)\right)}{1+\exp\left(-4*\left(1-\frac{r_1}{r_{tot}}-0.01\right)\right)}$

Table 4-4: The estimated diffusion expressions for NO and NO_2, used in the shrinking core model with mass transfer coefficient of 0.05 m/s

Apart from the reaction rates, the mass transfer coefficient between the gas and the washcoat can also play an important role in the storage dynamics. The lower bound was estimated as discussed earlier in this section. The effect of increasing the mass transfer coefficient beyond the initially selected value of 0.05 m/s was also studied and it was found that, for any new value that is assumed for the mass transfer coefficient, the diffusion and the reaction rate parameters need to be recalculated in order to maintain the fitting with respect to the data as in Figure 4-6. Accordingly the model was tuned for a higher value of 0.15 m/s and the rate constants and the diffusion coefficient expressions were estimated again to match the experimental data. The revised fitting of the NOx profile with a mass transfer coefficient of 0.15 m/s is shown in Figure 4-7. The revised estimated NO oxidation rate constant is as follows:

$$2.15 * 10^6 * \exp\left(-\frac{40000}{8.314 * 573}\right) \quad \text{... (4.10)}$$

The rate constants of the NOx storage reactions could be kept to be the same as the ones used for the lower mass transfer coefficients but the diffusion expressions have to be re-estimated and the revised values are listed in Table 4-5.

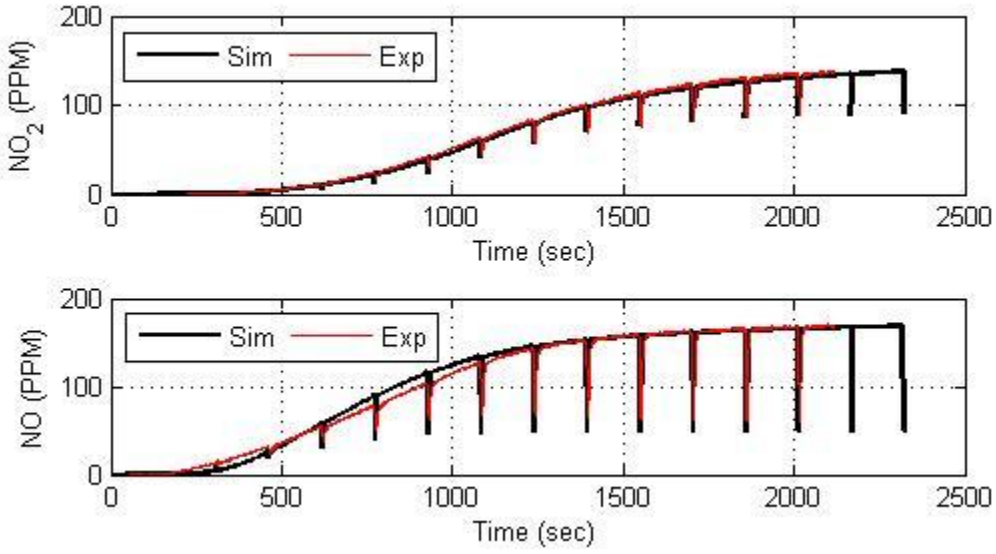

Figure 4-7: The simulated and experimental NOx profiles with the proposed modifications in the model structure and the mass transfer coefficient of 0.15 m/s

Species	Diffusion Expression
D_{NO_2}	$10 * 10^{-9} * \frac{exp\left(-7.5 * \left(1 - \frac{r_1}{r_{tot}} - 0.15\right)\right)}{1 + exp\left(-7.5 * \left(1 - \frac{r_1}{r_{tot}} - 0.15\right)\right)}$
D_{NO}	$1.15 * 10^{-9} * \frac{\exp\left(-3.5 * \left(1 - \frac{r_1}{r_{tot}} - 0.01\right)\right)}{1 + \exp\left(-3.5 * \left(1 - \frac{r_1}{r_{tot}} - 0.01\right)\right)}$

Table 4-5: The estimated diffusion expressions for NO and NO_2, used in the shrinking core model with mass transfer coefficient of 0.15 m/s

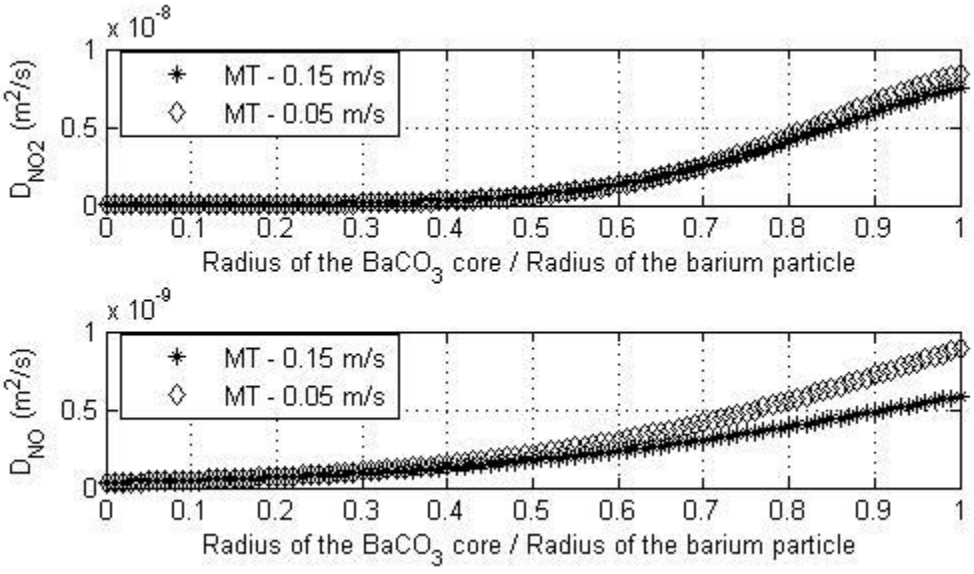

Figure 4-8: The comparison of estimated diffusion coefficient expressions for two mass different transfer coefficient values

The estimated diffusion expressions reported in Table 4-4 and Table 4-5 are plotted together in Figure 4-8 as a function of the ratio of the barium carbonate core and the particle radius. As shown in Figure 4-8, for the higher mass transfer coefficient, the corresponding value of the diffusion coefficient is lower than the value of the diffusion corresponding to the lower mass transfer coefficient. This is a logical result since both the mass transfer coefficient and the diffusion represent mechanisms to mass transfer resistance between the gas and the wash-coat. Thus, the data can be properly fitted with either a combination of high mass transfer coefficient and low diffusion or with a combination of low mass transfer coefficient with a higher diffusion. This also indicates that even if there is any error in the estimation of mass transfer coefficient, this error can be properly compensated for by the choice of the diffusion coefficient thus resulting in a similar storage dynamics.

4.2 Cyclic Data with 1.5% CO

In this section, the estimation of the rate constants for reductant based reactions occurring during the rich phase is presented. In principle, the NSR catalyst is exposed during the rich phase to reductants after certain duration of the lean phase in order to regenerate the barium storage sites. In this part of the study, data obtained from a cyclic experiment was used where the completely regenerated catalyst was exposed to the lean phase gas composition for 150 seconds, followed by the rich phase compositions for 5 seconds and this cyclic mode of operation was repeated again and again until a steady periodic mode of operation was achieved. The experimental NOx concentration data corresponding to this operating scenario is shown in Figure 4-9. The CO feed concentration that was used in the rich phase was 1.5%.

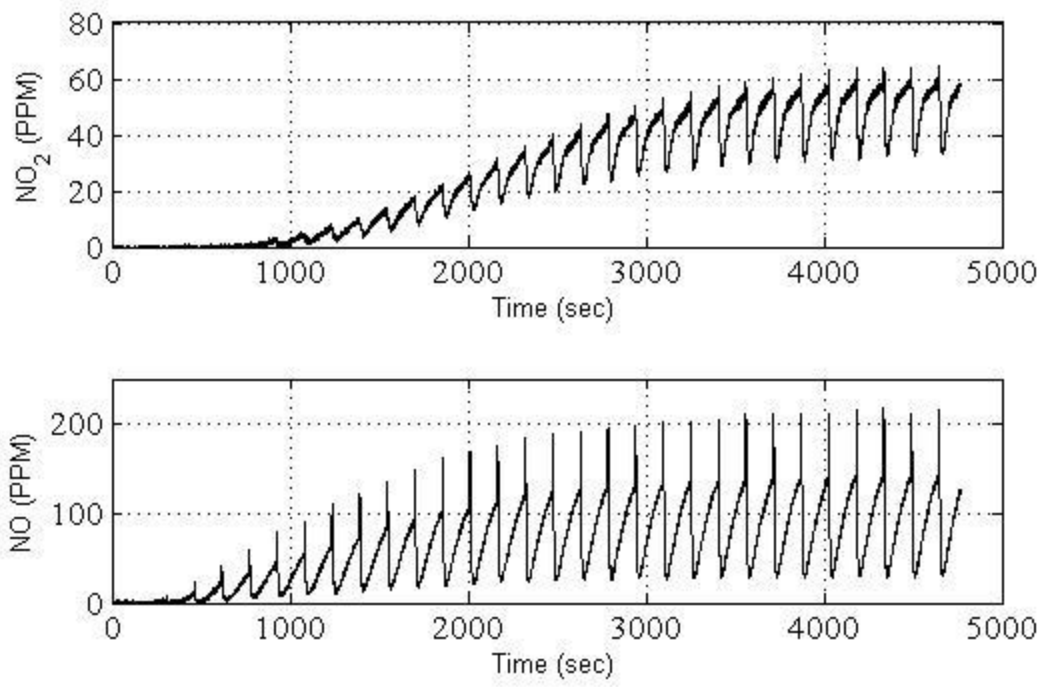

Figure 4-9: The experimental exit NOx profiles in a cyclic run with 1.5% CO

As discussed in the last chapter, there are total of 11 reactions that take place in the rich phase as follows:

$$CO + \frac{1}{2}O_2 \xrightarrow{r_5} CO_2 \quad \text{... (4.11)}$$

$$H_2 + \frac{1}{2}O_2 \xrightarrow{r_6} H_2O \quad \text{... (4.12)}$$

$$H_2O + CO \xleftrightarrow{r_7} H_2 + CO_2 \quad \text{... (4.13)}$$

$$CO + 2CeO_2 \xrightarrow{r_8} CO_2 + Ce_2O_3 \quad \text{... (4.14)}$$

$$H_2 + 2CeO_2 \xrightarrow{r_9} H_2O + Ce_2O_3 \quad \text{... (4.15)}$$

$$3CO + Ba(NO_3)_2 \xrightarrow{r_{10}} BaCO_3 + 2NO + 2CO_2 \quad \text{... (4.16)}$$

$$3H_2 + CO_2 + Ba(NO_3)_2 \xrightarrow{r_{11}} BaCO_3 + 2NO + 3H_2O \quad \text{... (4.17)}$$

$$5CO + Ba(NO_3)_2 \xrightarrow{r_{12}} BaCO_3 + N_2 + 4CO_2 \quad \text{... (4.18)}$$

$$5H_2 + CO_2 + Ba(NO_3)_2 \xrightarrow{r_{13}} BaCO_3 + N_2 + 5H_2O \quad \text{... (4.19)}$$

$$CO + NO \xrightarrow{r_{14}} CO_2 + \frac{1}{2}N_2 \quad \text{... (4.20)}$$

$$H_2 + NO \xrightarrow{r_{15}} H_2O + \frac{1}{2}N_2 \quad \text{... (4.21)}$$

Although these reactions have been studied separately in different research works, very few studies have considered these reactions collectively (Guthenke et al., 2007; Koci et al., 2007). Unfortunately, these studies that have considered all these reactions together have not reported detailed data about the rate constants. Therefore, it was decided to collect the rate constants' data from different studies in the literature that have considered subsets of these reactions and to use these data as initial guesses for model calibration. Table 1.4 summarized the rate constants available in the literature. As seen from the Table 1.4, there is no single study reporting the estimated rate constants for all these reactions. Moreover, the rate constants for the H_2 based reactions, as given by equations r_9, r_{11}, r_{13} and r_{15}, have not been reported by any of the authors. It has been observed that at 300^{o}C, using similar feed concentrations of CO or H_2 result in similar performance in terms of the percentage of NOx conversion (Mahzoul et al. 1999). Therefore, in this study, the kinetics for the H_2 based reactions were selected equal to the kinetic parameters of the CO based reactions. The water shift reaction was calibrated separately by using the data from a separate experiment, conducted by Al-Harbi (Al-Harbi Thesis, 2008) to study the extent of the water gas shift reaction at different temperatures. For these experiments, the maximum percentage conversion of CO at 300 ^{o}C was reported to be 62.4%. For calibration purposes, the present model was simulated with only the water gas reaction and the inlet conditions specified in the experiment by Al-Harbi. The rate constant was estimated to be 16.07 moles/m^3 with the error between predicted (62.68%) and experimental (62.4%) percentage CO conversion to be 0.28%.

Reactions	Rate Constants		
	Jirat et al. (1999)	Olsson et al. (2006)	Tuttlies et al. (2006)
r_5	$5 * 10^{16} * \exp(-\frac{95000}{8.314 * T})$	$7.8 * 10^{15} * \exp(-\frac{104400}{8.314 * T})$	
r_6	$5 * 10^{16} * \exp(-\frac{95000}{8.314 * T})$		
r_8	$3 * 10^{8} * \exp(-\frac{90000}{8.314 * T})$		
r_{10}		$3.7 * 10^{5} * \exp(-\frac{72700}{8.314 * T})$	$4.29 * 10^{5}$
r_{12}	$3 * 10^{7} * \exp(-\frac{90000}{8.314 * T})$		
r_{14}	$1.5 * 10^{6} * \exp(-\frac{70000}{8.314 * T})$	$8.5 * 10^{12} * \exp(-\frac{50500}{8.314 * T})$	$2.03 * 10^{-3}$

Table 4-6: The rate constants reported in different studies in the literature

Since the proposed model for the rich phase contains a large number of reactions, a corresponding large number of rate constants can be potentially changed to fit the experimental results. Adjusting all the parameters together may result in a very tedious trial and error exercise and it may also lead to the sensitivity to measurement errors if there is a large correlation between the parameters. Therefore, it was decided to conduct a sensitivity analysis with two goals: to identify the parameters that have the most impact on the outputs of the model and to test the overall robustness of the model with respect to possible inaccuracies in parameter values. A first order sensitivity analysis was used to check which rate constants are highly sensitive to the percentage conversion of NOx at the catalyst exit and which are almost insensitive. In this way, the number of parameters to be estimated was reduced to 4. All

the 10 reactions except the water gas shift reaction were included in this analysis. The nominal values for the rate constants were selected from the literature based on following considerations:

1. When the rate constants for CO and H_2 oxidation reactions, as reported in the studies by Jirat et al. (1999) and Olsson et al. (2005), were used, the model predicted 100% conversions for both reactions, too high based on the values observed in the experiments. Moreover, perturbing the rate constant values by $\pm$ 20% also resulted in 100% conversions. It was concluded that these reported rate constant values are too high and even if the percentage NOx conversion may slightly change with respect to these rate constants, any $\pm$ 20% change around the nominal values will never affect the sensitivity results. Since the values reported by Koltsakis et al. (2002), in the context of 3-way catalytic converters, were observed to predict the percentage conversion of around 6% in the oxidation reactions, these reported values were used in the sensitivity study.
2. The reactions involved in the regeneration of barium nitrate sites can proceed along two different pathways: one produces NO and the other produces directly N_2. Although the kinetics for the first pathway have been reported by both Olsson et al. (2005) and Tuttlies et al. (2006), the values reported by Olsson et al. (2005) were used as nominal values for the sensitivity study. For the second pathway, the kinetic parameters have been reported only by Jirat et al. (1999) and they were consequently used as nominal estimates.
3. The kinetics for the NO reduction reaction has been reported in all the three studies as summarized in the Table 4-6. However, the values reported by Jirat et al. (1999) were used as nominal values.
4. The regeneration of ceria in the context of NSR system has been studied by several authors, but the values have been reported only by Jirat et al. (1999) and these were consequently used as nominal values for the analysis.

To calculate the sensitivity of the percentage NOx conversion to a change in the kinetic parameters, each one of the kinetic parameters were perturbed by $\pm$ 20%, one at a time and the change in percentage conversion in the NOx at the catalyst exit over a period of 5 cycles was calculated using the following expressions:

$$\%\ NOx\ Conversion = \frac{NO_{inlet} - \int_{t=0}^{t=155*5} NO\ dt + \int_{t=0}^{t=155*5} NO_2\ dt}{NO_{inlet}} * 100 \qquad \ldots (4.22)$$

$$\Delta\,\%\,conv\ of\ NOx = \%\,NOx\ Conversion|_{k_{i-20\%}} - \%\,NOx\ Conversion|_{k_{i+20\%}}$$

... (4.23)

The nominal values for the rate constants of 14 reactions used for sensitivity analysis are listed in the Table 4-7 and the results from sensitivity analysis are summarized in the Table 4-8.

Reactions	The nominal values of the rate constants
r_5	$2 * 10^{13} * \exp(-95000/8.314/T)$
r_6	$2 * 10^{13} * \exp(-95000/8.314/T)$
r_8	$3 * 10^{8} * \exp(-90000/8.314/T)$
r_9	$3 * 10^{8} * \exp(-90000/8.314/T)$
r_{10}	$3.7 * 10^{5} * \exp(-72700/8.314/T)$
r_{11}	$3.7 * 10^{5} * \exp(-72700/8.314/T)$
r_{12}	$3 * 10^{7} * \exp(-90000/8.314/T)$
r_{13}	$3 * 10^{7} * \exp(-90000/8.314/T)$
r_{14}	$1.5 * 10^{6} * \exp(-70000/8.314/T)$
r_{15}	$1.5 * 10^{6} * \exp(-70000/8.314/T)$

Table 4-7: The summary of nominal values for the rate constants, selected from the literature for sensitivity analysis.

Reactions	Perturbation in the kinetic parameters				
	-20%		20%		Net Change
	NOx out (ppm)	% Conversion	NOx out (ppm)	% Conversion	% Conversion
r_5	30766	87.56929	30765	87.5697	0.000
r_6	30766	87.56929	30766	87.56929	0.000
r_8	31362	87.32848	30207	87.79515	0.467
r_9	30850	87.53535	30686	87.60162	0.066
r_{10}	29095	88.24444	32708	86.78465	1.460
r_{11}	30548	87.65737	31021	87.46626	0.191
r_{12}	31709	87.18828	29741	87.98343	0.795
r_{13}	30881	87.52283	30635	87.62222	0.099
r_{14}	30766	87.56929	30764	87.5701	0.001
r_{15}	30766	87.56929	30765	87.5697	0.000

Table 4-8: The results from the preliminary sensitivity analysis based on perturbation level of $\pm$ 20% in the nominal values.

Reactions	The kinetic parameters				
	Nominal Values (Jirat et al., 1999)		Increased Values (x1000)		Net Change
	NOx out (ppm)	% Conversion	NOx out (ppm)	% Conversion	% Conversion
r_{14}	30766	87.56929	29057	88.2598	0.690505
r_{15}	30766	87.56929	30481	87.6844	0.115152

Table 4-9: The results from the revised sensitivity analysis for NO reduction reactions

It can be seen from the Table 4-8 that the CO and H_2 oxidation reactions and the NO reduction reactions by CO and H_2 are the reactions that contribute the least to the sensitivity in percentage NOx conversion around the selected nominal values of their rate constants. However, there is a possibility that at the higher rate constant values, the change in the percentage NOx conversion may become sensitive to these reactions. To test this point, a few more simulations were carried out where the rate constants of these reactions were perturbed outside the $\pm$ 20% range around the nominal values.

The model was simulated with only CO and H_2 oxidation reactions and from these simulations, the lower bounds for the individual rate constant values were selected to be the ones that result in model predictions of 0% conversion whereas the upper bounds were selected to be the values that predicted 100% conversion. In the cyclic model, the rate constant values for the CO and H_2 oxidation reactions were then perturbed with respect to these calculated upper and lower bound values and the percentage NOx conversion was calculated as before. From the simulation results, a very small change in the percentage NOx conversion (< 0.01%) was observed with respect to the nominal values used earlier and therefore, it was decided to fix the rate constants values to the nominal values.

For the NO reduction reactions, a significant change in the percentage NOx conversion was obtained when the rate constants were increased by a factor of a 1000 and the results are summarized in the Table 4-9. From these results, it was concluded that the NO reduction reactions may also contribute to sensitivity in the percentage NOx conversion. This effect was not observable in the preliminary sensitivity analysis because the rate constants values, reported by Jirat et al. (1999) that were originally used were not sufficiently large to affect the percentage NOx conversion. Therefore, for the parameter estimation step, the higher rate constant values for the NO reduction reactions were used as an initial guess.

Since the kinetic parameters used for the reactions involving H_2 were the same as the ones used for the reactions involving CO and it was observed that a significant amount of CO (64%) will convert into H_2 (Al-Harbi Thesis, 2008), the sensitivity in the percentage NOx conversion with respect to the changes in kinetic parameters of the H_2 reactions was expected to be similar to the sensitivity with respect to the kinetic parameters of the CO reactions. However, the sensitivity analysis revealed that the CO and H_2 based reactions do not affect the percentage NOx conversion equally as shown in Table 4-8. A possible explanation for this observation is that the experiment of Meshari where he observed significant conversion of CO to H_2 was done in the absence of NO. However, in the actual operation NO is present and for that case the amount of H_2 being produced by the water gas shift reaction has been observed to be relatively small. This in turn can be attributed to the fact that CO is

involved in regeneration reactions with ceria and barium and therefore, the amount of CO available for water gas shift reactions may be very low.

Based on this discussion, the rate constants for only following reactions will be estimated:

$$CO + 2CeO_2 \xrightarrow{r_8} CO_2 + Ce_2O_3 \quad \text{... (4.24)}$$

$$3CO + Ba(NO_3)_2 \xrightarrow{r_{10}} BaCO_3 + 2NO + 2CO_2 \quad \text{... (4.25)}$$

$$5CO + Ba(NO_3)_2 \xrightarrow{r_{12}} BaCO_3 + N_2 + 4CO_2 \quad \text{... (4.26)}$$

$$CO + NO \xrightarrow{r_{14}} CO_2 + \frac{1}{2}N_2 \quad \text{... (4.27)}$$

4.2.1 Parameter Estimation

There are two reactions, represented by r_{10} and r_{12}, which are governing the regeneration of barium carbonate in the rich phase. However, reaction r_{10} also governs the release of NO, which is then reduced to N_2 by reaction r_{14}. If only reaction r_{10} is considered to be contributing towards regeneration of carbonates, it may result in higher NO concentrations as compared to experimental observations and consequently, the kinetics of the reaction r_{14} may have to be increased to fit the predicted NO concentrations. In another approach, the net NO release can be fitted by adjusting the kinetics of reaction r_{10} to a somewhat lower value but then the estimated kinetic parameters may not be large enough to regenerate the required carbonate amounts. In such a case, the kinetics of reaction r_{12} can be adjusted to any required level to regenerate the carbonates because as NO is not a product of $r_{12,}$ this adjustment will not affect the exit NO concentrations. Therefore, there exists a strong correlation between these three reactions. Accordingly, these reactions should be collectively adjusted in order to regenerate a sufficient amount of barium carbonate while maintaining the released NO concentrations within the limits shown in Figure 4-9.

As can be seen from the cyclic data in Figure 4-9, the NOx amount being stored in every cycle is progressively decreasing. This implies that only a fraction of barium nitrates formed during a lean phase is being converted back to barium carbonates in the subsequent rich phase, therefore decreasing the net amount of barium carbonate available for NOx storage during the next lean phase. Otherwise the same amount of NOx would have been stored in every subsequent lean phase. On the other hand it can be observed from the cyclic data shown in Figure 4-9 that during the initial few seconds in each lean phase, nearly the same amount of NOx is being stored, i.e. the lower values of the oscillating

response are similar. A possible explanation to this behaviour is that the fraction of barium carbonate regenerated during the rich phase corresponds to the barium carbonates present in the outer layer in the shrinking core model, which can trap the NOx very easily. Based on this explanation, Figure 4-10 illustrates the pictorial representation of the ideal particle assumed to represent the distribution of nitrates and carbonates in the shrinking core model during one complete cycle.

In Figure 4-10(a) the schematic represents a particle that it is completely regenerated with barium carbonate corresponding to the situation at the beginning of the cyclic operation shown in Figure 4-9. As cyclic operation proceeds, during a lean phase the barium carbonate core decreases in diameter as more and more carbonate is being consumed in the storage process. In the subsequent rich phase, since the regeneration reaction depends on the nitrate concentration and the nitrate shell has grown during the last lean phase, the amount of carbonate regenerated also increases and therefore in the subsequent rich phases, the outer carbonate shell increases in thickness. Since the barium particle at the end of the rich phase does not exhibit the same nitrates-carbonates content as the barium particle at the start of a cyclic operation corresponding to time=0 seconds in Figure 4-9, the same expression used to calculate the carbonate-nitrate reaction front for fresh catalyst cannot be used for the barium particle in cyclic operation.

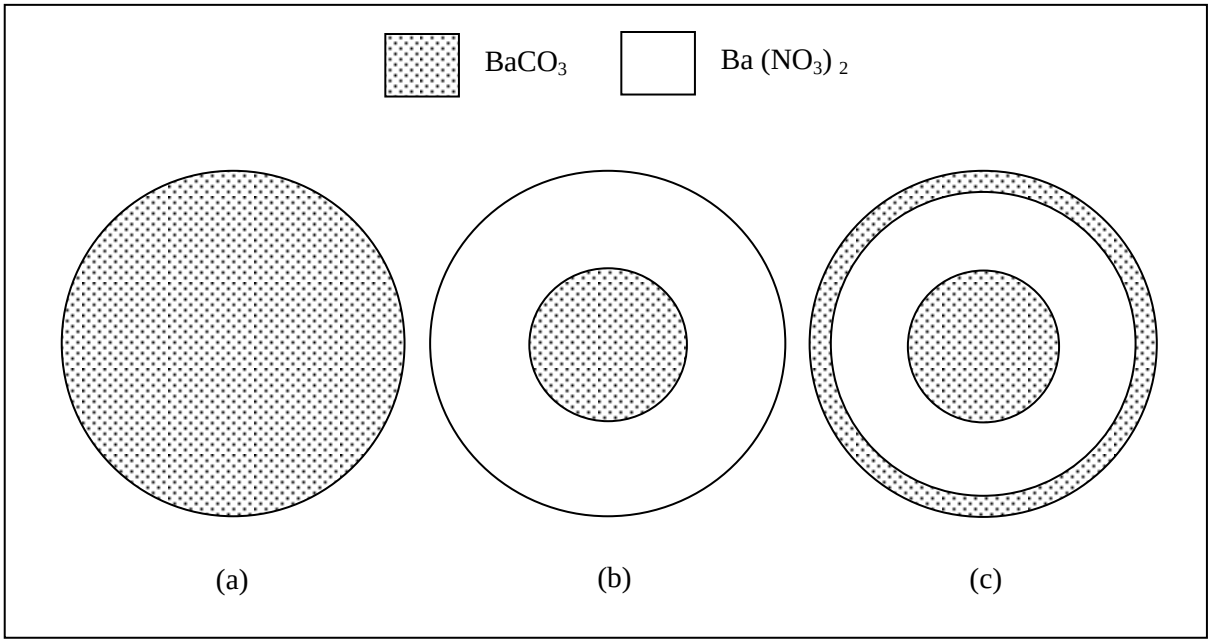

Figure 4-10: Pictorial representation of the barium particle undergoing conversions between carbonate and nitrate. (a) In the fresh catalyst before the start of cyclic operation (b) After the first lean phase (c) After the first rich phase

During the storage process in the second and subsequent lean phases, the barium carbonate in the outer shell will be consumed first and therefore, as this carbonate layer gets consumed, a newly formed nitrate layer grows in thickness and the position of this carbonate-nitrate interface, where the reaction occurs, will be given by:

$$r_1^{'} = r_{tot} * \left(\frac{\left(1 - 0.5 * \theta_{BaCO_3}\right) * \left(\frac{r^{'}}{r_{tot}}\right)^3 - \left(1 - 0.5 * \theta_{BaCO_3}\right) * \left(\frac{r^{''}}{r_{tot}}\right)^3 - 0.5 * \theta_{BaCO_3})}{0.5 * \theta_{BaCO_3} - 1} \right)^{\frac{1}{3}}$$

... (4.28)

where, r' is the radius of inner barium carbonate core and r'' is the radius of the interface between barium nitrate and the outer barium carbonate shell in the Figure 4-10c.

After the consumption of the outermost layer of the barium carbonate the NOx species has to diffuse through an already present nitrate layer and then the inner core of barium carbonate will be consumed. At that point, the barium particle exhibits a very simple structure with a carbonate shell surrounded by a nitrate shell as shown in Figure 4-10b. In this situation, the position of the carbonate-nitrate interface, as this layer gets consumed, can be calculated as follows:

$$r_1^{''} = r_{tot} * \left(\frac{0.5 * \theta_{BaCO_3}}{1 - 0.5 * \theta_{BaCO_3}} \right)^{\frac{1}{3}} \quad \text{... (4.29)}$$

After solving the first cycle, when the model was simulated for the second lean phase, the solver did not converge. As it can be seen from the Figure 4-10 (c), after consuming the outermost barium carbonate layer, the location of the reaction interface between carbonates and nitrates immediately shifts to the lower value r'' which results in a discontinuity in the model parameters. To overcome the numerical problems, the discontinuity corresponding to this sudden change in the radius of the interface from r' to r'' was approximated by a sigmoid around the radius value r' to provide for a relatively smoother transition as follows:

$$r = (r_1^{'} - r_1^{''}) * \left(flc2hs\left(\theta_{BaCO_3} - \theta_{BaCO_3}^{'} + 0.005, 0.005\right)\right) + r_1^{''} \quad \text{... (4.30)}$$

where, $\theta_{BaCO_3}^{'}$ is the carbonate fraction obtained at the end of the last lean cycle corresponding to the radius of inner carbonate core given by equation 1.21 above and flc2hs is the COMSOL function, used to represent a sigmoid.

The model was then simulated for the first 10 cycles leading to the preliminary results shown in Figure 4-11. Figure 4-11 (a) shows the simulated and experimental NOx concentrations at the catalyst exit for the first 10 cycles. For these simulations, the rate constants of the reactions, r_{10} and r_{14} were changed with respect to the nominal values used in the sensitivity analysis whereas the rate constants of the other two reactions were kept at their nominal value. It can be seen that after the third cycle, the simulated NOx profiles are higher than the experimental data and the possible reason is that the amount of barium carbonate regenerated in the previous rich phase is not sufficient to store the NOx in the subsequent lean phase. The barium carbonate fraction profiles along the catalyst length at the end of lean and rich phase for different cycles are shown in Figure 4-11b. It can be seen that only the front 30-35% of the reactor is being regenerated which may not be sufficient to store the required amount of NOx in subsequent cycles. Based on these results, it was concluded that the amount of barium carbonate being regenerated in the rich phase has to be higher than the one regenerated in the above simulations. However, whether the barium carbonate is to be regenerated mostly in the front part of the catalyst or uniformly along the catalyst length it is unclear and it cannot be confirmed by experiments. .

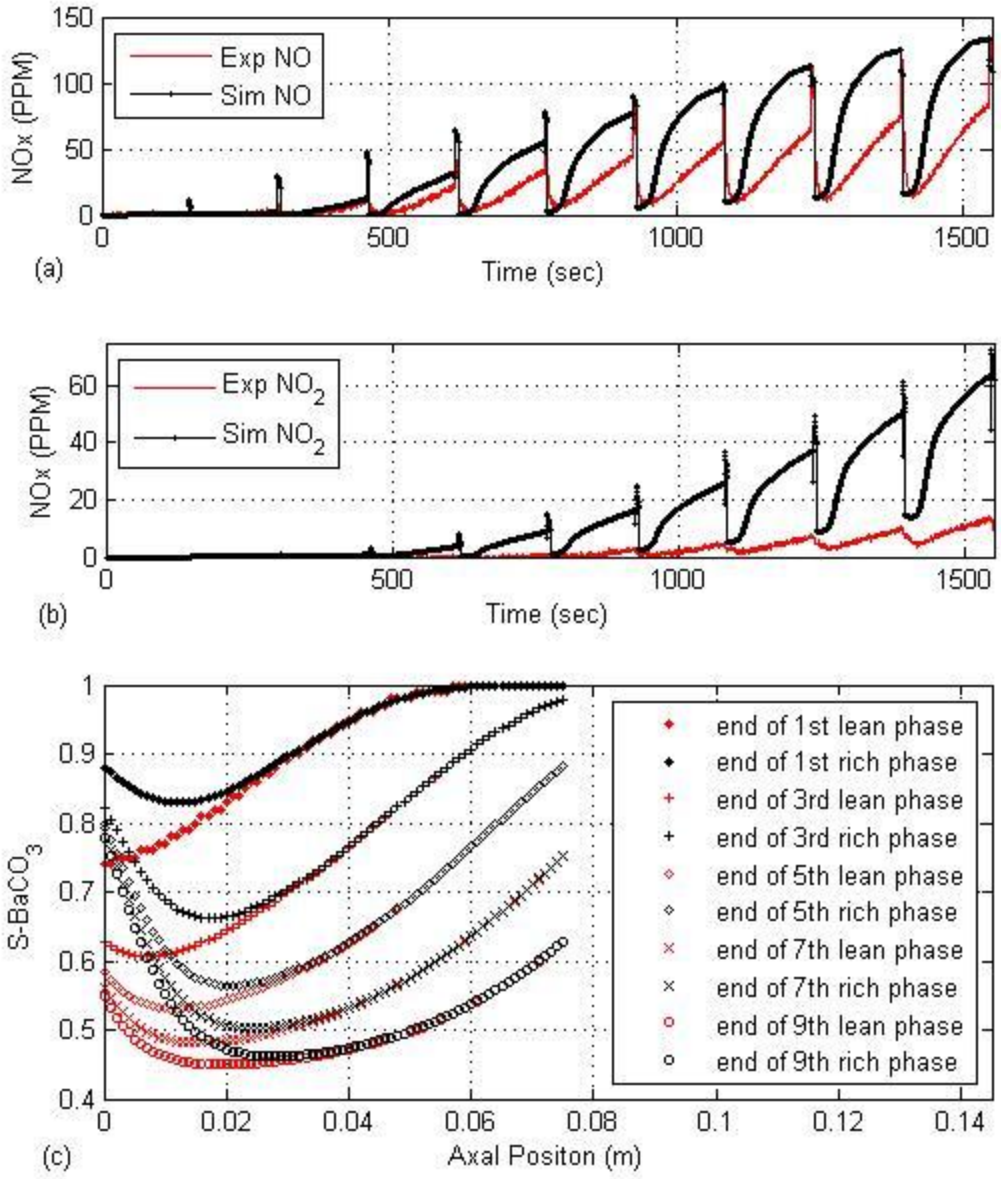

Figure 4-11: The preliminary results from the simulated model over first 10 cycles. (a) The exit NO concentrations. (b) The exit NO_2 concentrations. (c) The barium carbonate fraction as the function of catalyst length for different cycles.

The typical simulation time was around 2-3 hours which was considered to be too high for the parameter estimation step during which a large number of simulations is required. Thus the use of the sigmoid to avoid the discontinuity in the carbonate storage was not sufficient to speed up the simulation times. Therefore, since it was not possible to solve the model in the transient regime in a

reasonable time, it was decided to simulate the model in steady state cyclic regime corresponding to the time larger than 3000 seconds in Figure 4-9, so that more information can be gained about the changes in the coverage profiles that might have occurred in the catalyst till it reaches the steady periodic operation.

During the rich phase in the transient cyclic operation, the innermost barium carbonate layer gradually shrinks and the outermost carbonate layer gradually grows as the number of cycles is increasing. But when this operation reaches the steady state cyclic regime, only the outermost layer of the barium carbonate is being consumed in the lean phase and then is being regenerated during the rich phase. Due to this expected pattern of carbonate storage and in order to avoid the long simulation times arising from the steep changes in properties between the outer carbonate layer and the inner carbonate core, it was decided to approximate the imaginary particles used in the shrinking core model by a simpler configuration. This configuration assumed that the barium is present only in the carbonate form as in the case of fresh catalyst and as the storage proceeds only a small outermost layer of the barium carbonate will be consumed. However, to account for the fact that only the outer layer of the carbonate was reactive during cyclic operation instead of the entire volume of carbonate that participated in the reaction in the fresh catalyst, the diffusion expressions used to account for the NOx storage have to be adjusted accordingly.

From the experimental study by Meshari, it was also observed that with 1.5% CO in the rich phase, almost zero percent CO is present in the catalyst exit concentrations. The preliminary simulation also revealed that the CO got consumed in the first 30-35% of the reactor volume. Therefore, it was initially believed that in the reactor volume where the CO is available, the barium particles are present in the form as shown in Figure 4-10c and in the reactor volume after the axial position where the entire CO gets consumed, the barium particles are never regenerated and therefore they are present in the form as shown in Figure 4-10b. One numerically efficient approach to simulate the steady cycle operation is to assume initial axial profiles in concentrations and coverage for the beginning of the lean cycle, to solve for the lean and rich cycle and then to test whether the profiles at the end of the rich cycle coincide with the initially assumed profiles. Following this approach different initial profiles are assumed until convergence between the profiles after the rich cycle and the initial profiles coincide with each other. It was also found that the convergence is mostly sensitive to the initially assumed profile in barium carbonate coverage along the reactor. Based on the simpler configuration assumed to represent the barium particles in the first 30-35% of reactor, the barium carbonate fraction was considered as equal to one in this part of the reactor. For rest of the reactor, where the barium carbonate is present in the form as shown in Figure 4-10b, the carbonate fraction was considered to be

equal to some random value, which can be based on the preliminary simulation results in the transient operation. The typical profile used as an initial guess is shown in Figure 4-12.

The rate constants for the four selected reactions, r_8, r_{10}, r_{12} and r_{14} that mostly determine the barium carbonate profile at the end of the rich phase along with the parameters describing the diffusion expressions for NOx storage were estimated to obtain fitting between experiments and simulations. In addition to these parameters, the rate constant for the NO oxidation reaction was also modified. After an extensive trial and error procedure, the results obtained from the final simulation are shown in the Figure 4-13.

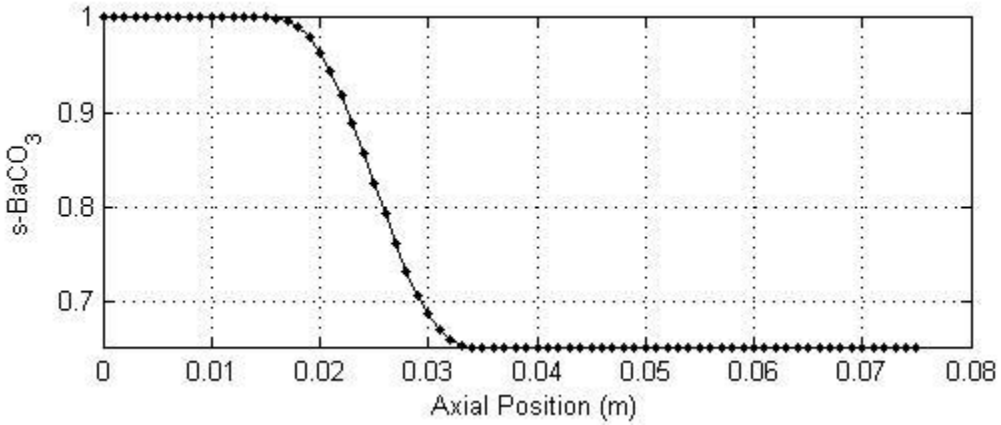

Figure 4-12: Initial guess for the barium carbonate fraction as a function of the catalyst length

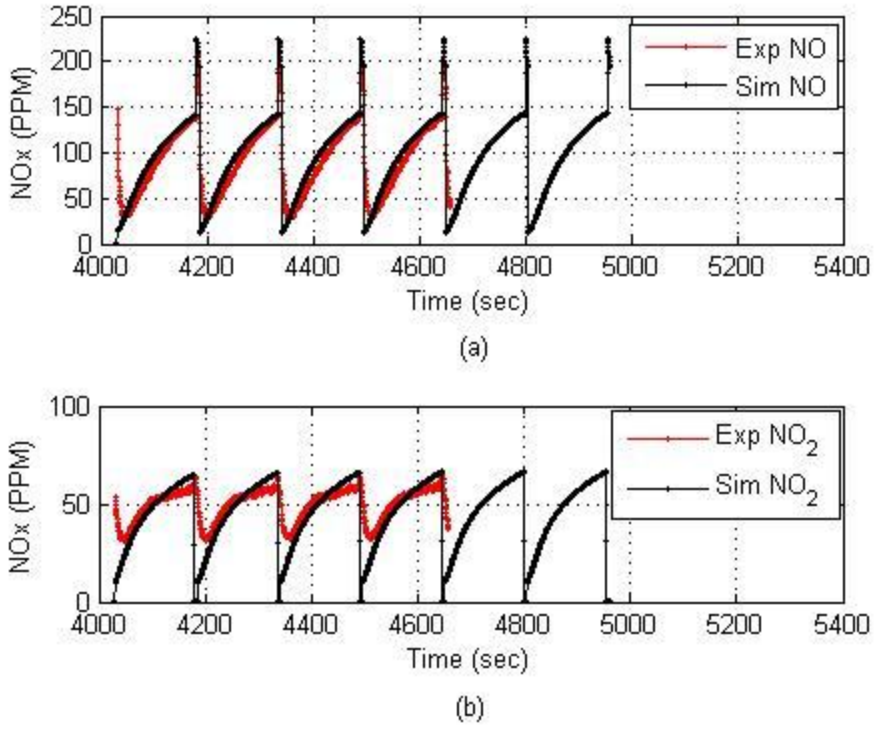

Figure 4-13: Fitting of the simulated NOx concentrations at the catalyst exit with the experimental data (a) NO concentrations (b) NO_2 concentrations

As stated before, the barium carbonate fraction in the imaginary particles used for the shrinking core model was assumed to be 1 for the first 30-35% of reactor and it was observed from the simulations that in order to regenerate the barium carbonate back to its original value, a mass transfer coefficient of 0.15 m/s had to be used in the rich phase. However, this does not necessarily mean that the actual mass transfer coefficient is 0.15 m/s since the particle used for analysis is only an approximate description of the barium particles in the bed. Since coverage cannot be measured at this point it is not possible to assess the accuracy of the assumed particle description. Due to the use of a high mass transfer coefficient and higher rate constants for the regeneration and reduction reactions, the convergence of the solution during the rich phase in Figure 4-13 was relatively slow with a simulation time of almost 1 hour as compared to a simulation time of 10 minutes required for simulating the lean phase. In order to reduce the computation time, the model was solved only for the first 40% of the reactor length and the coverage profiles in the remaining 60% of the reactor length were assumed to remain unchanged. Correspondingly, the concentration profiles in the last 60% of the reactor were assumed to be the same as the concentrations at the end of the first 40% of reactor.

The fraction of the barium carbonate along the catalyst length is shown in Figure 4-14. As it can be seen from Figure 4-14, the barium carbonate is being regenerated only in the first 30-35 % of the catalyst length. Therefore, the assumption that the coverage profiles remain constant for the last 60% of the reactor was found to be valid.

An additional modification that was done to improve the fitting between the experiments and the simulations was to reduce the rate constant of the NO oxidation reaction by half with respect to the values obtained for the long lean scenario (see equation 1.12). One possible reason for this modification is related to the fact that in the current simulations, only the first 30-35% of the reactor was assumed to store NOx. Since the rest of the catalyst, nearly 65-70%, cannot store the NOx, the NO_2 concentrations were observed to be very high as compared to the experimental data with the previously estimated rate constant values for the NO oxidation reaction. Therefore, in order to decrease the NO_2 concentrations to the level observed in the experiment, the rate constant values for the NO oxidation reaction had to be decreased.

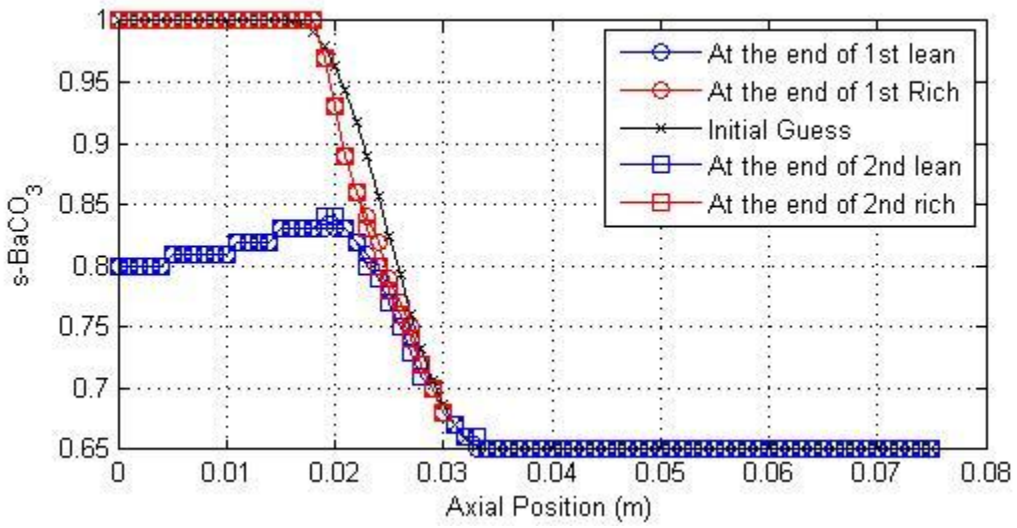

Figure 4-14: The predicted barium-carbonate profiles as the function of catalyst length during the steady state cyclic operation

This also suggests that the assumption by which only the first 30-35% of the reactor volume is regenerated and consequently the NOx is stored only in the front of the catalyst may not be correct. Therefore, it is necessary to solve the problem by regenerating more than 30-35% of the reactor where the barium carbonate will be much smoother as compared to the simulated results shown in Figure 4-11b. However, solving the problem in this direction is left for the future research.

The diffusion coefficient functions identified for the long lean experiment and for the cyclic experiment were compared in order to assess whether the differences can be explained by physical arguments. The comparison of the estimated diffusion coefficient functions is shown in the Figure 4-15 where the case 2 represents the diffusion expression for the fresh catalyst having the completely regenerated barium particles and the case 1 represents the diffusion expressions for the partially regenerated barium particles during the steady state cyclic regime with 1.5% CO. As can be seen from Figure 4-15, for the barium particles with the approximate configuration proposed above, the diffusion drops immediately after the formation of the barium nitrate layer. This supports that in the actual barium particle, as represented by Figure 4-10c, after the consumption of outer barium carbonate layer, the NOx species has to diffuse through the relatively larger layer of the barium nitrate.

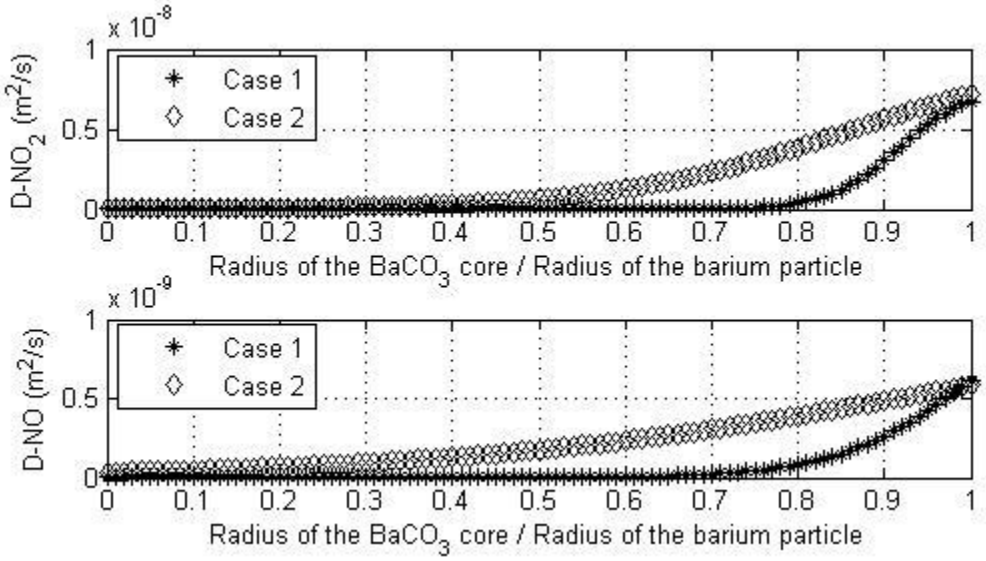

Figure 4-15: Comparison of the diffusion function. Case 1: Diffusion functions for the partially regenerated barium particles during the steady state regime of the cyclic experiment with 1.5% CO. Case 2: Diffusion functions for the fresh catalyst having the completely regenerated barium particles.

The corresponding drastic decrease in diffusivity represents the fact that only the outer carbonate core reacts during steady cyclic operation. As explained in this chapter the decrease in diffusivity with respect to distance from the surface of the imaginary particle is related to an increasing distance of the nitrate from a Pt site that is essential for the occurrence of the reaction. On the other hand, one would expect that at least the diffusivity of the outer layer of the particle will be the same for the catalyst during cyclic operation (Figure 4-10c) as for the fresh catalyst (Figure 4-10a). However, it can be seen from the Figure 4-15, that the diffusion values for the outer layer of the particle corresponding to a thickness of ~10%-13% of the particle radius are not equal. The possible explanations are as follows:

1. In the artificial configuration of the barium particle, the amount of regenerated barium carbonate in the outer layer was assumed to be nearly uniform along the axis. However, in reality, the thickness of outer layer is varying along the axis as shown in Figure 4.11.
2. The barium particle proposed in this modelling work represents the different barium particles in terms of their Pt/Ba proximity. Although the barium carbonate in the outer layer is easier to be consumed during the lean phase as discussed in the last chapter, the same may not be the true for the barium nitrate layer in the rich phase. It has been explained in the literature that H_2 has a "spill over" effect whereby H_2 can be equally reactive with nitrates located at different distances from Pt sites. If this spill over effect occurs, the configuration of barium particle at the end of rich phase will not be the same as shown in Figure 4-10c and a revised schematic description shown in Figure 4-16 may be necessary. In this revised configuration, all the barium particles that have been converted into the nitrates can be equally regenerated back to carbonates resulting in the occurrence of multiple rings of carbonate at the end of the rich phase. If the reductant spill over effect is prominent, then the multiple carbonate rings formed during the rich phase can also explain the discrepancy observed in the diffusion relation as discussed above.

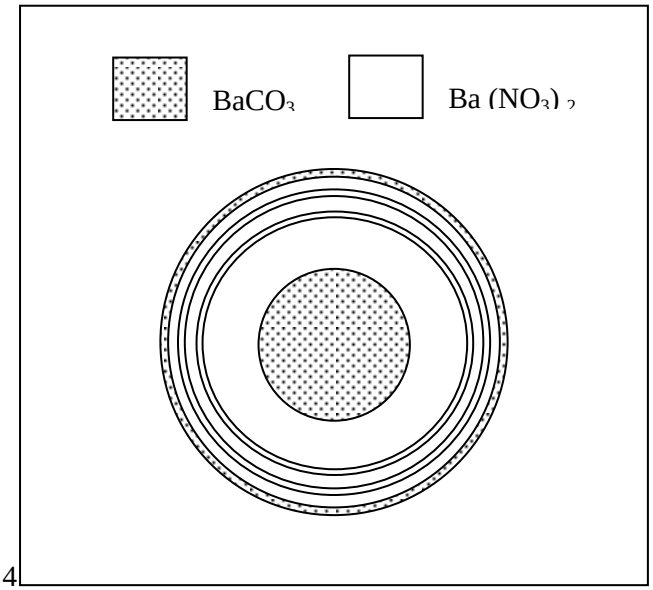

Figure 4-16: The representation of the artificial barium particle at the end of rich phase considering the reductant spillover effect.

In summary, a general approach to model the NOx storage dynamics has been presented. This approach can be easily adapted to any NSR formulation ranging from the basic to the most complex one by calibrating the diffusion function to account for any kind of resistance.

The proposed model was shown to be partially successful in predicting the NOx profiles for cyclic operation. The inaccuracies of the model are believed to be related to inaccurate assumptions regarding the patterns of regeneration of carbonates within the barium particles and along the catalyst length. Since these patterns have yet to be directly measured, the coverage profiles and the distribution of carbonates within the particles were based at this point on speculations. Improvement in the prediction accuracy of the model may be obtained by assuming a more uniform distribution of the regenerated carbonates along the catalyst bed. A better assumption regarding the carbonate profile and the multiple ring structure is expected to improve the predictions while requiring less adjustment of model parameters when simulating different operating scenarios and shorter simulation times.

Chapter 5
Conclusions and Future Work

In this thesis, a general approach to model the NOx storage during the lean phase of a NSR cycle is presented, which can be easily adapted to any NSR formulation. In addition, it also reveals important information about the possible barium carbonate profiles along the catalyst length at the end of rich phase in each cycle and also possible regeneration mechanisms that can explain the transient cyclic regime. Overall, the conclusions can be summarized as follows:

5.1 Shrinking core model

The resistance to NOx storage during the lean phase of NSR cycle, observed in the experiments, is attributed to either Pt/Ba proximity or in general different storage site types. In the context of Pt/Ba proximity, the barium particles that are close to the Pt sites can store the NOx at faster rates as compared to the barium particle away from the Pt sites. The rate of storage decreases as the distance of barium particles from the Pt sites increases. Due to confidentiality reasons, the catalyst structure is not completely known and therefore, it cannot be confirmed what types of different sites might be present. In the absence of a complete picture regarding the catalyst structure, an imaginary barium particle, assumed to be spherical in shape, has been proposed, where the outer layer represents, as an example, the barium particles that are either close to the Pt sites. The subsequent inner layers represent the particles with decreasing reactivity corresponding to their increasing distance from the Pt sites. A varying diffusivity, which decreases with a decrease in particle radius, was used to account for the decreasing reactivity as a function of particle depth.

5.2 Estimation of kinetics in the lean phase reactions

Since the feed compositions used for the lean phase has no reductants, the kinetics for the lean phase reactions: NO oxidation reaction, NO storage reaction and NO_2 storage reaction, can be estimated by independent experiments where the catalyst is to be exposed to only lean phase gas compositions. When the barium particles reach their saturation limit to store the NOx, the exit NO and NO_2 concentrations were believed to be governed by the equilibrium of NO oxidation reaction. Therefore, the kinetics of NO oxidation were estimated to predict the steady state NO and NO_2 concentrations. In the initial simulations, the barium was assumed to be present as $BaCO_3$ and therefore, the NOx reactions involving only $BaCO_3$ were considered. The model was simulated in a cyclic manner with 330 ppm of NO and 10% O_2 in the lean phase and no NO and O_2 in the rich phase to study the reversibility of the NOx storage reactions. It was concluded from the simulation results that the NOx

storage reactions are reversible, but the equilibrium constant between $BaCO_3$ and $Ba(NO_3)_2$, calculated from the thermodynamic calculations cannot explain the experimental NOx profiles. This indicates the presence of barium in other forms as well. Since the feed compositions contain significant amounts of CO_2 and H_2O, the barium can be present as both $BaCO_3$ and $Ba(OH)_2$. However, in order to explain the storage dynamics with the minimum possible number of reactions, only the reactions with $BaCO_3$ were used. In fitting the model predictions and the experimental NOx profiles, the forward and the backward rate kinetics of the reversible storage reactions were estimated separately and consequently the estimated rate constants give a lumped representation of the kinetics of both $BaCO_3$ and $Ba(OH)_2$ based reactions. With the higher mass transfer coefficient, the values of diffusion function within the imaginary barium particle were observed to be lower than the values estimated for lower mass transfer coefficient. Since both the mass transfer coefficient and the diffusivity in the barium particle represent the mass transfer resistance between the bulk phase concentrations and the concentration at barium carbonate-nitrate interface, the data can be fitted with either a combination of high mass transfer coefficient and low diffusion or with a combination of low mass transfer coefficient with a higher diffusion.

5.3 Parametric sensitivity analysis

The data from the cyclic experiment with 1.5% CO was used to estimate the kinetics of the rich phase reactions. Since the total number of rate constants to be estimated was 11, a parametric sensitivity analysis was performed to estimate the change in percentage NOx conversion in a complete NSR cycle with respect to $\pm$ 20% change in the nominal values of the rate constants, selected from the literature. The results from the sensitivity analysis conclude that the change in percentage NOx conversion is almost insensitive to any percentage change in the rate constants for CO and H_2 oxidation whereas it is most sensitive to four CO based reactions including regeneration of nitrates, reaction with ceria and the reduction of NO. Moreover, the change in percentage NOx conversion is observed to be less sensitive to the change in rate constants of H_2 based reactions as compared to CO based reactions. This indicates that the percentage conversion of CO to H_2 due to the water gas shift reaction is comparatively smaller in the presence of NO in the feed as compared to the situation where the feed contains zero amounts of NO. The reactions of CO with barium nitrates and ceria were suggested as possibly responsible for smaller CO to H_2 conversions. Based on the sensitivity analysis, the rate constants for only four CO based reactions: reaction with ceria, regeneration of nitrates with the release of NO, regeneration of nitrates with the release of N_2 and reduction of NO, were decided to be estimated by parameter estimation. The rate constants for these reactions based on H_2 were kept

the same as the estimated rate constants for the CO based reactions and the rate constant of CO and H_2 oxidation reaction were kept constant at the values reported in the literature.

5.4 Simulations in transient cyclic regime

In the transient cyclic operation, the effective NOx storage capacity of the catalyst progressively decreases as the number of cycle increases. Incomplete regeneration of the barium carbonate during each rich phase, resulting in the reduced amounts of barium carbonate available for the storage in subsequent lean phase, was proposed as a possible explanation to this observation. As an initial assumption, the barium nitrate close to the Pt sites was considered to be converted back into the carbonate earlier than one further away from the Pt sites. Based on this assumption and due to the incomplete regeneration of carbonate in the rich phase, the barium particle at the end of the rich phase is considered to have a carbonate core, which is surrounded by a nitrate layer and which is again surrounded by newly formed carbonate layer during the rich phase. During the subsequent lean phase in the transient, the outer carbonate layer will be consumed first, and then followed by the inner carbonate core until the inner carbonate core shrinks to a level which is inaccessible for the surface NOx. After that the cycle will be in steady state regime, where only the outer carbonate layer is being consumed in the lean phase and is being regenerated in the rich phase. The simulation of the model in the transient regime was taking much longer computational time at this stage, approximately 3-4 hours. Due to longer simulation time, the parameter estimation, where a large number of iterative runs are required, is very difficult to perform in reasonable time for the transient regime. Consequently, the possible regeneration mechanisms also cannot be verified. Therefore, in order to have an idea about the distribution of barium carbonate fraction along the catalyst length at the end of rich phase and the validation of the outer carbonate layer assumption as said above, the model was simulated in the steady state regime.

5.5 Simulations in steady state cyclic regime

From the preliminary simulation in the transient regime, the model predicted the regeneration to be occurring only in the first 30-35% of the reactor. In the steady state regime, based on this initial estimate, barium particles were considered to be present as sandwich type structure in the first 30-35% of the reactor whereas for rest of the reactor, a simpler configuration with an inner inaccessible carbonate core surrounded by a nitrate layer was considered. Since the inner barium carbonate core cannot store the NOx in steady state cyclic operation, the assumed sandwich type structure of the carbonate at the end of rich phase, was approximated by a completely regenerated barium carbonate particle which can store the NOx up to a smaller depth as compared to the completely regenerated

barium carbonate particle in the fresh catalyst. Therefore, the barium carbonate fraction with a value equal to one for the first 30-35% of reactor, and equal to some lower arbitrary value for the rest of reactor was assumed to solve the model. The rate constants for the four selected rich phase reactions along with the diffusion function describing the storage of NOx in the barium particle in the lean phase were estimated and very close fitting was obtained between the predicted and the experimental NOx concentrations. In addition, the NO oxidation kinetics were also modified. Since only the first 30-35% of the reactor was assumed to be consumed in the lean phase, the NO_2 concentration based on the earlier estimated kinetics for the NO oxidation reaction was observed to be higher than the experimental observation. The decrease in the NO oxidation kinetics to fit the data in steady state suggests that more than 30-35% of the reactor may have to be regenerated in the rich. The simulation results also reveal that the diffusion in the approximated barium-carbonate particle drops to a very low value drastically after a certain depth as compared to the diffusion in the fresh catalyst. This confirms that after consuming the outermost carbonate layer, the NOx has to diffuse through a relatively larger nitrate layer and the innermost carbonate is almost inaccessible for further reactions. The diffusion value in the approximated barium carbonate particle was expected to be the same as the one in the fresh catalyst for the uppermost carbonate layer but was observed to be relatively lower. One of the possible reasons for this discrepancy is the assumption of same thickness for the outer barium carbonate layer along the length of catalyst. However, in actual operation, the thickness is varying with respect to axial position due to different degree of regeneration along the catalyst length. Another reason could be the presence of multiple carbonate rings at the end of rich phase because the reductant may not be following the Pt/Ba proximity effect in the rich phase and can be equally reactive with the nitrates located at different distances from the Pt sites. If this is the case, then the results also indicate the possibility of a reductant spillover effect.

Although the storage mechanism has been explained well in this study, significant work has to be done in explaining the regeneration mechanism along the catalyst length. The results from the simulations in the transient and the steady state regime reveal the valuable information about the possibilities in regeneration mechanisms that can help in improving the predictions in future.

Based on these conclusions, the present work can be extended in the future in the following directions:

1. Although some of the possible mechanisms for the regeneration of carbonates in the rich phase have been presented in this study, the exact picture is still unclear. The immediate work in the future will be the estimation of rich phase reaction kinetics to predict the regeneration

along the larger catalyst length as compared to the predictions by preliminary simulations reported in this study.

2. If the larger spread of regeneration is insufficient to explain the transient data, the multiple carbonate rings at the end of the rich phase accounting for the reductant spillover effect may have to be considered. In one of the ways to model the multiple carbonate rings, the diffusion function has to be adapted from cycle to cycle.

3. In the cyclic operation, the required amounts of NOx can be stored in each lean phase only if sufficient amounts of storage sites have been regenerated in the previous rich phase. Since the regeneration depends on the amounts of fuel injected, there is a potential to address the optimal operating conditions to have better trade-off between the amount of fuel consumed and the amounts of NOx reduced.

4. At 300^{o}C, the temperature rise in the lean and the rich phase is not very significant for the conditions considered, leading to the assumption of isothermal conditions in this thesis. However, at higher temperatures where the temperature rise can be very significant, the model has to be solved with energy balance equations.

5. Estimation of the lean phase reaction kinetics has been presented at 300^{o}C. However, at different temperatures, the different types of barium particles can exhibit different storage dynamics and the corresponding diffusivity function may have to be estimated accordingly. Therefore, estimation of the rate kinetics and the diffusion function at different temperatures involve a significant amount of work in order to understand the storage dynamics over the range of temperatures.

Appendix A

The reactions used in the proposed model

Reaction	Rate Expressions
$NO + \frac{1}{2}O_2 \overset{r_1}{\leftrightarrow} NO_2$	$r_1 = k_1 * \left(c_{NO} * c_{O_2}^{0.5} - \frac{c_{NO_2}}{K_1^{eq}}\right) \Big/ \left(1 + K_1 * c_{NO_2}^{0.7}\right)$
$2NO_2 + \frac{1}{2}O_2 + BaCO_3 \overset{r_2}{\rightarrow} Ba(NO_3)_2 + CO_2$	$r_2 = \psi_{NOx} * \frac{k_2}{1 + k_2 \frac{r_{tot} - r_i}{D_{eff_{NO_2}}} \frac{r_i}{r_{tot}} \theta_{BaCO_3}} * c_{NO_2} * \theta_{BaCO_3} * c_{O_2}^{0.25}$
$2NO + \frac{3}{2}O_2 + BaCO_3 \overset{r_3}{\rightarrow} Ba(NO_3)_2 + CO_2$	$r_3 = \psi_{NOx} * \frac{k_3}{1 + k_3 \frac{r_{tot} - r_i}{D_{eff_{NO_2}}} \frac{r_i}{r_{tot}} \theta_{BaCO_3}} * c_{NO} * \theta_{BaCO_3} * c_{O_2}^{0.75}$
$Ce_2O_3 + \frac{1}{2}O_2 \overset{r_4}{\rightarrow} 2CeO_2$	$r_4 = k_4 \, \psi_{O_2} C_{O_2} \left(1 - \theta_{CeO_2}\right)$
$CO + 2CeO_2 \overset{r_5}{\rightarrow} CO_2 + Ce_2O_3$	$r_5 = k_5 \, \psi_{O_2} C_{CO} \theta_{CeO_2}$
$H_2 + 2CeO_2 \overset{r_6}{\rightarrow} H_2O + Ce_2O_3$	$r_6 = k_6 \, \psi_{O_2} C_{H_2} \theta_{CeO_2}$
$CO + \frac{1}{2}O_2 \overset{r_7}{\rightarrow} CO_2$	$r_7 = k_7 \frac{C_{CO} C_{O_2}}{(1 + K_7 C_{CO})^2 (1 + K_1 C_{NO}^{0.7})}$
$H_2 + \frac{1}{2}O_2 \overset{r_8}{\rightarrow} H_2O$	$r_8 = k_8 \frac{C_{H_2} C_{O_2}}{(1 + K_8 C_{CO})^2 (1 + K_1 C_{NO}^{0.7})}$
$H_2O + CO \overset{r_9}{\leftrightarrow} H_2 + CO_2$	$r_9 = k_9 \left(C_{CO} C_{H_2O} - \frac{C_{CO_2} C_{H_2}}{K_9^{eq}}\right)$
$Ba(NO_3)_2 + CO_2 \overset{r_{10}}{\rightarrow} 2NO + \frac{3}{2}O_2 + BaCO_3$	$r_{10} = k_{10} * \psi_{NOx} * \frac{1}{\left(1 + \exp\left(-X_1 * \left(\theta_{Ba(NO_3)_2} - Y_1\right)\right)\right)}$
$Ba(NO_3)_2 + CO_2 \overset{r_{11}}{\rightarrow} 2\,NO_2 + \frac{1}{2}O_2 + BaCO_3$	$r_{11} = k_{11} * \psi_{NOx} * \frac{1}{\left(1 + \exp\left(-X_2 * \left(\theta_{Ba(NO_3)_2} - Y_2\right)\right)\right)}$

Reaction	Rate Expressions
$3CO + Ba(NO_3)_2 \xrightarrow{r_{12}} BaCO_3 + 2NO + 2CO_2$	$r_{12} = k_{12} * \psi_{NOx} * C_{CO} * \theta_{Ba(NO_3)_2}$
$3H_2 + Ba(NO_3)_2 \xrightarrow{r_{13}} BaCO_3 + 2NO + 2H_2O$	$r_{13} = k_{13} * \psi_{NOx} * C_{H_2} * \theta_{Ba(NO_3)_2}$
$CO + NO \xrightarrow{r_{14}} CO_2 + \frac{1}{2}N_2$	$r_{14} = k_{14} * C_{CO} * C_{NO}$
$H_2 + NO \xrightarrow{r_{15}} H_2O + \frac{1}{2}N_2$	$r_{15} = k_{15} * C_{H_2} * C_{NO}$

Appendix B

COMSOL Code

```
% Start of the algorithm

function F = modelfile

clear all
clc

% vector of parameters related to the rich phase reactions
w=[600 0 15 3];

% vector of parameters related to the lean phase reactions
v=[10 1.15 7.5 3.5 0.15 0.01 2.15 1 1.15 1.15];

flclear fem

% COMSOL version
clear vrsn
vrsn.name = 'COMSOL 3.4';
vrsn.ext = '';
vrsn.major = 0;
vrsn.build = 248;
vrsn.rcs = '$Name:  $';
vrsn.date = '$Date: 2007/10/10 16:07:51 $';
fem.version = vrsn;

% Geometry
g1=solid1([0,0.075]);

% Analyzed geometry
clear s
s.objs={g1};
s.name={'I1'};
s.tags={'g1'};

fem.draw=struct('s',s);
fem.geom=geomcsg(fem);

% Initialize mesh
fem.mesh=meshinit(fem,'hmax',0.001);

% Application mode 1 (defining the gas phase mass balance equations)
clear appl
appl.mode.class = 'FlPDEG';
appl.dim = {'c_NO','c_NO2','c_O2','c_CO','c_H2','c_CO2','c_H2O', ...
  'c_N2','c_NO_t','c_NO2_t','c_O2_t','c_CO_t','c_H2_t', ...
  'c_CO2_t','c_H2O_t','c_N2_t'};
appl.name = 'B_C';
appl.gporder = 4;
appl.cporder = 2;
appl.assignsuffix = '_B_C';
clear bnd
```

```
bnd.r = {{'-c_NO';'-c_NO2';'-c_O2';'-c_CO';'-c_H2';'-c_CO2'; ...
  '-c_H2O';'-c_N2'},{'-c_NO+c_NO_in';'-c_NO2+c_NO2_in';'-c_O2+c_O2_in';'-
c_CO+c_CO_in'; ...
  '-c_H2+c_H2_in';'-c_CO2+c_CO2_in';'-c_H2O+c_H2O_in'; ...
  '-c_N2+c_N2_in'}};
bnd.type = {'neu','dir'};
bnd.ind = [2,1];
appl.bnd = bnd;
clear equ
equ.f = {{'(-c_NOx*v)+kc*Sg*((cs_NO.*(cs_NO>0))-(c_NO.*(c_NO>0)))'; ...
    '(-c_NO2x*v)+kc*Sg*((cs_NO2.*(cs_NO2>0))-(c_NO2.*(c_NO2>0)))'; ...
    '(-c_O2x*v)+kc*Sg*((cs_O2.*(cs_O2>0))-(c_O2.*(c_O2>0)))'; ...
    '(-c_COx*v)+kc*Sg*((cs_CO.*(cs_CO>0))-(c_CO.*(c_CO>0)))'; ...
    '(-c_H2x*v)+kc*Sg*((cs_H2.*(cs_H2>0))-(c_H2.*(c_H2>0)))'; ...
    '(-c_CO2x*v)+kc*Sg*((cs_CO2.*(cs_CO2>0))-(c_CO2.*(c_CO2>0)))'; ...
    '(-c_H2Ox*v)+kc*Sg*((cs_H2O.*(cs_H2O>0))-(c_H2O.*(c_H2O>0)))'; ...
    '(-c_N2x*v)+kc*Sg*((cs_N2.*(cs_N2>0))-(c_N2.*(c_N2>0)))'}};
equ.ga = 0;
equ.ind = [1];
appl.equ = equ;
fem.appl{1} = appl;

% Application mode 2 (defining the washcoat phase mass balance equations)
clear appl
appl.mode.class = 'FlPDEG';
appl.dim = {'cs_NO','cs_NO2','cs_O2','cs_CO','cs_H2','cs_CO2', ...
  'cs_H2O','cs_N2','cs_NO_t','cs_NO2_t','cs_O2_t','cs_CO_t','cs_H2_t', ...
  'cs_CO2_t','cs_H2O_t','cs_N2_t'};
appl.name = 'W_C';
appl.gporder = 4;
appl.cporder = 2;
appl.assignsuffix = '_W_C';
clear bnd
bnd.type = 'neu';
bnd.ind = [1,1];
appl.bnd = bnd;
clear equ
equ.f = {{'(kc*Ss*((c_NO.*(c_NO>0))-(cs_NO.*(cs_NO>0)))-r7-
2*r8+2*r10+2*r11-r14-r15+2*r16)/e_s'; ...
  '(kc*Ss*((c_NO2.*(c_NO2>0))-(cs_NO2.*(cs_NO2>0)))+r7-2*r9+2*r17)/e_s';
...
  '(kc*Ss*((c_O2.*(c_O2>0))-(cs_O2.*(cs_O2>0)))-0.5*r1-0.5*r2-0.5*r4-
0.5*r7-2*0.75*r8-2*0.25*r9+2*0.75*r16+2*0.25*r17)/e_s'; ...
  '(kc*Ss*((c_CO.*(c_CO>0))-(cs_CO.*(cs_CO>0)))-r1-r3-r5-3*r10-5*r12-
r14)/e_s'; ...
  '(kc*Ss*((c_H2.*(c_H2>0))-(cs_H2.*(cs_H2>0)))-r2+r3-r6-3*r11-5*r13-
r15)/e_s'; ...
  '(kc*Ss*((c_CO2.*(c_CO2>0))-
(cs_CO2.*(cs_CO2>0)))+r1+r3+r5+2*0.5*r8+2*0.5*r9+3*r10-r11+4*r12-r13+r14-
2*0.5*r16-2*0.5*r17)/e_s'; ...
  '(kc*Ss*((c_H2O.*(c_H2O>0))-(cs_H2O.*(cs_H2O>0)))+r2-
r3+r6+3*r11+5*r13+r15)/e_s'; ...
  '(kc*Ss*((c_N2.*(c_N2>0))-
(cs_N2.*(cs_N2>0)))+r12+r13+0.5*r14+0.5*r15)/e_s'}};
equ.ga = 0;
equ.ind = [1];
appl.equ = equ;
```

```
fem.appl{2} = appl;

% Application mode 3 (defining the mass balance equations for surface
species)

clear appl
appl.mode.class = 'FlPDEG';
appl.dim = {'s_Ce2O3','s_CeO2','s_BaCO3','s_Ba_NO3_2', ...
  's_Ce2O3_t','s_CeO2_t','s_BaCO3_t','s_Ba_NO3_2_t'};
appl.name = 'coverages';
appl.gporder = 4;
appl.cporder = 2;
appl.assignsuffix = '_coverages';
clear bnd
bnd.type = 'neu';
bnd.ind = [1,1];
appl.bnd = bnd;
clear equ
equ.f = {{'(-r4+r5+r6)/sigmaO2'; ...
    '(r4-r5-r6)/sigmaO2'; ...
    '(-0.5*2*r8-0.5*2*r9+r10+r11+r12+r13+2*0.5*r16+2*0.5*r17)/sigmaNOx';
...
    '(0.5*2*r8+0.5*2*r9-r10-r11-r12-r13-2*0.5*r16-2*0.5*r17)/sigmaNOx'}};
equ.init = {{1;0;1;0;0;0;0;0}};
equ.ga = 0;
equ.ind = [1];
appl.equ = equ;
fem.appl{3} = appl;

% Application mode 4 (defining the arbitrary model parameters used to
solve the model in cyclic mode)

clear appl
appl.mode.class = 'FlPDEG';
appl.dim =
{'R_1','R_2','R_3','theta_1','theta_3','R_1_t','R_2_t','R_3_t','theta_1_t'
,'theta_3_t'};
appl.name = 'coupling';
appl.gporder = 4;
appl.cporder = 2;
appl.assignsuffix = '_coupling';
clear bnd
bnd.type = 'neu';
bnd.ind = [1,1];
appl.bnd = bnd;
clear equ
equ.f = {{'R_1-Rm';'R_2-Rm';'R_3-Rm';'theta_1-s_BaCO3';'theta_3-
s_BaCO3'}};
equ.init = {{0;0;0;0;0;0;0;0;0;0}};
equ.da = 0;
equ.ga = 0;
equ.ind = [1];
appl.equ = equ;
fem.appl{4} = appl;
fem.frame = {'ref'};
fem.border = 1;
```

```
clear units;
units.basesystem = 'SI';
fem.units = units;

 % Constants
fem.const = {'T_in','573', ...
  'Rg','8.314', ...
  'Sg','(2*0.000625)/(.000625^2)', ...
  'Ss','(2*0.000625)/(.000665^2-0.000625^2)', ...
  'e_g','(0.000625^2)/(0.000665^2)', ...
  'F','(T_in*10^6*8.314)/(101325)', ...
  'e_s','0.95', ...
  'kc','0.05'};

% duration of the lean phase
lt=150;

% duration of the rich phase
rt=5;

% Starting Time
time=0;

tic

% Start of the cycle
cycle=1;

while (cycle<=15)

% Expressions for first lean phase

    if (cycle==1)

% Global expressions
fem.globalexpr = {'c_NO_in','(0.00033*101325*(flc2hs(t-
0.25,0.25)))/(8.314*T_in)', ...
  'c_O2_in','(0.1*101325*(flc2hs(t-0.25,0.25)))/(8.314*T_in)', ...
  'c_CO2_in','(0.05*101325*(flc2hs(t-0.25,0.25)))/(8.314*T_in)', ...
  'c_H2O_in','(0.05*101325*(flc2hs(t-0.25,0.25)))/(8.314*T_in)', ...
  'c_N2_in','(0.7997*101325*(flc2hs(t-0.25,0.25)))/(8.314*T_in)', ...
  'c_NO2_in','0', ...
  'c_H2_in','0', ...
  'c_CO_in','0', ...
  'v','(14.32/(1000*60*169))/(.000625^2*3.14)', ...
  'D','0', ...
  'sigmaNOx','650', ...
  'sigmaO2','600', ...
  'r1','(k1*(cs_CO.*(cs_CO>0))*(cs_O2.*(cs_O2>0)))/G1', ...
  'r2','(k2*(cs_H2.*(cs_H2>0))*(cs_O2.*(cs_O2>0)))/G1', ...
  'r3','k3*(((cs_CO.*(cs_CO>0))*(cs_H2O.*(cs_H2O>0)))-
(((cs_CO2.*(cs_CO2>0))*(cs_H2.*(cs_H2>0)))/K3_eq))', ...
  'r4','k4*sigmaO2*((cs_O2.*(cs_O2>0)))*(1-s_CeO2)', ...
  'r5','k5*sigmaO2*(cs_CO.*(cs_CO>0))*s_CeO2', ...
  'r6','k6*sigmaO2*(cs_H2.*(cs_H2>0))*s_CeO2', ...
```

```
'r7','(k7/1/(1+K4*((cs_NO2.*(cs_NO2>0))^inhibit))^1)*(((cs_NO.*(cs_NO>0))*
((cs_O2.*(cs_O2>0))^0.5))-((cs_NO2.*(cs_NO2>0))/K7_eq))', ...

'r8','sigmaNOx*(k8f*(cs_NO.*(cs_NO>0))*((cs_O2.*(cs_O2>0))^0.75)*(s_BaCO3.
*(s_BaCO3>0)))', ...

'r9','sigmaNOx*(k9f*(cs_NO2.*(cs_NO2>0))*((cs_O2.*(cs_O2>0))^0.25)*(s_BaCO
3.*(s_BaCO3>0)))', ...
  'r10','(k10*sigmaNOx*((cs_CO.*(cs_CO>0))^1)*(s_Ba_NO3_2^PowerNO3))', ...
  'r11','(k11*sigmaNOx*((cs_H2.*(cs_H2>0))^1)*(s_Ba_NO3_2^PowerNO3))', ...
  'r12','(k12*sigmaNOx*((cs_CO.*(cs_CO>0))^1)*(s_Ba_NO3_2^PowerNO3))', ...
  'r13','(k13*sigmaNOx*((cs_H2.*(cs_H2>0))^1)*(s_Ba_NO3_2^PowerNO3))', ...
  'r14','k14*(cs_CO.*(cs_CO>0))*((cs_NO.*(cs_NO>0))^PowerNO)', ...
  'r15','k15*(cs_H2.*(cs_H2>0))*((cs_NO.*(cs_NO>0))^PowerNO)', ...
  'r16','(k16*sigmaNOx/(1+exp(-20*(s_Ba_NO3_2-0.3))))', ...
  'r17','(k17*sigmaNOx/(1+exp(-20*(s_Ba_NO3_2-0.5))))', ...
  'k1','A1*10^14*exp(-95000/Rg/Ts)', ...
  'k2','A2*10^14*exp(-95000/Rg/Ts)', ...
  'k3','A3*10^10*exp(-90000/Rg/Ts)', ...
  'k4','A4*10^7*exp(-90000/Rg/Ts)', ...
  'k5','A5*10^8*exp(-90000/Rg/Ts)', ...
  'k6','A6*10^8*exp(-90000/Rg/Ts)', ...
  'k7','A7*10^6*exp(-40000/Rg/Ts)*(flc2hs(t-0.25,0.25))', ...
  'k8','A8*10^2*exp(-20000/Rg/Ts)*(flc2hs(t-0.25,0.25))', ...
  'k9','A9*10^7*exp(-80000/Rg/Ts)*(flc2hs(t-0.25,0.25))', ...
  'k10','A10*10^7*exp(-90000/Rg/Ts)', ...
  'k11','A11*10^7*exp(-90000/Rg/Ts)', ...
  'k12','A12*10^8*exp(-90000/Rg/Ts)', ...
  'k13','A13*10^8*exp(-90000/Rg/Ts)', ...
  'k14','A14*10^9*exp(-70000/Rg/Ts)', ...
  'k15','A15*10^9*exp(-70000/Rg/Ts)', ...
  'k16','A16*2*0.375*10^-4', ...
  'k17','A17*2*10^-4', ...
  'A1','0.2', ...
  'A2','0.2', ...
  'A3','1', ...
  'A4','10', ...
  'A5',w(4), ...
  'A6',w(4), ...
  'A7',v(7), ...
  'A8',v(8), ...
  'A9','100', ...
  'A10',w(3), ...
  'A11',w(3), ...
  'A12',w(2), ...
  'A13',w(2), ...
  'A14',w(1), ...
  'A15',w(1), ...
  'A16',v(9), ...
  'A17',v(10), ...
  'inhibit','0.7', ...
  'K3_eq','exp(-4.33+(4577.8/Ts))', ...
  'K7_eq','exp((57100-Ts*73)/(8.314*Ts))*((Rg*Ts/100000)^0.5)', ...
  'G1','((1+K1*(cs_CO.*(cs_CO>0)))^2)*(1+K4*((cs_NO2.*(cs_NO2>0))^0.7))',
...
  'K1','65.55*exp(961/Ts)', ...
```

```
  'K2','2.08*1000*exp(361/Ts)', ...
  'K3','3.98*exp(11611/Ts)', ...
  'K4','4.79*10^5*exp(-3733/Ts)', ...
  'rbase_c','(50-50/1)*flc2hs(x-0.02,0.01)+50/1', ...
  'rbase_n','(62.5-62.5/1)*flc2hs(x-0.02,0.01)+62.5/1', ...
  'rtot','((rbase_n-rbase_c)*(flc2hs(s_Ba_NO3_2-
0.5,0.45))+rbase_c)/(10^9)', ...
  'l','rtot-Rm', ...
  'D_NO2',v(1), ...
  'D_NO',v(2), ...
  'slope_NO2',v(3), ...
  'slope_NO',v(4), ...
  'limit_NO2',v(5), ...
  'limit_NO',v(6), ...
  'Deff_NO2','(D_NO2*10^-9)*exp(-slope_NO2*(1-Rm/rtot-limit_NO2))/(1+exp(-
slope_NO2*(1-Rm/rtot-limit_NO2)))', ...
  'Deff_NO','(D_NO*10^-9)*exp(-slope_NO*(1-Rm/rtot-limit_NO))/(1+exp(-
slope_NO*(1-Rm/rtot-limit_NO)))', ...
  'k8f','k8/(1+k8*(l/Deff_NO)*(Rm/rtot)*s_BaCO3)', ...
  'k9f','k9/(1+k9*(l/Deff_NO2)*(Rm/rtot)*s_BaCO3)', ...
  'Rm','(rtot*(0.5*s_BaCO3/(1-0.5*s_BaCO3))^(1/3))', ...
  'PowerNO','1', ...
  'PowerNO3','1', ...
  'Ts','T_in'};

% Multiphysics
fem=multiphysics(fem);

% Extend mesh
fem.xmesh=meshextend(fem);

% Solve problem
fem.sol=femtime(fem, ...

'solcomp',{'R_1','theta_1','c_CO','c_N2','cs_CO','c_CO2','s_Ce2O3','s_Ba_N
O3_2','cs_H2','c_NO2','c_H2','cs_CO2','cs_O2','c_H2O','cs_NO','s_CeO2','cs
_N2','cs_H2O','cs_NO2','s_BaCO3','c_NO','c_O2'}, ...

'outcomp',{'R_1','R_2','R_3','theta_1','theta_3','c_CO','c_N2','cs_CO','c_
CO2','s_Ce2O3','s_Ba_NO3_2','cs_H2','c_NO2','c_H2','cs_CO2','cs_O2','c_H2O
','cs_NO','s_CeO2','cs_N2','cs_H2O','cs_NO2','s_BaCO3','c_NO','c_O2'}, ...
                'tlist',[0:0.5:lt], ...
                'atol',{'1e-6'}, ...
                'rtol',1e-4, ...
                'maxorder',2, ...
                'tout','tlist');

fem1=fem;

% Saving the data to text files

dlmwrite('c_NO.txt',[postinterp(fem1,'t',0,'solnum','all')+time
postinterp(fem1,'c_NO*F',fem1.mesh.p,'solnum','all')], 'delimiter',
'\t','precision', '%.2f');
```

```
dlmwrite('c_NO2.txt',[postinterp(fem1,'t',0,'solnum','all')+time
postinterp(fem1,'c_NO2*F',fem1.mesh.p,'solnum','all')], 'delimiter',
'\t','precision', '%.2f');
dlmwrite('s_CeO2.txt',[postinterp(fem1,'t',0,'solnum','all')+time
postinterp(fem1,'s_CeO2',fem1.mesh.p,'solnum','all')], 'delimiter',
'\t','precision', '%.2f');
dlmwrite('s_BaCO3.txt',[postinterp(fem1,'t',0,'solnum','all')+time
postinterp(fem1,'s_BaCO3',fem1.mesh.p,'solnum','all')], 'delimiter',
'\t','precision', '%.2f');
dlmwrite('c_CO.txt',[postinterp(fem1,'t',0,'solnum','all')+time
postinterp(fem1,'c_CO*(F/10^6)',fem1.mesh.p,'solnum','all')], 'delimiter',
'\t','precision', '%.2f');

toc

% Expressions for even lean phase

    elseif(rem(cycle,2)==0)

% Global expressions
fem.globalexpr = {'c_NO_in','(0.00033*101325*(flc2hs(t-
0.25,0.25)))/(8.314*T_in)', ...
  'c_O2_in','(0.1*101325*(flc2hs(t-0.25,0.25)))/(8.314*T_in)', ...
  'c_CO2_in','(0.05*101325)/(8.314*T_in)', ...
  'c_H2O_in','(0.05*101325)/(8.314*T_in)', ...
  'c_N2_in','(0.7997*101325)/(8.314*T_in)', ...
  'c_NO2_in','0', ...
  'c_H2_in','0', ...
  'c_CO_in','(0.015*101325*(1-flc2hs(t-0.25,0.25)))/(8.314*T_in)', ...
  'v','(14.32/(1000*60*169))/(.000625^2*3.14)', ...
  'D','0', ...
  'sigmaNOx','650', ...
  'sigmaO2','600', ...
  'r1','(k1*(cs_CO.*(cs_CO>0))*(cs_O2.*(cs_O2>0)))/G1', ...
  'r2','(k2*(cs_H2.*(cs_H2>0))*(cs_O2.*(cs_O2>0)))/G1', ...
  'r3','k3*(((cs_CO.*(cs_CO>0))*(cs_H2O.*(cs_H2O>0)))-
(((cs_CO2.*(cs_CO2>0))*(cs_H2.*(cs_H2>0)))/K3_eq))', ...
  'r4','k4*sigmaO2*((cs_O2.*(cs_O2>0)))*(1-s_CeO2)', ...
  'r5','k5*sigmaO2*(cs_CO.*(cs_CO>0))*s_CeO2', ...
  'r6','k6*sigmaO2*(cs_H2.*(cs_H2>0))*s_CeO2', ...

'r7','(k7/1/(1+K4*((cs_NO2.*(cs_NO2>0))^inhibit))^1)*(((cs_NO.*(cs_NO>0))*
((cs_O2.*(cs_O2>0))^0.5))-((cs_NO2.*(cs_NO2>0))/K7_eq))', ...

'r8','sigmaNOx*(k8f*(cs_NO.*(cs_NO>0))*((cs_O2.*(cs_O2>0))^0.75)*(s_BaCO3.
*(s_BaCO3>0)))', ...

'r9','sigmaNOx*(k9f*(cs_NO2.*(cs_NO2>0))*((cs_O2.*(cs_O2>0))^0.25)*(s_BaCO
3.*(s_BaCO3>0)))', ...
  'r10','(k10*sigmaNOx*((cs_CO.*(cs_CO>0))^1)*(s_Ba_NO3_2^PowerNO3))', ...
  'r11','(k11*sigmaNOx*((cs_H2.*(cs_H2>0))^1)*(s_Ba_NO3_2^PowerNO3))', ...
  'r12','(k12*sigmaNOx*((cs_CO.*(cs_CO>0))^1)*(s_Ba_NO3_2^PowerNO3))', ...
  'r13','(k13*sigmaNOx*((cs_H2.*(cs_H2>0))^1)*(s_Ba_NO3_2^PowerNO3))', ...
  'r14','k14*(cs_CO.*(cs_CO>0))*((cs_NO.*(cs_NO>0))^PowerNO)', ...
  'r15','k15*(cs_H2.*(cs_H2>0))*((cs_NO.*(cs_NO>0))^PowerNO)', ...
  'r16','(k16*sigmaNOx/(1+exp(-20*(s_Ba_NO3_2-0.3))))', ...
```

```
  'r17','(k17*sigmaNOx/(1+exp(-20*(s_Ba_NO3_2-0.5))))', ...
  'k1','A1*10^14*exp(-95000/Rg/Ts)*(1-flc2hs(t-0.25,0.25))', ...
  'k2','A2*10^14*exp(-95000/Rg/Ts)*(1-flc2hs(t-0.25,0.25))', ...
  'k3','A3*10^10*exp(-90000/Rg/Ts)*(1-flc2hs(t-0.25,0.25))', ...
  'k4','A4*10^7*exp(-90000/Rg/Ts)*(flc2hs(t-0.25,0.25))', ...
  'k5','A5*10^8*exp(-90000/Rg/Ts)*(1-flc2hs(t-0.25,0.25))', ...
  'k6','A6*10^8*exp(-90000/Rg/Ts)*(1-flc2hs(t-0.25,0.25))', ...
  'k7','A7*10^6*exp(-40000/Rg/Ts)*(flc2hs(t-0.25,0.25))', ...
  'k8','A8*10^2*exp(-20000/Rg/Ts)*(flc2hs(t-0.25,0.25))', ...
  'k9','A9*10^7*exp(-80000/Rg/Ts)*(flc2hs(t-0.25,0.25))', ...
  'k10','A10*10^7*exp(-90000/Rg/Ts)*(1-flc2hs(t-0.25,0.25))', ...
  'k11','A11*10^7*exp(-90000/Rg/Ts)*(1-flc2hs(t-0.25,0.25))', ...
  'k12','A12*10^8*exp(-90000/Rg/Ts)*(1-flc2hs(t-0.25,0.25))', ...
  'k13','A13*10^8*exp(-90000/Rg/Ts)*(1-flc2hs(t-0.25,0.25))', ...
  'k14','A14*10^9*exp(-70000/Rg/Ts)*(1-flc2hs(t-0.25,0.25))', ...
  'k15','A15*10^9*exp(-70000/Rg/Ts)*(1-flc2hs(t-0.25,0.25))', ...
  'k16','A16*2*0.375*10^-4', ...
  'k17','A17*2*10^-4', ...
  'A1','0.2', ...
  'A2','0.2', ...
  'A3','1', ...
  'A4','10', ...
  'A5',w(4), ...
  'A6',w(4), ...
  'A7',v(7), ...
  'A8',v(8), ...
  'A9','100', ...
  'A10',w(3), ...
  'A11',w(3), ...
  'A12',w(2), ...
  'A13',w(2), ...
  'A14',w(1), ...
  'A15',w(1), ...
  'A16',v(9), ...
  'A17',v(10), ...
  'inhibit','0.7', ...
  'K3_eq','exp(-4.33+(4577.8/Ts))', ...
  'K7_eq','exp((57100-Ts*73)/(8.314*Ts))*((Rg*Ts/100000)^0.5)', ...
  'G1','((1+K1*(cs_CO.*(cs_CO>0)))^2)*(1+K4*((cs_NO2.*(cs_NO2>0))^0.7))',
...
  'K1','65.55*exp(961/Ts)', ...
  'K2','2.08*1000*exp(361/Ts)', ...
  'K3','3.98*exp(11611/Ts)', ...
  'K4','4.79*10^5*exp(-3733/Ts)', ...
  'rbase_c','(50-50/1)*flc2hs(x-0.02,0.01)+50/1', ...
  'rbase_n','(62.5-62.5/1)*flc2hs(x-0.02,0.01)+62.5/1', ...
  'rtot','((rbase_n-rbase_c)*(flc2hs(s_Ba_NO3_2-
0.5,0.45))+rbase_c)/(10^9)', ...
  'l','rtot-Rm', ...
  'D_NO2',v(1), ...
  'D_NO',v(2), ...
  'slope_NO2',v(3), ...
  'slope_NO',v(4), ...
  'limit_NO2',v(5), ...
  'limit_NO',v(6), ...
  'Deff_NO2','(D_NO2*10^-9)*exp(-slope_NO2*(1-Rm/rtot-limit_NO2))/(1+exp(-
slope_NO2*(1-Rm/rtot-limit_NO2)))', ...
```

```
  'Deff_NO','(D_NO*10^-9)*exp(-slope_NO*(1-Rm/rtot-limit_NO))/(1+exp(-
slope_NO*(1-Rm/rtot-limit_NO)))', ...
  'k8f','k8/(1+k8*(l/Deff_NO)*(Rm/rtot)*s_BaCO3)', ...
  'k9f','k9/(1+k9*(l/Deff_NO2)*(Rm/rtot)*s_BaCO3)', ...
  'Rm','(R1-R2)*flc2hs(s_BaCO3-theta_1-0.005,0.005)+R2', ...
  'R1','(rtot*(((1-0.5*s_BaCO3)*((R_1/rtot)^3)-(1-
0.5*s_BaCO3)*((R_2/rtot)^3)-0.5*s_BaCO3)/(0.5*s_BaCO3-1))^(1/3))', ...
  'R2','(rtot*(0.5*s_BaCO3/(1-0.5*s_BaCO3))^(1/3))', ...
  'PowerNO','1', ...
  'PowerNO3','1', ...
  'Ts','T_in'};

% Multiphysics
fem=multiphysics(fem);

% Extend mesh
fem.xmesh=meshextend(fem);

% Mapping stored solution to extended mesh
init = asseminit(fem,'init',fem1.sol,'solnum',length(fem1.sol.tlist));

% Solve problem
fem.sol=femtime(fem, ...
                'init',init, ...

'solcomp',{'R_3','theta_3','c_CO','c_N2','cs_CO','c_CO2','s_Ce2O3','s_Ba_N
O3_2','cs_H2','c_NO2','c_H2','cs_CO2','cs_O2','c_H2O','cs_NO','s_CeO2','cs
_N2','cs_H2O','cs_NO2','s_BaCO3','c_NO','c_O2'}, ...

'outcomp',{'R_1','R_2','R_3','theta_1','theta_3','c_CO','c_N2','cs_CO','c_
CO2','s_Ce2O3','s_Ba_NO3_2','cs_H2','c_NO2','c_H2','cs_CO2','cs_O2','c_H2O
','cs_NO','s_CeO2','cs_N2','cs_H2O','cs_NO2','s_BaCO3','c_NO','c_O2'}, ...
                'tlist',[0:0.5:lt], ...
                'atol',{'1e-6'}, ...
                'rtol',1e-4, ...
                'maxorder',2, ...
                'tout','tlist');

fem1=fem;

% Saving the data to text files

dlmwrite('c_NO.txt',[postinterp(fem1,'t',0,'solnum','all')+time
postinterp(fem1,'c_NO*F',fem1.mesh.p,'solnum','all')],  '-
append','delimiter', '\t','precision', '%.6f');
dlmwrite('c_NO2.txt',[postinterp(fem1,'t',0,'solnum','all')+time
postinterp(fem1,'c_NO2*F',fem1.mesh.p,'solnum','all')],  '-
append','delimiter', '\t','precision', '%.6f');
dlmwrite('s_CeO2.txt',[postinterp(fem1,'t',0,'solnum','all')+time
postinterp(fem1,'s_CeO2',fem1.mesh.p,'solnum','all')], '-append',
'delimiter', '\t','precision', '%.6f');
dlmwrite('s_BaCO3.txt',[postinterp(fem1,'t',0,'solnum','all')+time
postinterp(fem1,'s_BaCO3',fem1.mesh.p,'solnum','all')], '-append',
'delimiter', '\t','precision', '%.6f');
```

```
dlmwrite('c_CO.txt',[postinterp(fem1,'t',0,'solnum','all')+time
postinterp(fem1,'c_CO*(F/10^6)',fem1.mesh.p,'solnum','all')], '-append',
'delimiter', '\t','precision', '%.6f');

toc

% Expressions for odd lean phase

    elseif(rem(cycle,2)==1)

% Global expressions
fem.globalexpr = {'c_NO_in','(0.00033*101325*(flc2hs(t-
0.25,0.25)))/(8.314*T_in)', ...
  'c_O2_in','(0.1*101325*(flc2hs(t-0.25,0.25)))/(8.314*T_in)', ...
  'c_CO2_in','(0.05*101325)/(8.314*T_in)', ...
  'c_H2O_in','(0.05*101325)/(8.314*T_in)', ...
  'c_N2_in','(0.7997*101325)/(8.314*T_in)', ...
  'c_NO2_in','0', ...
  'c_H2_in','0', ...
  'c_CO_in','(0.015*101325*(1-flc2hs(t-0.25,0.25)))/(8.314*T_in)', ...
  'v','(14.32/(1000*60*169))/(.000625^2*3.14)', ...
  'D','0', ...
  'sigmaNOx','650', ...
  'sigmaO2','600', ...
  'r1','(k1*(cs_CO.*(cs_CO>0))*(cs_O2.*(cs_O2>0)))/G1', ...
  'r2','(k2*(cs_H2.*(cs_H2>0))*(cs_O2.*(cs_O2>0)))/G1', ...
  'r3','k3*(((cs_CO.*(cs_CO>0))*(cs_H2O.*(cs_H2O>0)))-
(((cs_CO2.*(cs_CO2>0))*(cs_H2.*(cs_H2>0)))/K3_eq))', ...
  'r4','k4*sigmaO2*((cs_O2.*(cs_O2>0)))*(1-s_CeO2)', ...
  'r5','k5*sigmaO2*(cs_CO.*(cs_CO>0))*s_CeO2', ...
  'r6','k6*sigmaO2*(cs_H2.*(cs_H2>0))*s_CeO2', ...

'r7','(k7/1/(1+K4*((cs_NO2.*(cs_NO2>0))^inhibit))^1)*(((cs_NO.*(cs_NO>0))*
((cs_O2.*(cs_O2>0))^0.5))-((cs_NO2.*(cs_NO2>0))/K7_eq))', ...

'r8','sigmaNOx*(k8f*(cs_NO.*(cs_NO>0))*((cs_O2.*(cs_O2>0))^0.75)*(s_BaCO3.
*(s_BaCO3>0)))', ...

'r9','sigmaNOx*(k9f*(cs_NO2.*(cs_NO2>0))*((cs_O2.*(cs_O2>0))^0.25)*(s_BaCO
3.*(s_BaCO3>0)))', ...
  'r10','(k10*sigmaNOx*((cs_CO.*(cs_CO>0))^1)*(s_Ba_NO3_2^PowerNO3))', ...
  'r11','(k11*sigmaNOx*((cs_H2.*(cs_H2>0))^1)*(s_Ba_NO3_2^PowerNO3))', ...
  'r12','(k12*sigmaNOx*((cs_CO.*(cs_CO>0))^1)*(s_Ba_NO3_2^PowerNO3))', ...
  'r13','(k13*sigmaNOx*((cs_H2.*(cs_H2>0))^1)*(s_Ba_NO3_2^PowerNO3))', ...
  'r14','k14*(cs_CO.*(cs_CO>0))*((cs_NO.*(cs_NO>0))^PowerNO)', ...
  'r15','k15*(cs_H2.*(cs_H2>0))*((cs_NO.*(cs_NO>0))^PowerNO)', ...
  'r16','(k16*sigmaNOx/(1+exp(-20*(s_Ba_NO3_2-0.3))))', ...
  'r17','(k17*sigmaNOx/(1+exp(-20*(s_Ba_NO3_2-0.5))))', ...
  'k1','A1*10^14*exp(-95000/Rg/Ts)*(1-flc2hs(t-0.25,0.25))', ...
  'k2','A2*10^14*exp(-95000/Rg/Ts)*(1-flc2hs(t-0.25,0.25))', ...
  'k3','A3*10^10*exp(-90000/Rg/Ts)*(1-flc2hs(t-0.25,0.25))', ...
  'k4','A4*10^7*exp(-90000/Rg/Ts)*(flc2hs(t-0.25,0.25))', ...
  'k5','A5*10^8*exp(-90000/Rg/Ts)*(1-flc2hs(t-0.25,0.25))', ...
  'k6','A6*10^8*exp(-90000/Rg/Ts)*(1-flc2hs(t-0.25,0.25))', ...
  'k7','A7*10^6*exp(-40000/Rg/Ts)*(flc2hs(t-0.25,0.25))', ...
  'k8','A8*10^2*exp(-20000/Rg/Ts)*(flc2hs(t-0.25,0.25))', ...
```

```
  'k9','A9*10^7*exp(-80000/Rg/Ts)*(flc2hs(t-0.25,0.25))', ...
  'k10','A10*10^7*exp(-90000/Rg/Ts)*(1-flc2hs(t-0.25,0.25))', ...
  'k11','A11*10^7*exp(-90000/Rg/Ts)*(1-flc2hs(t-0.25,0.25))', ...
  'k12','A12*10^8*exp(-90000/Rg/Ts)*(1-flc2hs(t-0.25,0.25))', ...
  'k13','A13*10^8*exp(-90000/Rg/Ts)*(1-flc2hs(t-0.25,0.25))', ...
  'k14','A14*10^9*exp(-70000/Rg/Ts)*(1-flc2hs(t-0.25,0.25))', ...
  'k15','A15*10^9*exp(-70000/Rg/Ts)*(1-flc2hs(t-0.25,0.25))', ...
  'k16','A16*2*0.375*10^-4', ...
  'k17','A17*2*10^-4', ...
  'A1','0', ...
  'A1','0.2', ...
  'A2','0.2', ...
  'A3','1', ...
  'A4','10', ...
  'A5',w(4), ...
  'A6',w(4), ...
  'A7',v(7), ...
  'A8',v(8), ...
  'A9','100', ...
  'A10',w(3), ...
  'A11',w(3), ...
  'A12',w(2), ...
  'A13',w(2), ...
  'A14',w(1), ...
  'A15',w(1), ...
  'A16',v(9), ...
  'A17',v(10), ...
  'inhibit','0.7', ...
  'K3_eq','exp(-4.33+(4577.8/Ts))', ...
  'K7_eq','exp((57100-Ts*73)/(8.314*Ts))*((Rg*Ts/100000)^0.5)', ...
  'G1','((1+K1*(cs_CO.*(cs_CO>0)))^2)*(1+K4*((cs_NO2.*(cs_NO2>0))^0.7))',
...
  'K1','65.55*exp(961/Ts)', ...
  'K2','2.08*1000*exp(361/Ts)', ...
  'K3','3.98*exp(11611/Ts)', ...
  'K4','4.79*10^5*exp(-3733/Ts)', ...
  'rbase_c','(50-50/1)*flc2hs(x-0.02,0.01)+50/1', ...
  'rbase_n','(62.5-62.5/1)*flc2hs(x-0.02,0.01)+62.5/1', ...
  'rtot','((rbase_n-rbase_c)*(flc2hs(s_Ba_NO3_2-
0.5,0.45))+rbase_c)/(10^9)', ...
  'l','rtot-Rm', ...
  'D_NO2',v(1), ...
  'D_NO',v(2), ...
  'slope_NO2',v(3), ...
  'slope_NO',v(4), ...
  'limit_NO2',v(5), ...
  'limit_NO',v(6), ...
  'Deff_NO2','(D_NO2*10^-9)*exp(-slope_NO2*(1-Rm/rtot-limit_NO2))/(1+exp(-
slope_NO2*(1-Rm/rtot-limit_NO2)))', ...
  'Deff_NO','(D_NO*10^-9)*exp(-slope_NO*(1-Rm/rtot-limit_NO))/(1+exp(-
slope_NO*(1-Rm/rtot-limit_NO)))', ...
  'k8f','k8/(1+k8*(l/Deff_NO)*(Rm/rtot)*s_BaCO3)', ...
  'k9f','k9/(1+k9*(l/Deff_NO2)*(Rm/rtot)*s_BaCO3)', ...
  'Rm','(R1-R2)*flc2hs(s_BaCO3-theta_3-0.005,0.005)+R2', ...
  'R1','(rtot*(((1-0.5*s_BaCO3)*((R_3/rtot)^3)-(1-
0.5*s_BaCO3)*((R_2/rtot)^3)-0.5*s_BaCO3)/(0.5*s_BaCO3-1))^(1/3))', ...
  'R2','(rtot*(0.5*s_BaCO3/(1-0.5*s_BaCO3))^(1/3))', ...
```

```
  'PowerNO','1', ...
  'PowerNO3','1', ...
  'Ts','T_in'};

% Multiphysics
fem=multiphysics(fem);

% Extend mesh
fem.xmesh=meshextend(fem);

% Mapping stored solution to extended mesh
init = asseminit(fem,'init',fem1.sol,'solnum',length(fem1.sol.tlist));

% Solve problem
fem.sol=femtime(fem, ...
                'init',init, ...

'solcomp',{'R_1','theta_1','c_CO','c_N2','cs_CO','c_CO2','s_Ce2O3','s_Ba_N
O3_2','cs_H2','c_NO2','c_H2','cs_CO2','cs_O2','c_H2O','cs_NO','s_CeO2','cs
_N2','cs_H2O','cs_NO2','s_BaCO3','c_NO','c_O2'}, ...

'outcomp',{'R_1','R_2','R_3','theta_1','theta_3','c_CO','c_N2','cs_CO','c_
CO2','s_Ce2O3','s_Ba_NO3_2','cs_H2','c_NO2','c_H2','cs_CO2','cs_O2','c_H2O
','cs_NO','s_CeO2','cs_N2','cs_H2O','cs_NO2','s_BaCO3','c_NO','c_O2'}, ...
                'tlist',[0:0.5:lt], ...
                'atol',{'1e-6'}, ...
                'rtol',1e-4, ...
                'maxorder',2, ...
                'tout','tlist');

fem1=fem;

% Saving the data to text files

dlmwrite('c_NO.txt',[postinterp(fem1,'t',0,'solnum','all')+time
postinterp(fem1,'c_NO*F',fem1.mesh.p,'solnum','all')],  '-
append','delimiter', '\t','precision', '%.6f');
dlmwrite('c_NO2.txt',[postinterp(fem1,'t',0,'solnum','all')+time
postinterp(fem1,'c_NO2*F',fem1.mesh.p,'solnum','all')],  '-
append','delimiter', '\t','precision', '%.6f');
dlmwrite('s_CeO2.txt',[postinterp(fem1,'t',0,'solnum','all')+time
postinterp(fem1,'s_CeO2',fem1.mesh.p,'solnum','all')], '-append',
'delimiter', '\t','precision', '%.6f');
dlmwrite('s_BaCO3.txt',[postinterp(fem1,'t',0,'solnum','all')+time
postinterp(fem1,'s_BaCO3',fem1.mesh.p,'solnum','all')], '-append',
'delimiter', '\t','precision', '%.6f');
dlmwrite('c_CO.txt',[postinterp(fem1,'t',0,'solnum','all')+time
postinterp(fem1,'c_CO*(F/10^6)',fem1.mesh.p,'solnum','all')], '-append',
'delimiter', '\t','precision', '%.6f');

toc

    end

time=time+lt;
```

```
% Expressions for odd rich phase

if(rem(cycle,2)==1)

% Global expressions
fem.globalexpr = {'c_NO_in','(0.00033*101325*(1-flc2hs(t-
0.25,0.25)))/(8.314*T_in)', ...
  'c_O2_in','(0.1*101325*(1-flc2hs(t-0.25,0.25)))/(8.314*T_in)', ...
  'c_CO2_in','(0.05*101325)/(8.314*T_in)', ...
  'c_H2O_in','(0.05*101325)/(8.314*T_in)', ...
  'c_N2_in','(0.7997*101325)/(8.314*T_in)', ...
  'c_NO2_in','0', ...
  'c_H2_in','0', ...
  'c_CO_in','(0.015*101325*(flc2hs(t-0.25,0.25)))/(8.314*T_in)', ...
  'v','(14.32/(1000*60*169))/(.000625^2*3.14)', ...
  'D','0', ...
  'sigmaNOx','650', ...
  'sigmaO2','600', ...
  'r1','(k1*(cs_CO.*(cs_CO>0))*(cs_O2.*(cs_O2>0)))/G1', ...
  'r2','(k2*(cs_H2.*(cs_H2>0))*(cs_O2.*(cs_O2>0)))/G1', ...
  'r3','k3*(((cs_CO.*(cs_CO>0))*(cs_H2O.*(cs_H2O>0)))-
(((cs_CO2.*(cs_CO2>0))*(cs_H2.*(cs_H2>0)))/K3_eq))', ...
  'r4','k4*sigmaO2*((cs_O2.*(cs_O2>0)))*(1-s_CeO2)', ...
  'r5','k5*sigmaO2*(cs_CO.*(cs_CO>0))*s_CeO2', ...
  'r6','k6*sigmaO2*(cs_H2.*(cs_H2>0))*s_CeO2', ...

'r7','(k7/1/(1+K4*((cs_NO2.*(cs_NO2>0))^inhibit))^1)*(((cs_NO.*(cs_NO>0))*
((cs_O2.*(cs_O2>0))^0.5))-((cs_NO2.*(cs_NO2>0))/K7_eq))', ...

'r8','sigmaNOx*(k8f*(cs_NO.*(cs_NO>0))*((cs_O2.*(cs_O2>0))^0.75)*(s_BaCO3.
*(s_BaCO3>0)))', ...

'r9','sigmaNOx*(k9f*(cs_NO2.*(cs_NO2>0))*((cs_O2.*(cs_O2>0))^0.25)*(s_BaCO
3.*(s_BaCO3>0)))', ...
  'r10','(k10*sigmaNOx*((cs_CO.*(cs_CO>0))^1)*(s_Ba_NO3_2^PowerNO3))', ...
  'r11','(k11*sigmaNOx*((cs_H2.*(cs_H2>0))^1)*(s_Ba_NO3_2^PowerNO3))', ...
  'r12','(k12*sigmaNOx*((cs_CO.*(cs_CO>0))^1)*(s_Ba_NO3_2^PowerNO3))', ...
  'r13','(k13*sigmaNOx*((cs_H2.*(cs_H2>0))^1)*(s_Ba_NO3_2^PowerNO3))', ...
  'r14','k14*(cs_CO.*(cs_CO>0))*((cs_NO.*(cs_NO>0))^PowerNO)', ...
  'r15','k15*(cs_H2.*(cs_H2>0))*((cs_NO.*(cs_NO>0))^PowerNO)', ...
  'r16','(k16*sigmaNOx/(1+exp(-20*(s_Ba_NO3_2-0.3))))', ...
  'r17','(k17*sigmaNOx/(1+exp(-20*(s_Ba_NO3_2-0.5))))', ...
  'k1','A1*10^14*exp(-95000/Rg/Ts)*(flc2hs(t-0.25,0.25))', ...
  'k2','A2*10^14*exp(-95000/Rg/Ts)*(flc2hs(t-0.25,0.25))', ...
  'k3','A3*10^10*exp(-90000/Rg/Ts)*(flc2hs(t-0.25,0.25))', ...
  'k4','A4*10^7*exp(-90000/Rg/Ts)*(1-flc2hs(t-0.25,0.25))', ...
  'k5','A5*10^8*exp(-90000/Rg/Ts)*(flc2hs(t-0.25,0.25))', ...
  'k6','A6*10^8*exp(-90000/Rg/Ts)*(flc2hs(t-0.25,0.25))', ...
  'k7','A7*10^6*exp(-40000/Rg/Ts)*(1-flc2hs(t-0.25,0.25))', ...
  'k8','A8*10^2*exp(-20000/Rg/Ts)*(1-flc2hs(t-0.25,0.25))', ...
  'k9','A9*10^7*exp(-80000/Rg/Ts)*(1-flc2hs(t-0.25,0.25))', ...
  'k10','A10*10^7*exp(-90000/Rg/Ts)*(flc2hs(t-0.25,0.25))', ...
  'k11','A11*10^7*exp(-90000/Rg/Ts)*(flc2hs(t-0.25,0.25))', ...
  'k12','A12*10^8*exp(-90000/Rg/Ts)*(flc2hs(t-0.25,0.25))', ...
  'k13','A13*10^8*exp(-90000/Rg/Ts)*(flc2hs(t-0.25,0.25))', ...
  'k14','A14*10^9*exp(-70000/Rg/Ts)*(flc2hs(t-0.25,0.25))', ...
  'k15','A15*10^9*exp(-70000/Rg/Ts)*(flc2hs(t-0.25,0.25))', ...
```

```
  'k16','A16*2*0.375*10^-4', ...
  'k17','A17*2*10^-4', ...
  'A1','0.2', ...
  'A2','0.2', ...
  'A3','1', ...
  'A4','10', ...
  'A5',w(4), ...
  'A6',w(4), ...
  'A7',v(7), ...
  'A8',v(8), ...
  'A9','100', ...
  'A10',w(3), ...
  'A11',w(3), ...
  'A12',w(2), ...
  'A13',w(2), ...
  'A14',w(1), ...
  'A15',w(1), ...
  'A16',v(9), ...
  'A17',v(10), ...
  'inhibit','0.7', ...
  'K3_eq','exp(-4.33+(4577.8/Ts))', ...
  'K7_eq','exp((57100-Ts*73)/(8.314*Ts))*((Rg*Ts/100000)^0.5)', ...
  'G1','((1+K1*(cs_CO.*(cs_CO>0)))^2)*(1+K4*((cs_NO2.*(cs_NO2>0))^0.7))',
...
  'K1','65.55*exp(961/Ts)', ...
  'K2','2.08*1000*exp(361/Ts)', ...
  'K3','3.98*exp(11611/Ts)', ...
  'K4','4.79*10^5*exp(-3733/Ts)', ...
  'rbase_c','(50-50/1)*flc2hs(x-0.02,0.01)+50/1', ...
  'rbase_n','(62.5-62.5/1)*flc2hs(x-0.02,0.01)+62.5/1', ...
  'rtot','((rbase_n-rbase_c)*(flc2hs(s_Ba_NO3_2-
0.5,0.45))+rbase_c)/(10^9)', ...
  'l','rtot-Rm', ...
  'D_NO2',v(1), ...
  'D_NO',v(2), ...
  'slope_NO2',v(3), ...
  'slope_NO',v(4), ...
  'limit_NO2',v(5), ...
  'limit_NO',v(6), ...
  'Deff_NO2','(D_NO2*10^-9)*exp(-slope_NO2*(1-Rm/rtot-limit_NO2))/(1+exp(-
slope_NO2*(1-Rm/rtot-limit_NO2)))', ...
  'Deff_NO','(D_NO*10^-9)*exp(-slope_NO*(1-Rm/rtot-limit_NO))/(1+exp(-
slope_NO*(1-Rm/rtot-limit_NO)))', ...
  'k8f','k8/(1+k8*(l/Deff_NO)*(Rm/rtot)*s_BaCO3)', ...
  'k9f','k9/(1+k9*(l/Deff_NO2)*(Rm/rtot)*s_BaCO3)', ...
  'Rm','rtot*((1+(1-0.5*s_BaCO3)*((R_1/rtot)^3)-s_BaCO3)/(1-
0.5*s_BaCO3))^(1/3)', ...
  'PowerNO','1', ...
  'PowerNO3','1', ...
  'Ts','T_in'};

% Multiphysics
fem=multiphysics(fem);

% Extend mesh
fem.xmesh=meshextend(fem);
```

```
% Mapping stored solution to extended mesh
init = asseminit(fem,'init',fem1.sol,'solnum',length(fem1.sol.tlist));

% Solve problem
fem.sol=femtime(fem, ...
                'init',init, ...

'solcomp',{'R_2','c_CO','c_N2','cs_CO','c_CO2','s_Ce2O3','s_Ba_NO3_2','cs_
H2','c_NO2','c_H2','cs_CO2','cs_O2','c_H2O','cs_NO','s_CeO2','cs_N2','cs_H
2O','cs_NO2','s_BaCO3','c_NO','c_O2'}, ...

'outcomp',{'R_1','R_2','R_3','theta_1','theta_3','c_CO','c_N2','cs_CO','c_
CO2','s_Ce2O3','s_Ba_NO3_2','cs_H2','c_NO2','c_H2','cs_CO2','cs_O2','c_H2O
','cs_NO','s_CeO2','cs_N2','cs_H2O','cs_NO2','s_BaCO3','c_NO','c_O2'}, ...
                'tlist',[0:0.5:rt], ...
                'atol',{'1e-6'}, ...
                'rtol',1e-4, ...
                'maxstep', 0.05, ...
                'maxorder',2, ...
                'tout','tlist');

fem1=fem;

% Saving the data to text files

dlmwrite('c_NO.txt',[postinterp(fem1,'t',0,'solnum','all')+time
postinterp(fem1,'c_NO*F',fem1.mesh.p,'solnum','all')],  '-
append','delimiter', '\t','precision', '%.6f');
dlmwrite('c_NO2.txt',[postinterp(fem1,'t',0,'solnum','all')+time
postinterp(fem1,'c_NO2*F',fem1.mesh.p,'solnum','all')],  '-
append','delimiter', '\t','precision', '%.6f');
dlmwrite('s_CeO2.txt',[postinterp(fem1,'t',0,'solnum','all')+time
postinterp(fem1,'s_CeO2',fem1.mesh.p,'solnum','all')], '-append',
'delimiter', '\t','precision', '%.6f');
dlmwrite('s_BaCO3.txt',[postinterp(fem1,'t',0,'solnum','all')+time
postinterp(fem1,'s_BaCO3',fem1.mesh.p,'solnum','all')], '-append',
'delimiter', '\t','precision', '%.6f');
dlmwrite('c_CO.txt',[postinterp(fem1,'t',0,'solnum','all')+time
postinterp(fem1,'c_CO*(F/10^6)',fem1.mesh.p,'solnum','all')], '-append',
'delimiter', '\t','precision', '%.6f');

toc

% Expressions for even rich phase

elseif(rem(cycle,2)==0)

% Global expressions
fem.globalexpr = {'c_NO_in','(0.00033*101325*(1-flc2hs(t-
0.25,0.25)))/(8.314*T_in)', ...
  'c_O2_in','(0.1*101325*(1-flc2hs(t-0.25,0.25)))/(8.314*T_in)', ...
  'c_CO2_in','(0.05*101325)/(8.314*T_in)', ...
  'c_H2O_in','(0.05*101325)/(8.314*T_in)', ...
  'c_N2_in','(0.7997*101325)/(8.314*T_in)', ...
  'c_NO2_in','0', ...
```

```
  'c_H2_in','0', ...
  'c_CO_in','(0.015*101325*(flc2hs(t-0.25,0.25)))/(8.314*T_in)', ...
  'v','(14.32/(1000*60*169))/(.000625^2*3.14)', ...
  'D','0', ...
  'sigmaNOx','650', ...
  'sigmaO2','600', ...
  'r1','(k1*(cs_CO.*(cs_CO>0))*(cs_O2.*(cs_O2>0)))/G1', ...
  'r2','(k2*(cs_H2.*(cs_H2>0))*(cs_O2.*(cs_O2>0)))/G1', ...
  'r3','k3*(((cs_CO.*(cs_CO>0))*(cs_H2O.*(cs_H2O>0)))-
(((cs_CO2.*(cs_CO2>0))*(cs_H2.*(cs_H2>0)))/K3_eq))', ...
  'r4','k4*sigmaO2*((cs_O2.*(cs_O2>0)))*(1-s_CeO2)', ...
  'r5','k5*sigmaO2*(cs_CO.*(cs_CO>0))*s_CeO2', ...
  'r6','k6*sigmaO2*(cs_H2.*(cs_H2>0))*s_CeO2', ...

'r7','(k7/1/(1+K4*((cs_NO2.*(cs_NO2>0))^inhibit))^1)*(((cs_NO.*(cs_NO>0))*
((cs_O2.*(cs_O2>0))^0.5))-((cs_NO2.*(cs_NO2>0))/K7_eq))', ...

'r8','sigmaNOx*(k8f*(cs_NO.*(cs_NO>0))*((cs_O2.*(cs_O2>0))^0.75)*(s_BaCO3.
*(s_BaCO3>0)))', ...

'r9','sigmaNOx*(k9f*(cs_NO2.*(cs_NO2>0))*((cs_O2.*(cs_O2>0))^0.25)*(s_BaCO
3.*(s_BaCO3>0)))', ...
  'r10','(k10*sigmaNOx*((cs_CO.*(cs_CO>0))^1)*(s_Ba_NO3_2^PowerNO3))', ...
  'r11','(k11*sigmaNOx*((cs_H2.*(cs_H2>0))^1)*(s_Ba_NO3_2^PowerNO3))', ...
  'r12','(k12*sigmaNOx*((cs_CO.*(cs_CO>0))^1)*(s_Ba_NO3_2^PowerNO3))', ...
  'r13','(k13*sigmaNOx*((cs_H2.*(cs_H2>0))^1)*(s_Ba_NO3_2^PowerNO3))', ...
  'r14','k14*(cs_CO.*(cs_CO>0))*((cs_NO.*(cs_NO>0))^PowerNO)', ...
  'r15','k15*(cs_H2.*(cs_H2>0))*((cs_NO.*(cs_NO>0))^PowerNO)', ...
  'r16','(k16*sigmaNOx/(1+exp(-20*(s_Ba_NO3_2-0.3))))', ...
  'r17','(k17*sigmaNOx/(1+exp(-20*(s_Ba_NO3_2-0.5))))', ...
  'k1','A1*10^14*exp(-95000/Rg/Ts)*(flc2hs(t-0.25,0.25))', ...
  'k2','A2*10^14*exp(-95000/Rg/Ts)*(flc2hs(t-0.25,0.25))', ...
  'k3','A3*10^10*exp(-90000/Rg/Ts)*(flc2hs(t-0.25,0.25))', ...
  'k4','A4*10^7*exp(-90000/Rg/Ts)*(1-flc2hs(t-0.25,0.25))', ...
  'k5','A5*10^8*exp(-90000/Rg/Ts)*(flc2hs(t-0.25,0.25))', ...
  'k6','A6*10^8*exp(-90000/Rg/Ts)*(flc2hs(t-0.25,0.25))', ...
  'k7','A7*10^6*exp(-40000/Rg/Ts)*(1-flc2hs(t-0.25,0.25))', ...
  'k8','A8*10^2*exp(-20000/Rg/Ts)*(1-flc2hs(t-0.25,0.25))', ...
  'k9','A9*10^7*exp(-80000/Rg/Ts)*(1-flc2hs(t-0.25,0.25))', ...
  'k10','A10*10^7*exp(-90000/Rg/Ts)*(flc2hs(t-0.25,0.25))', ...
  'k11','A11*10^7*exp(-90000/Rg/Ts)*(flc2hs(t-0.25,0.25))', ...
  'k12','A12*10^8*exp(-90000/Rg/Ts)*(flc2hs(t-0.25,0.25))', ...
  'k13','A13*10^8*exp(-90000/Rg/Ts)*(flc2hs(t-0.25,0.25))', ...
  'k14','A14*10^9*exp(-70000/Rg/Ts)*(flc2hs(t-0.25,0.25))', ...
  'k15','A15*10^9*exp(-70000/Rg/Ts)*(flc2hs(t-0.25,0.25))', ...
  'k16','A16*2*0.375*10^-4', ...
  'k17','A17*2*10^-4', ...
  'A1','0.2', ...
  'A2','0.2', ...
  'A3','1', ...
  'A4','10', ...
  'A5',w(4), ...
  'A6',w(4), ...
  'A7',v(7), ...
  'A8',v(8), ...
  'A9','100', ...
  'A10',w(3), ...
```

```
  'A11',w(3), ...
  'A12',w(2), ...
  'A13',w(2), ...
  'A14',w(1), ...
  'A15',w(1), ...
  'A16',v(9), ...
  'A17',v(10), ...
  'inhibit','0.7', ...
  'K3_eq','exp(-4.33+(4577.8/Ts))', ...
  'K7_eq','exp((57100-Ts*73)/(8.314*Ts))*((Rg*Ts/100000)^0.5)', ...
  'G1','((1+K1*(cs_CO.*(cs_CO>0)))^2)*(1+K4*((cs_NO2.*(cs_NO2>0))^0.7))',
...
  'K1','65.55*exp(961/Ts)', ...
  'K2','2.08*1000*exp(361/Ts)', ...
  'K3','3.98*exp(11611/Ts)', ...
  'K4','4.79*10^5*exp(-3733/Ts)', ...
  'rbase_c','(50-50/1)*flc2hs(x-0.02,0.01)+50/1', ...
  'rbase_n','(62.5-62.5/1)*flc2hs(x-0.02,0.01)+62.5/1', ...
  'rtot','((rbase_n-rbase_c)*(flc2hs(s_Ba_NO3_2-
0.5,0.45))+rbase_c)/(10^9)', ...
  'l','rtot-Rm', ...
  'D_NO2',v(1), ...
  'D_NO',v(2), ...
  'slope_NO2',v(3), ...
  'slope_NO',v(4), ...
  'limit_NO2',v(5), ...
  'limit_NO',v(6), ...
  'Deff_NO2','(D_NO2*10^-9)*exp(-slope_NO2*(1-Rm/rtot-limit_NO2))/(1+exp(-
slope_NO2*(1-Rm/rtot-limit_NO2)))', ...
  'Deff_NO','(D_NO*10^-9)*exp(-slope_NO*(1-Rm/rtot-limit_NO))/(1+exp(-
slope_NO*(1-Rm/rtot-limit_NO)))', ...
  'k8f','k8/(1+k8*(l/Deff_NO)*(Rm/rtot)*s_BaCO3)', ...
  'k9f','k9/(1+k9*(l/Deff_NO2)*(Rm/rtot)*s_BaCO3)', ...
  'Rm','rtot*((1+(1-0.5*s_BaCO3)*((R_3/rtot)^3)-s_BaCO3)/(1-
0.5*s_BaCO3))^(1/3)', ...
  'PowerNO','1', ...
  'PowerNO3','1', ...
  'Ts','T_in'};

% Multiphysics
fem=multiphysics(fem);

% Extend mesh
fem.xmesh=meshextend(fem);

% Mapping stored solution to extended mesh
init = asseminit(fem,'init',fem1.sol,'solnum',length(fem1.sol.tlist));

% Solve problem
fem.sol=femtime(fem, ...
                'init',init, ...

'solcomp',{'R_2','c_CO','c_N2','cs_CO','c_CO2','s_Ce2O3','s_Ba_NO3_2','cs_
H2','c_NO2','c_H2','cs_CO2','cs_O2','c_H2O','cs_NO','s_CeO2','cs_N2','cs_H
2O','cs_NO2','s_BaCO3','c_NO','c_O2'}, ...
```

```
'outcomp',{'R_1','R_2','R_3','theta_1','theta_3','c_CO','c_N2','cs_CO','c_
CO2','s_Ce2O3','s_Ba_NO3_2','cs_H2','c_NO2','c_H2','cs_CO2','cs_O2','c_H2O
','cs_NO','s_CeO2','cs_N2','cs_H2O','cs_NO2','s_BaCO3','c_NO','c_O2'}, ...
                'tlist',[0:0.5:rt], ...
                'atol',{'1e-6'}, ...
                'rtol',1e-4, ...
                'maxstep', 0.05, ...
                'maxorder',2, ...
                'tout','tlist');

fem1=fem;

% Saving the data to text files

dlmwrite('c_NO.txt',[postinterp(fem1,'t',0,'solnum','all')+time
postinterp(fem1,'c_NO*F',fem1.mesh.p,'solnum','all')],  '-
append','delimiter', '\t','precision', '%.6f');
dlmwrite('c_NO2.txt',[postinterp(fem1,'t',0,'solnum','all')+time
postinterp(fem1,'c_NO2*F',fem1.mesh.p,'solnum','all')],  '-
append','delimiter', '\t','precision', '%.6f');
dlmwrite('s_CeO2.txt',[postinterp(fem1,'t',0,'solnum','all')+time
postinterp(fem1,'s_CeO2',fem1.mesh.p,'solnum','all')], '-append',
'delimiter', '\t','precision', '%.6f');
dlmwrite('s_BaCO3.txt',[postinterp(fem1,'t',0,'solnum','all')+time
postinterp(fem1,'s_BaCO3',fem1.mesh.p,'solnum','all')], '-append',
'delimiter', '\t','precision', '%.6f');
dlmwrite('c_CO.txt',[postinterp(fem1,'t',0,'solnum','all')+time
postinterp(fem1,'c_CO*(F/10^6)',fem1.mesh.p,'solnum','all')], '-append',
'delimiter', '\t','precision', '%.6f');

toc

end

time=time+rt;
cycle=cycle+1;
end

% End of the algorithm
```

Bibliography

Abdulhamid H., E. Fridell, and M. Skoglundh, "The reduction phase in NOx storage catalysis: Effect of type of precious metal and reducing agent" Applied Catalysis B: Environmental, 62 (2006) 319-328.

Al-Harbi M. and Epling W.S. "Personal Communication" (2009)

Al-Harbi M. "M.A.Sc. Thesis - Environmental Technology Management: Performance and Reaction Activity Changes of a NOX Storage/Reduction Catalyst as a Function of Regeneration Mixture and Thermal Degradation", UW-Space (2008)

Amberntsson Annika, Persson Hans, Engström Per, Kasemo Bengt. "NOx release from a noble metal/BaO catalyst: dependence on gas composition." Applied Catalysis B: Environmental 31 (2001)27-38.

Forzatti P., L. Castoldi, I. Nova, L. Lietti, E. Tronconi "NO_x removal catalysis under lean conditions" Catalysis Today 117 (2006) 316–320

Fridell Erik, Skoglundh Magnus, Westerberg Björn, Johansson Stefan, Smedler Gudmund. "NOx Storage in Barium-Containing Catalysts" Journal of Catalysis 183 (1999) 196-209.

Fridell E., Hans Persson, Louise Olsson, BjörnWesterberg, Annika Amberntsson, and Magnus Skoglundh. "Model studies of NOx storage and sulphur deactivation of NOx storage catalysts" Topics in Catalysis, 16/17 (2001) 1-4.

Güthenke, A., et al. "Development and Application of a Model for a NOx Storage and Reduction Catalyst." Chemical Engineering Science 62.18-20 SPEC. ISS. (2007): 5357-63.

Jirát, J., M. Kubíček, and M. Marek. "Mathematical Modelling of Catalytic Monolithic Reactors with Storage of Reaction Components on the Catalyst Surface." Catalysis Today 53.4 (1999): 583-96.

Kočí, P., et al. "Modelling of Catalytic Monolith Converters with Low- and High-Temperature NOx Storage Compounds and Differentiated Washcoat." Chemical Engineering Journal 97.2-3 (2004): 131-9.

Kočí, P., et al. "Nonlinear Dynamics of Automobile Exhaust Gas Converters: The Role of Nonstationary Kinetics." Chemical Engineering Science 59.22-23 (2004): 5597-605.

Kočí, P., et al. "Transient Behaviour of Catalytic Monolith with NOx Storage Capacity." Catalysis Today 119.1-4 (2007): 64-72.

Koltsakis, G. C., P. A. Konstantinidis, and A. M. Stamatelos. "Development and Application Range of Mathematical Models for 3-Way Catalytic Converters." Applied Catalysis B: Environmental 12.2-3 (1997): 161-91.

Koltsakis, G. C., and A. M. Stamatelos. "Modeling Dynamic Phenomena in 3-Way Catalytic Converters." Chemical Engineering Science 54.20 (1999): 4567-78.

Mahzoul H., Brilhac J.F., Gilot P. "Experimental and mechanistic study of NOx adsorption over NOx trap catalysts" Applied Catalysis B: Environmental 20 (1999) 47-55.

Mahzoul H., Gilot, P., Brilhac J.-F., and Stanmore B.R. "Reduction of NOx over a NOx-Trap Catalyst and the Regeneration Behaviour of Adsorbed SO_2" Topics in Catalysis 16 (2001) 293-298.

Nova I., Lidia Castoldi, Luca Lietti, Enrico Tronconi, and Pio Forzatti. "On the dynamic behavior of "NOx storage/reduction" Pt–Ba/Al_2O_3 catalyst" Catalysis Today 75 (2002) 431–437.

Ohtsuka, H., and T. Tabata. "Roles of Palladium and Platinum in the Selective Catalytic Reduction of Nitrogen Oxides by Methane on Palladium-Platinum-Loaded Sulfated Zirconia." Applied Catalysis B: Environmental 29.3 (2001): 177-83.

Ohtsuka, H. "The Selective Catalytic Reduction of Nitrogen Oxides by Methane on Noble Metal-Loaded Sulfated Zirconia." Applied Catalysis B: Environmental 33.4 (2001): 325-33.

Olsson, L., R. J. Blint, and E. Fridell. "Global Kinetic Model for Lean NOx Traps." Industrial and Engineering Chemistry Research 44.9 (2005): 3021-32.

Olsson, L., et al. "Mean Field Modelling of NOx Storage on Pt/BaO/Al_2O_3." Catalysis Today 73.3-4 (2002): 263-70.

Olsson, L., D. Monroe, and R. J. Blint. "Global Kinetic Modelling of a Supplier Barium- and Potassium-Containing Lean NOx Trap." Industrial and Engineering Chemistry Research 45.26 (2006): 8883-90.

Olsson, L., Hans Persson, Erik Fridell, Magnus Skoglundh, and Bengt Andersson. "A Kinetic Study of NO Oxidation and NOx Storage on Pt/Al_2O_3 and $Pt/BaO/Al_2O_3$." Journal of Physical Chemistry B 105.29 (2001): 6895-6906.

Prinetto F., Ghiotti G.,Nova I., Lietti L., Tronconi E., Forzatti P. "FT-IR and TPD Investigation of the NOX Storage Properties of BaO/Al_2O_3 and $Pt–BaO/Al_2O_3$ Catalysts" Journal of Physical Chemistry B. 105 (2001) 12732-12745.

Salasc, S., M. Skoglundh, and E. Fridell. "A Comparison between Pt and Pd in NOx Storage Catalysts." Applied Catalysis B: Environmental 36.2 (2002): 145-60.

Schmeißer, V., U. Tuttlies, and G. Eigenberger. "Towards a Realistic Simulation Model for NOx-Storage Catalyst Dynamics." Topics in Catalysis 42-43.1-4 (2007): 77-81.

Scotti, Andrea, et al. "Kinetic Study of Lean NOx Storage over the $Pt–Ba/Al_2O_3$ System." Industrial & Engineering Chemistry Research 43.16 (2004): 4522-34.

Tomašić, V. "Application of the Monoliths in DeNOx Catalysis." Catalysis Today 119.1-4 (2007): 106-13.

Toops T. J., Bruce G. Bunting, Ke Nguyen, Ajit Gopinath. "Effect of engine based thermal aging on surface morphology and performance of Lean NOx Traps" Catalysis Today 123 (2007) 285–292.

Tsinoglou, D. N., G. C. Koltsakis, and J. C. Peyton Jones. "Oxygen Storage Modeling in Three Way Catalytic Converters." Industrial and Engineering Chemistry Research 41.5 (2002): 1152-65.

Tuttlies, U., V. Schmeißer, and G. Eigenberger. "A Mechanistic Simulation Model for NOx Storage Catalyst Dynamics." Chemical Engineering Science 59.22-23 (2004): 4731-8.

Voltz, S. E., et al. "Kinetic Study of Carbon Monoxide and Propylene Oxidation on Platinum Catalysts." Industrial & Engineering Chemistry Product Research and Development 12.4 (1973): 294-301.

Watanabe, Y., et al. "Development of a Model for the Lean NOx Catalytic Reaction with Hydrocarbon Adsorption and Desorption." Applied Catalysis B: Environmental 31.3 (2001): 221-8.

William S. Epling, Larry E. Campbell, Aleksey Yezerets, Neal W.Currier, and James E. Parks II. “Overview of the fundamental reactions and degradation mechanisms of NOx storage/ reduction catalyst”. Catalysis Review 46 (2004) 163.

Xue, E., K. Seshan, and J. R. H. Ross. "Roles of Supports, Pt Loading and Pt Dispersion in the Oxidation of NO to NO_2 and of SO_2 to SO_3." Applied Catalysis B: Environmental 11.1 (1996): 65-79.